



UNIVERSITY OF THE
WITWATERSRAND,
JOHANNESBURG

*Investigating telomere dynamics using standard and AuNP-based assays and
developing an LRP-based nanoparticle drug*

by

Martin Bernert

(375076)

Thesis

Submitted in fulfilment of the requirements for the degree

Philosophiae Doctor

in

Molecular and Cell Biology

in the Faculty of Science, University of the Witwatersrand, Johannesburg, South Africa

Supervisors: Prof Stefan FT Weiss and Dr. Eloise van der Merwe

November 2023

Declaration

I, Martin Bernert (375076), am a student registered for the degree of Doctor of Philosophy Science by Thesis (PhD) in the academic year 2023.

I hereby declare the following:

- I am aware that plagiarism (the use of someone else's work without their permission and/or without acknowledging the original source) is wrong.
- I confirm that the work submitted for assessment for the above degree is my own unaided work except where explicitly indicated otherwise.
- I have not submitted this work before for any other degree or examination at this or any other University.
- I have followed the required conventions in referencing the thoughts and ideas of others.
- I understand that the University of the Witwatersrand may take disciplinary action against me if there is a belief that this is not my own unaided work or that I have failed to acknowledge the source of the ideas or words in my writing.

Signed: 6th day of November 2023

A handwritten signature in black ink, appearing to be 'M. Bernert', written in a cursive style with a long horizontal stroke extending to the right.

Abstract

Telomere dynamics, specifically telomerase activity have been implicated in age-related diseases, such as CVD, Alzheimer's disease, and cancer. This makes the accurate detection of telomerase activity within cell cultures and tissue samples a necessity. Conventional techniques have many drawbacks, including their very high cost. Therefore, this research aimed to develop a gold nanoparticle (AuNP)-based assay to determine telomerase activity. In the assay the extracted telomerase leads to a colour change in the solution through the addition of telomeric repeats and subsequent elongation of the synthetic telomeres attached to the AuNPs. This colour change is detectable using spectrophotometric readings and represents telomerase activity. This assay would be useful as an alternative to expensive existing telomerase activity kits as large batches of AuNPs can be synthesised inexpensively. Telomerase activity was successfully detected in both HEK-293 and WHCO-5 cells using this novel technique, although the sensitivity of the AuNP-based telomerase activity assay is currently lower than a commercially available qPCR-based telomerase activity kit. In addition, telomerase activity is directly affected by the LRP protein, a highly conserved non-integrin transmembrane receptor, which has been shown to have therapeutic effects in ageing, Alzheimer's disease, Parkinson's disease, diabetes, and cardiovascular disease models. Recently it has been found that overexpression of LRP::FLAG, by plasmid transfection, leads to a significant increase in telomerase activity in cell culture models. This may indicate that upregulation of LRP can be used to treat various age-related diseases, however, transfection is not a viable treatment strategy and therefore, a protein-based drug was created. For a protein-based drug, a suitable delivery system needed to be developed and nano-capsules, such as those synthesised using Poly(lactic-co-glycolic acid) (PLGA), are able to contain the therapeutic protein. The molecules contained within the nanoparticles also gain the benefit of having increased stability compared to unprotected molecules and the capsules have the capacity for surface modifications for targeted therapy. These polymer-based nanoparticles are also biodegradable and biocompatible, making them a safe delivery agent. Thus, this research further aimed to develop a PLGA-based LRP drug delivery system for the 37 kDa Laminin receptor protein. Both synthesis of the nanoparticles and encapsulation of the LRP protein were successfully optimised and the completed drug was tested in a cell culture model, where treatment increased cell viability and telomerase activity in HEK-293 cells. Therefore, this LRP drug delivery system has great potential to assist in the translation of our *in vitro* studies into an *in vivo* context. Due to the wide range of applications elevating LRP levels has in the treatment of different disorders, this could represent a safer alternative to plasmid transfection treatment and could potentially be used for the treatment of age-related diseases, through its ability to increase telomerase activity.

Acknowledgements

Firstly, I would like to thank Dr. Eloise van der Merwe for being not just an incredible supervisor but an amazing friend. Your excitement for your work is infectious and this has kept me motivated through rough times. You have pushed and encouraged me to take on new and challenging scientific techniques and I cannot thank you enough for this. Throughout my entire postgraduate journey, you have been a constant source of knowledge and support, without which I would never have come as far as I have.

I would also like to thank my parents, Albert, and Monika Kopp, for everything they have done to support me throughout my PhD. Your genuine interest in everything I do has been an incredible motivator and I don't have the words to adequately convey the love and respect I have for you both. Thank you for being the best parents I could have wished for. And Albert, I am happy to finally have a satisfactory answer to your question: yes, it is finally done!

I would also like to thank my girlfriend, Claire Tinderholm. Thank you for your infinite patience in dealing with my ups and downs, your presence alone has made my life so much better. I could not have done this without your help and support, and I cannot thank you enough.

Thank you to my friends, Nick, Gen, Bacci, Bradley, Dave and Andi. You guys are awesome, thank you for the games, intellectual and not so intellectual conversations as well as looking out for me. You guys kept me motivated.

I would like to give a very special thank you to Dr. Tyrone Otgaar, Dr. Monique Bignoux and Dr. Gavin Morris. Tyrone, you have been the rock that kept our lab together and I am grateful to have you as one of my friends. Your passion for science is evident in every conversation we have

had, and I have learned a so much from you. Monique, you bring a vibe to the lab I can't fully explain, you can make the heaviest subject fun and see a lack of a smile on your colleagues faces as a personal challenge. Thank you for all your help and support over the years. Gavin, you have been a fantastic friend and roommate to me, your assistance during my PhD has been invaluable and your insights profound. You are one of the smartest people I know (and I know a lot of smart people), thank you for everything you have done for me. I thoroughly enjoyed our lengthy troubleshooting sessions together and I wish you three all the best for the future.

Thank you to my colleagues of Weiss lab and the Cell Biology and Signalling Research lab, you all have made an impact on me. It has been a privilege to see so many of you become the amazing scientists you are today. I would like to specifically acknowledge Chandni Madhav and Sichumiso Gqeba for your assistance with the protein work. It was tough stuff.

Finally, I would like to thank my late supervisors Dr. Boitelo Letsolo and Prof. Stefan Weiss. Although you are no longer with us, your fierce intelligences and personalities have made an impact on the world. Dr. Letsolo was my first supervisor and the reason I fell in love with molecular biology. You strove to not only make me a better scientist but also a better person. Similarly, Prof. Weiss was not just a supervisor, he was a force of nature and everyone who knew him was better off for it. He encouraged me to challenge and to better myself in all things. I will always remember being hurriedly pulled out of the culture lab just to play a round of darts with you. You both are dearly missed.

Financial aid:

Wits Postgraduate Merit Award (PGMA) (2015-2016)

National Research Foundation (NRF) – Free Standing (2016)

Technology Innovation Agency (TIA) Seed Fund (2017-2023)

University of the Witwatersrand seed fund (2021)

Research outputs

Publications:

- Bignoux MJ, Otgaar TC, Bernert M, Weiss SFT and Ferreira E (2022) siRNA- mediated downregulation of LRP/LR inhibits multiple cancer hallmarks in lung cancer cells. FEBS One Bio (under review).
- Vania L, Morris G, Otgaar TC, Bignoux MJ, Bernert M, Burns J, Gabathuse A, Singh E, Ferreira E and Weiss SFT (2019) Patented therapeutic approaches targeting LRP/LR for cancer treatment. Expert Opinion on Therapeutic Patents. 29(12):987-1009
- Otgaar TC, Ferreira E, Malindisa S, Bernert M, Letsolo BT and Weiss SFT (2017) 37 kDa LRP::FLAG enhances telomerase activity and reduces senescent markers *in vitro*. Oncotarget. 8(49):86646-86656. doi:10.18632/oncotarget.21278.
- Naidoo K, Malindisa ST, Otgaar TC, Bernert M, Da Costa Dias B, Ferreira E, Reusch U, Knackmuss S, Little M, Weiss SFT and Letsolo BT (2015) Knock-down of the 37kDa/67kDa laminin receptor LRP/LR impedes telomerase activity. Plos One. 10(11)

Patents:

- South Africa patent application WO/2019/116334 is in the name of the University of the Witwatersrand entitled: "A Nanoparticle-Based Telomerase Assay." Inventors: Stefan Weiss, Boitelo Teresa Letsolo, Martin Bernert.

- South Africa patent application WO/2020/008442A3 is in the name of the University of the Witwatersrand entitled: “Biopharmaceutical agents for use in reducing lipid content in cells”. Inventors: Stefan Weiss, Eloise van der Merwe, Martin Bernert and Tyrone Otgaar.

Conference outputs:

- Bernert M., Letsolo B. T. Metformin Reduces Telomerase Activity in Oesophageal Carcinoma Cells Expressing Wild-Type p53. Poster Presentation. Molecular Biosciences Research Thrust (MBRT) Research Day, Johannesburg, South Africa. 2014
- Bernert M., Otgaar T. C., Baichan P., Malindisa S.T., Weiss S.F.T, Veale R. B., Moeno S. and Letsolo B.T. Investigating Telomere Dynamics in Oesophageal Squamous Carcinoma Cells using Standard and Nanoparticle-based Assays. Poster Presentation. Molecular Biosciences Research Thrust (MBRT) Research Day. Johannesburg, South Africa. 2016.
- Bernert M., Kondiah K., Veale R.B., Moeno S., Letsolo B.T., and Weiss S.F.T. Investigating Telomere Dynamics in Oesophageal Squamous Carcinoma Cells using Standard and Nanoparticle-based Assays. Poster presentation. Molecular Biosciences Research Thrust (MBRT) Research Day, Johannesburg, South Africa. 2017
- Bernert M., Kondiah K., Veale R.B., Moeno S., Letsolo B.T., and Weiss S.F.T. Investigating Telomere Dynamics in Oesophageal Squamous Carcinoma Cells using Standard and Nanoparticle-based Assays. Oral presentation. South African Society for Biochemistry and Molecular Biology (SASBMB). Potchefstroom, South Africa. 2018.

- Bernert M., Kondiah K., Veale R.B., Moeno S., Letsolo B.T., and Weiss S.F.T. Investigating Telomere Dynamics in Oesophageal Squamous Carcinoma Cells using Standard and Nanoparticle-based Assays. Poster presentation. South African Society for Biochemistry and Molecular Biology (SASBMB). Potchefstroom, South Africa. 2018.
- Bernert M., Morris G., Veale R., Ferreira E., and Weiss S.F.T. Developing Nanoparticle-based Systems for the Detection of Telomerase Activity as well as Drug Delivery. Poster presentation. Molecular Biosciences Research Thrust (MBRT) Research Day, Johannesburg, South Africa. 2019
- Ferreira E., Otgaar T.C., Bernert M., Morris G., Baichan P., Letsolo B.T. and Weiss S.F.T. *In vivo* investigation of the effect of LRP::FLAG overexpression on the ageing process and telomere dynamics in mice. Oral presentation, OLC International Biotechnology Conference, Chicago, USA, 23-24 September 2019

Table of Contents

Declaration.....	ii
Abstract.....	iii
Acknowledgements.....	iv
Research outputs	vi
Table of Contents.....	ix
List of Figures	xiii
List of Tables	xv
List of Abbreviations	xvi
1. Introduction and Literature Review.....	1
1.1. Telomeres.....	1
1.1.1. Function	1
1.1.2. Structure	3
1.1.3. Telomerase.....	5
1.1.4. Extratelomeric functions of hTERT	8
1.2. Telomeres in diseases	8
1.2.1. Telomeres and cancer.....	8
1.2.2. The role of telomeres in age related disorders	13
1.2.3. The role of telomeres in neurodegenerative disorders.....	14
1.3. Telomerase modulators	15
1.3.1. Metformin inhibits telomerase activity	15
1.3.1. The MST-312 telomerase inhibitor	17
1.3.2. The TA-65 telomerase enhancer.....	17

1.4.	37 kDa laminin receptor precursor/67 kDa high affinity laminin receptor	18
1.4.1.	Structure and function	18
1.4.2.	LRP/LR and telomerase	19
1.4.3.	The role of LRP/LR in cancer	20
1.4.4.	The role of LRP/LR in neurodegenerative disease	21
1.5.	Applications of nanoparticles in drug delivery and research.....	22
1.5.1.	PLGA nano-capsules as drug delivery agents	22
1.5.2.	Nanoparticles in telomerase activity assays	23
1.6.	Research rationale.....	26
2.	Aims and Objectives.....	28
2.1.	Aim 1: Optimise the gold nanoparticle telomerase activity assay and improve the stability of the functionalised AuNPs by redesigning separate linker and extension strands.	28
2.2.	Aim 2: Create an LRP based nanoparticle drug.....	28
3.	Materials and Methods.....	29
3.1.	Cell culture	29
3.1.1.	Cell culture protocol	29
3.1.2.	Passaging of cells	29
3.1.3.	Cryo-preservation of cells	30
3.1.4.	Cell quantification	30
3.1.5.	Metformin and MST-312 Treatments.....	31
3.1.6.	MTT cell viability assay.....	32
3.1.7.	DNA quantification - agarose gel electrophoresis	32
3.1.8.	Telomerase activity.....	33
3.2.	Section 1: Gold nanoparticle telomerase activity assay	35

3.2.1.	AuNP synthesis.....	36
3.2.2.	AuNP DNA functionalisation	36
3.2.3.	AuNP based telomerase activity assay	38
3.2.4.	Electron microscopy (SEM and TEM) and spectrophotometry	40
3.3.	Section 2: LRP-based PLGA nanoparticle drug design	41
3.3.1.	Nanoparticle drug design.....	41
3.3.2.	BCA/ micro-BCA assay.....	43
3.3.3.	Western blot	43
3.3.4.	Telomerase activity.....	45
3.4.	Data analysis and statistical evaluation	45
4.	Results.....	46
4.1.	Section 1: AuNP-based telomerase activity assay	46
4.1.1.	Metallic nanoparticle synthesis	47
4.1.2.	AuNP characterisation	49
4.1.3.	Thiol-DNA Functionalisation of gold nanoparticles	53
4.1.4.	DNA functionalisation - pH dependent method.....	57
4.1.5.	AuNP-based telomerase activity assay.....	60
4.1.	Section 2: Encapsulated-LRP PLGA nano-capsules	65
4.1.1.	Optimisation of PLGA nano-capsule synthesis	66
4.1.2.	The effects of empty PLGA nano-capsules on cell viability	77
4.1.3.	Protein encapsulation using PLGA nano-capsules.....	79
4.1.4.	LRP protein encapsulation	83
4.1.5.	Effect of encapsulated LRP treatments on total LRP levels, cell viability and telomerase activity	85

5.	Discussion.....	90
5.1.	Section 1: AuNP-based telomerase activity assay	90
5.1.1.	Synthesis and characterisation	91
5.1.2.	DNA functionalisation	92
5.1.3.	AuNP-based telomerase activity assay	94
5.1.4.	AuNP section conclusion.....	97
5.1.5.	Future research for the AuNP-based telomerase activity assay	98
5.2.	Section 2: LRP-encapsulated PLGA nano-capsules	99
5.2.1.	Optimisation of synthesis	99
5.2.2.	Purification of PLGA nano-capsules	101
5.2.3.	Protein encapsulation trials	104
5.2.4.	LRP-PLGA nano-capsule treatments	106
5.2.5.	PLGA section conclusion	109
5.2.6.	Future research for the LRP-encapsulated PLGA nano-capsules	109
5.3.	Conclusion	110
6.	References	112
7.	Supplementary results	127
7.1.	Metformin treatment reduces telomerase activity on oesophageal cancer cells:.....	127
7.2.	LRP protein synthesis	128
8.	Supplementary information.....	137
8.1.	List of reagents and materials:.....	137
8.2.	List of equipment:	138
8.3.	List of software:.....	138

List of Figures

Figure 1.1: Schematic representation of the "end-replication" problem	2
Figure 1.2: Focused view of the shelterin complex	4
Figure 1.3: Telomere secondary structures and associated stabilising proteins	5
Figure 1.4: Schematic representation of the telomerase enzyme	6
Figure 1.5: The relationship between telomere shortening and cancer generation	10
Figure 1.6: Flow diagram of cellular crisis.....	11
Figure 1.7: Schematic representation of the LRP/LR transmembrane receptor, binding various biomolecules.....	19
Figure 1.8: Principles of a AuNP-based telomerase activity assay	26
Figure 3.1: Predicted results when using the improved AuNP-based telomerase activity assay	40
Figure 4.1: Optimisation of AuNP synthesis parameters.....	48
Figure 4.2: Spectrophotometric analysis of AuNP synthesis reactions	50
Figure 4.3: $A_{610/520}$ ratio confirms the consistency of the AuNP synthesis reactions.....	51
Figure 4.4: AuNP size distribution determined by TEM and ImageJ analysis.....	52
Figure 4.5: Schematic representation of the first iteration of the AuNP-based telomerase activity assay.....	54
Figure 4.6: Transmission electron microscopy analysis of 5' extension strand functionalised AuNPs.....	55
Figure 4.7: Schematic diagram of the Improved AuNP telomerase activity assay.....	56
Figure 4.8: Annealing of telomerase extension strand and thiolated linker DNA.....	57
Figure 4.9: Spectrophotometric comparison between thiol-DNA functionalised and non-functionalised AuNPs	58
Figure 4.10: Comparison of DNA-functionalised and non-functionalised AuNP, using the $A_{610/520}$ ratio.....	59
Figure 4.11: Transmission electron micrograph of DNA functionalized AuNPs	60
Figure 4.12: Successful detection of telomerase activity using the improved AuNP based telomerase activity assay.....	61

Figure 4.13: Relative telomerase activity of HEK-293 and WHCO-5 cells after MST-312 telomerase inhibitor and metformin treatment (TRAPEze® RT Telomerase Detection Kit)	62
Figure 4.14: Relative telomerase activity of HEK-293 and WHCO-5 cells after MST-312 telomerase inhibitor and metformin treatment (AuNP-based telomerase activity assay).....	64
Figure 4.15: Light microscope and TEM images of PLGA nano-capsules	67
Figure 4.16: Initial PLGA nano-capsule synthesis	68
Figure 4.17: The effect of initial PLGA (in solvent) concentration on nano-capsule polydispersity	70
Figure 4.18: PLGA nano-capsules purification by centrifugation at 8000 xg.....	71
Figure 4.19: PLGA nano-capsules purification by centrifugation at 10 000 xg.....	72
Figure 4.20: PLGA nano-capsules purification by centrifugation at 12 000 xg.....	73
Figure 4.21: PLGA nano-capsules purification by centrifugation at 14 000 xg.....	74
Figure 4.22: PLGA nano-capsules purification by 0.45 µl filtration and centrifugation at 500 xg	75
Figure 4.23: Evaluation of the size distribution of PLGA nano-capsules	77
Figure 4.24: HEK-293 cell viability after PLGA nano-capsule treatment	78
Figure 4.25: Scanning electron micrograph of protein encapsulated PLGA nanoparticles.....	79
Figure 4.26: BCA assay results of encapsulated-BSA PLGA nanoparticles	80
Figure 4.27: Micro-BCA assay results of encapsulated-GFP PLGA nano-capsules	82
Figure 4.28: Micro-BCA assay results of empty and encapsulated-LRP PLGA nanoparticles.....	84
Figure 4.29: Western blot analysis of encapsulated-LRP PLGA nanoparticle treatments on HEK-293 cells	86
Figure 4.30: Improved cell viability after LRP-nanoparticle treatment in vitro	87
Figure 4.31: LRP-nanoparticle treatment elevates telomerase activity in vitro	88
Figure 7.1: Metformin reduces telomerase activity in WHCO-1 cells	127
Figure 7.2: LRP protein sequence homology	129
Figure 7.3: Initial expression of LRP at 37 °C using varying IPTG concentrations	130
Figure 7.4: Initial IMAC purification of LRP.....	131
Figure 7.5: Coomassie blue stained SDS-PAGE gel of the purified LRP	132
Figure 7.6: Expression of LRP at 20 °C using varying IPTG concentrations.....	133

Figure 7.7: Purification of LRP using IMAC	133
Figure 7.8: Improved IMAC purification of LRP	134
Figure 7.9: Coomassie blue stained SDS-PAGE gel of the purified LRP	135
Figure 7.10: Confirmation of purified LRP via standard curve extrapolation.....	136

List of Tables

Table 3.1: Telomerase activity primers.....	35
Table 3.2: Oligo sequences for the improved AuNP-based telomerase activity assay.	38
Table 4.1: DLS results of PLGA nano-capsules	76

List of Abbreviations

Abbreviation	Meaning
μl	microliter
μM	micromolar
μm	micrometre
ALT	alternative lengthening of telomeres
AMP	adenosine monophosphate
AMPK	AMP-activated protein kinase
AMPK	adenosine monophosphate activated protein kinase
AuNP	gold nanoparticle
Aβ	amyloid-beta
BCA	bicinchoninic acid
BSA	bovine serum albumen
CHAPS	3-[(3-Cholamidopropyl)dimethylammonio]-1-propanesulfonate
CVD	cardiovascular disease
DCM	dichloromethane
d-loop	displacement loop
DLS	dynamic light scattering
DMEM	Dulbecco's modified eagle's medium
DMSO	dimethyl sulfoxide
DNA	deoxyribonucleic acid
dNTP	deoxyribonucleotide
dsDNA	double stranded DNA
EA	ethyl acetate
EDTA	ethylene diaminetetraacetic acid
EGCG	epigallocatechin gallate
EGTA	ethylene glycol-bis(β-aminoethyl ether)
ELISA	enzyme-linked immunosorbent assay
FBS	foetal bovine serum
GFP	green fluorescent protein
hTERC	human telomerase RNA component
hTERT	human telomerase reverse transcriptase component
IC50	50% inhibitory concentration
IMAC	immobilized metal chelate affinity chromatography
IPTG	Isopropyl β-D-1-thiogalactopyranoside
kbp	kilo base pairs
LDL	low-density lipoprotein
LKB1	liver kinase B1
LRP/LR	37 kDa laminin receptor precursor/67 kDa high affinity laminin receptor
M	molar
mg	milligram
min	minutes

ml	millilitre
mm	millimetre
mM	millimolar
mRNA	messenger ribonucleic acid
MTT	3-(4,5-dimethylthiazol-2-yl)-2,5-diphenyltetrazolium bromide
ng	nanogram
nm	nanometer
nM	nano molar
oxLDL	oxidised low-density lipoprotein
PAGE	polyacrylamide gel electrophoresis
PBS	phosphate buffered saline
PCR	polymerase chain reaction
PDI	polydispersity index
PEG	polyethylene glycol
PLGA	poly(lactic-co-glycolic acid)
POT1	protection of telomeres 1
pRb	phosphorylated Retinoblastoma protein
PrPc	scrapie prion protein
PrP ^{Sc}	scrapie prion protein
PVA	polyvinyl alcohol
qPCR	quantitative polymerase chain reaction
RAP1	human repressor activator protein
RIPA buffer	radioimmunoprecipitation assay buffer
RNA	ribonucleic acid
RNase	ribonuclease
ROS	reactive oxygen species
SDS	sodium dodecyl sulphate
SEM	scanning electron microscopy
SNPs	single nucleotide polymorphisms
ss-DNA	single stranded DNA
STELA	Single telomere length analysis
TBE	tris/borate/EDTA
TE	tris/EDTA
TEM	transmission electron microscopy
TIN2	TRF1-interacting nuclear protein 2
t-loop	telomere loop
TPP1	adrenocortical dysplasia protein
TRAP	telomeric repeat amplification protocol
TRF	telomeric repeat-binding factor 2
TRF1	telomeric repeat-binding factor 1
V	volts
VNTR	variable number of tandem repeats
Xg	times gravity

1. Introduction and Literature Review

1.1. Telomeres

1.1.1. Function

Telomeres are non-coding repetitive double stranded TTAGGG DNA repeats at the ends of chromosomes and are between 10-15 kbp in length in humans (Fleming & Burrows, 2013). These telomeres help stabilise and protect the ends of chromosomes. They carry out this protective function by preventing the erosion of important coding DNA by the “end-replication” problem (Levy et al., 1992). This loss of coding DNA occurs because of the incomplete synthesis of double stranded DNA, which is a characteristic of the mode of action of RNA dependant DNA polymerase (Figure 1.1). The polymerase utilises an RNA primer in order to synthesise a new DNA strand. Due to the degradation of this RNA primer, a single stranded overhang remains after lagging strand synthesis (Levy et al., 1992). This overhang is then removed, which results in the loss of small fragments of DNA after each synthesis reaction (reviewed in Denchi, 2009) and this, therefore, leads to the systematic erosion of the ends of chromosomes after cell division (Blackburn, 1991).

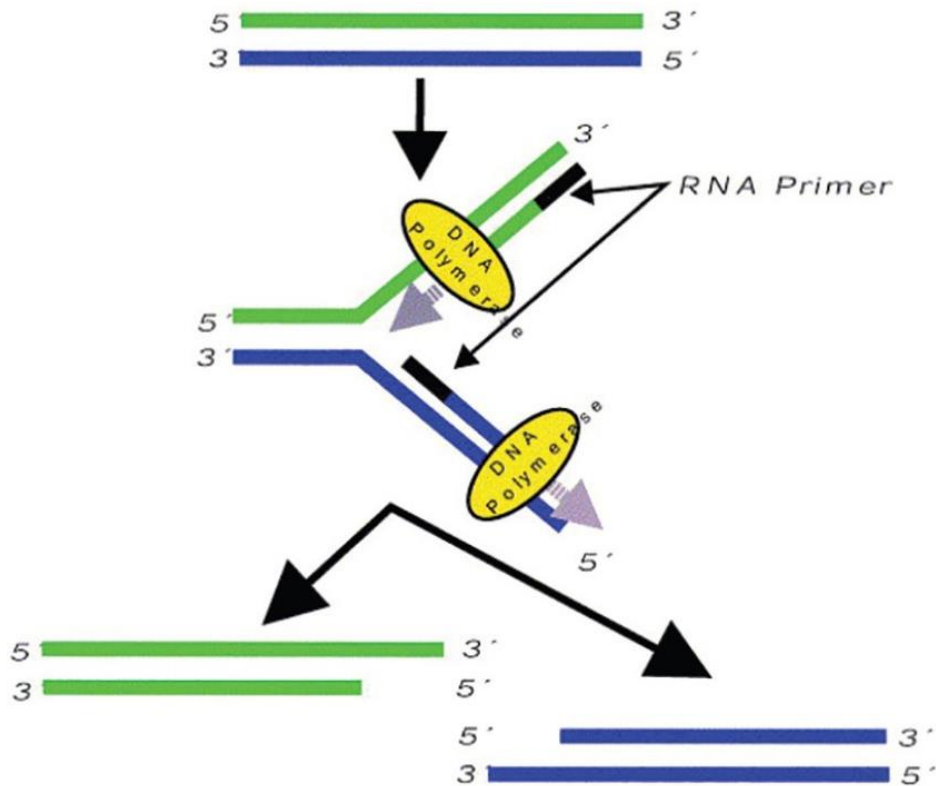


Figure 1.1: Schematic representation of the "end-replication" problem

The DNA synthesis reaction, performed by DNA polymerase, involves both the leading strand (green) and the lagging strand (blue) of the replication fork are shown with an attached RNA primer. As this RNA primer is degraded, the newly synthesised double stranded DNA is missing complimentary bases on the 5' end, leading to 3' overhangs in the template strand. This overhang is eventually degraded resulting in the shortening of the DNA strand (Klapper et al., 2001; Levy et al., 1992).

Telomeres act as a "buffer" zone to this erosion, however, if they are not continually maintained after each cell division, it can lead to the degradation of coding DNA, leading to a breakdown of normal functions if the cell does not enter a senescent state (where cells are metabolically active, but no longer replicate) (Shay & Wright, 2005). Telomerase, a multi-subunit enzyme, maintains and elongates the telomeres. However, it has been shown to be nearly undetectable in most somatic cell lines (Kim et al., 1994). This is significant, as it means that many mammalian cells are therefore susceptible to genetic ageing and undergoing senescence (Shay & Wright, 2005). In

contrast, germ-line cells in addition to other highly proliferating cell types, such as intestinal and oesophageal cells, have been shown to have high telomerase activity. This is most likely due to these cell types requiring to undergo constant cell division (Kim et al., 1994; Wright et al., 1996). If the telomeres are not maintained, become short and a functional DNA repair mechanism, it could lead to replicative senescence or even the induction of apoptosis (programmed cell death) (Shay & Wright, 2005). Normally, somatic cells are only capable of undergoing a limited number of cell divisions because of the shortening of telomeres. This is known as the “Hayflick limit” (Hayflick & Moorhead, 1961). When approaching this limit, it can lead to the disruption of normal tissue function, which has been theorised to contribute to the ageing process (Carneiro et al., 2016; Sahin & Depinho, 2010). This is further supported by the fact that older individuals have shorter telomeres leading to the telomere theory of ageing.

1.1.2. Structure

The telomeric repeats, in conjunction with telomere stabilising proteins such as the shelterin complex (Figure 1.2), help stabilise the ends of chromosomes by maintaining telomere length and capping the ends of telomeres (Bailey & Murnane, 2006). The shelterin complex consists of multiple telomere-associated proteins namely, telomeric repeat-binding factor 1 and 2 (TRF1 and 2) and protection of telomeres 1 (POT1), which bind directly to the telomeric DNA, thereafter, allowing TRF1-interacting nuclear protein 2 (TIN2) to bind to TRF1 and TRF2 (Bailey & Murnane, 2006). Human repressor activator protein (RAP1) binds to TRF2, and adrenocortical dysplasia protein (TPP1) helps POT1 associate with the telomere. These proteins are also involved in the regulation of telomere length (Bailey & Murnane, 2006). The telomeres form secondary structures called the telomere loop (t-loop) and displacement loop (d-loop) (Figure 1.3). The t- and d-loops are formed when the telomere folds back on itself and integrates the 3' overhang back into the telomere (Bailey & Murnane, 2006; Greider, 1999). The shelterin complex in conjunction with the t- and d-loops prevent the degradation of the telomeres and chromosome

end-fusions (Bailey & Murnane, 2006; Greider, 1999; Ohno et al., 2016). Chromosome end-fusions are the result of destabilised/unprotected telomeres, where two chromosomes are fused at their telomeric ends, possibly resulting in the disruption of mitosis and even cancer formation (Ohno et al., 2016).

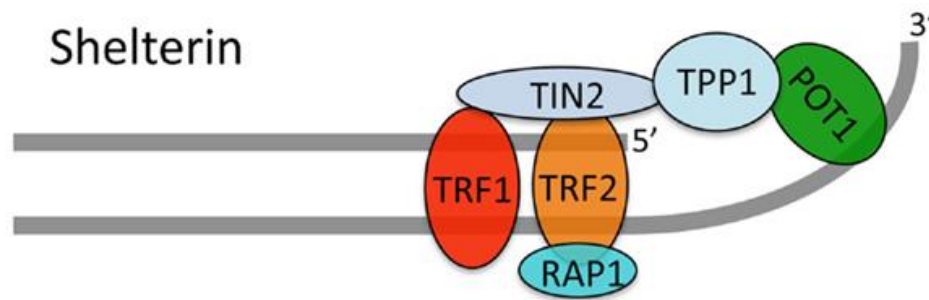


Figure 1.2: Focused view of the shelterin complex

The major components of the “shelterin” complex are: TRF1/2, TIN2, RAP1, TPP1, and POT1. Here TRF1/2 allow for the binding of the complex to the double stranded DNA and POT1 to single stranded DNA whereas the other components help stabilise the complex (Bailey & Murnane, 2006; Raffa et al., 2013).

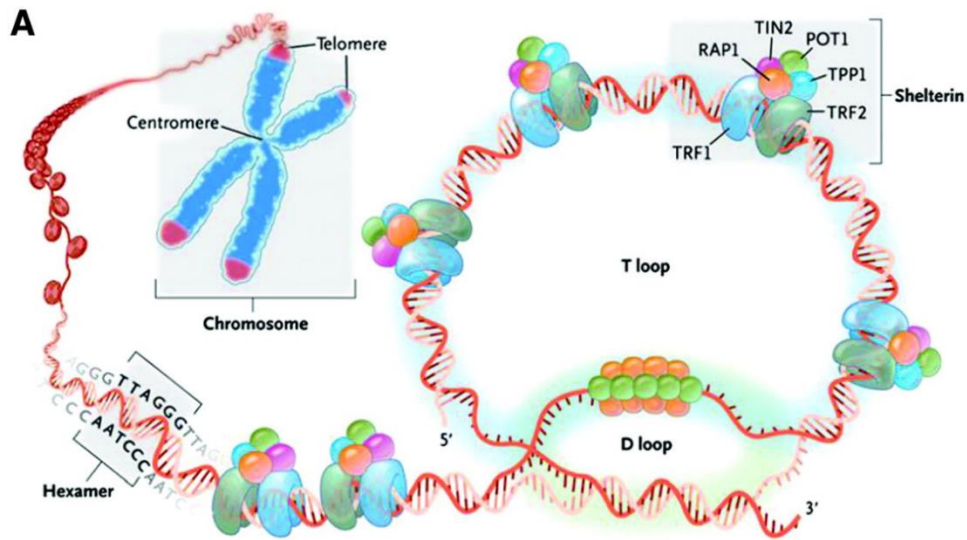


Figure 1.3: Telomere secondary structures and associated stabilising proteins

This image shows the formation of the shelterin complex and depicts its stabilisation role in conjunction with the telomere loop (t-loop) and displacement loop (d-loop). The t-loop forms as the 3' overhang folds in on itself (red DNA strand). The shelterin complex is shown with its major components; TRF1 (blue) and TRF2 (dark green) as stabilising the t-loop. The d-loop is formed as a result and is stabilised by RAP1 and POT1 (Bailey & Murnane, 2006; Greider, 1999; Kovacic et al., 2011).

1.1.3. Telomerase

The telomerase enzyme is a ribonucleoprotein consisting of multiple subunits, two of which are essential. These subunits perform the main function of the enzyme, by maintaining telomere length. The human telomerase RNA component (hTERC) functions as an RNA template for the human telomerase reverse transcriptase component (hTERT), which adds the telomeric repeats to the ends of telomeres (Figure 1.4) (Carlin et al., 1997). It has been found that overexpression of hTERT in non-immortalised cell lines leads to cell immortalisation, whereas the overexpression of hTERC did not, this makes hTERT the limiting factor for enzyme activity (Sheng et al., 2013; Wick et al., 1999). In fact, it has even been shown that the increase of hTERT expression at any

stage of the cell cycle results in the immortalisation of the cell line (Wick et al., 1999). This is further supported with the fact that hTERT mRNA levels are directly proportional to telomerase activity. This correlates to the high number of cancers (90%) that have elevated telomerase activity, as they also exhibit increased hTERT mRNA levels (Kirkpatrick et al., 2003).

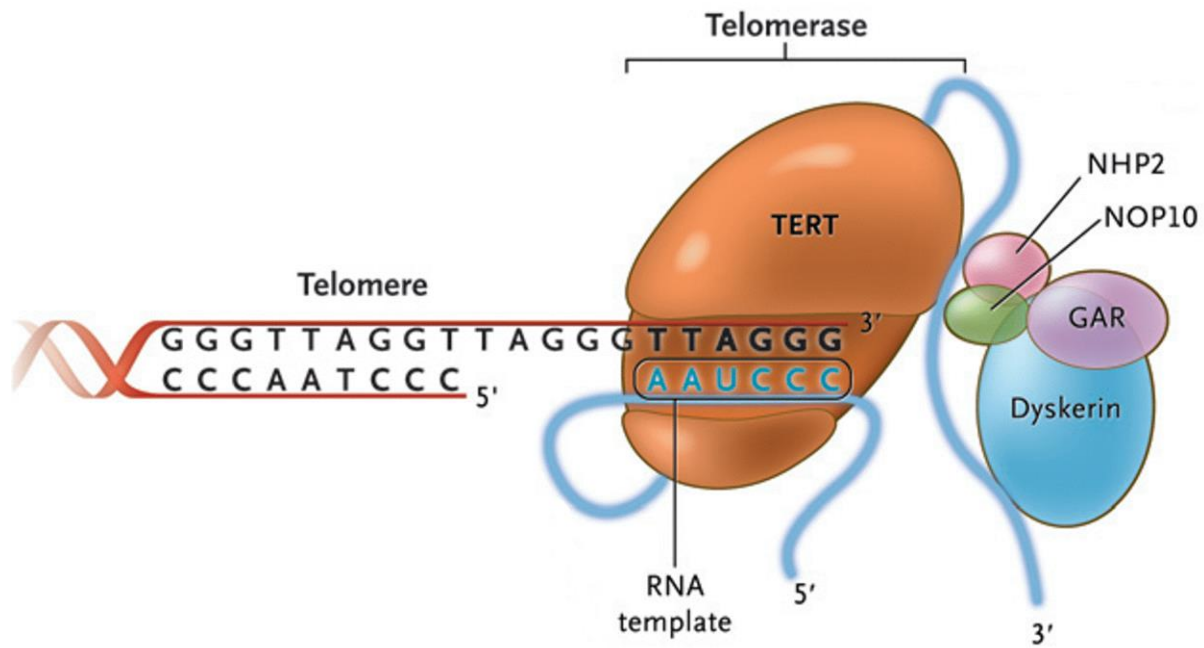


Figure 1.4: Schematic representation of the telomerase enzyme

The telomerase complex is made up of two major components: the telomerase reverse transcriptase component (TERT) and the telomerase RNA component/ template (TERC). The enzyme is stabilised by the presence of the proteins: dyskerin, GAR, NOP10 and NHP2. Telomerase maintains the telomeres by using TERC (blue) as a template for TERT (orange) to add additional telomeric repeats (TTAGGG) to the ends of chromosomes in a 3' to 5' direction, leaving a 3' overhang (Calado & Young, 2009).

Since hTERT is the limiting factor of telomerase, this suggests that influences on hTERT mRNA expression could greatly affect telomerase activity. There are multiple factors such as the variation of the hTERT minisatellite (MNS16A) in addition to mutations of the hTERT promoter sequence, which have both been associated with hTERT expression (Wang et al., 2003). Additionally, specific single nucleotide polymorphisms (SNPs) that can be found in the hTERT promoter affect hTERT expression. In fact, an increased risk to lymphoblastic leukaemia and increased hTERT mRNA expression has been linked to the SNP rs2735940 in the hTERT promoter region (Sheng et al., 2013).

Similarly, a genetic change in the hTERT minisatellite (MNS16A), which is a polymorphic tandem repeat downstream of the hTERT gene, has been linked to hTERT expression. It is thought that the antisense MNS16A gene is involved in the silencing of hTERT mRNA. This means that the shorter variant of the minisatellite has an increased ability to silence hTERT mRNA. The larger variants, on the other hand, would lead to decreased silencing due to a decrease in antisense transcription, and therefore cause an increase in hTERT expression (Wang et al., 2003). Further supporting this; the short allele of the variable number of tandem repeats (VNTR) of the MNS16A minisatellite (VNTR-274) has been found to downregulate hTERT mRNA expression (Hofer et al., 2013). This may lead to apoptosis or even senescence. VNTR-274 has even had a suggested protective role against prostate cancer (Hofer et al., 2013). In previous research, it was also found that cell lines containing the larger minisatellite variant had correspondingly high telomerase activity (Bernert et al., (unpublished); (Wang et al., 2003).

Comparably, the proto-oncogene, c-myc, has been shown to increase hTERT expression. C-myc directly targets the hTERT gene, leading to increased telomerase activity due to increased hTERT expression (Greenberg et al., 1999; Tang et al., 2016). Even the p53 transcription factor has been known to target the hTERT gene, where it is thought to directly bind the hTERT gene through the SP1 binding site. This is said to regulate hTERT expression in normal, healthy cells by decreasing hTERT transcription (Kanaya et al., 2000). This, however, means that if there should be a loss of function mutation in p53, that it could lead to an increase in cell proliferation.

1.1.4. Extratelomeric functions of hTERT

hTERT has been found to play a role not only in telomere maintenance and cell proliferation but has been implicated in a variety of extra-telomeric functions. During times of oxidative stress, hTERT is known to relocate to the mitochondria from the nucleus via a mitochondrial leader sequence present in the enzyme in order to improve mitochondrial function. This targeting sequence facilitates the shuttling of the enzyme into the mitochondria (Haendeler et al., 2009). The mitochondrial hTERT has been shown to improve mitochondrial function in times of oxidative stress, suggesting a potential protective role (Saretzki, 2009). Without this form of protection, it could lead to mitochondrial dysfunction, which can further cause the release of reactive oxygen species (ROS). Since ROS damage the genetic material of the cell (via oxidative damage), increased hTERT may protect mitochondrial DNA from damage by binding to it and preventing contact with ROS (Haendeler et al., 2009). Additionally, hTERT has been implicated in DNA damage response, as it helps recruit DNA repair proteins (Saretzki, 2014).

1.2. Telomeres in diseases

1.2.1. Telomeres and cancer

Cancer is one of the world's leading causes of death and is characterised by abnormal cell proliferation (Jemal et al., 2011). Over 10 million deaths, from over 19.3 million cases, were reported in 2020 (GLOBOCAN 2020). Telomeres are vital for continued cell proliferation, and therefore have an important role in cancer genetics. Since continued cell division leads to telomere shortening, DNA repair pathways such as the p53/p21 pathway can be triggered, causing cell cycle arrest (senescence) and even apoptosis (Figure 1.5) (Shay & Wright, 2005). This occurs when the telomeres become critically short, or DNA breaks are detected by gamma H2AX. It then aids in the formation of DNA repair foci which in turn promotes the p53/p21 DNA damage response. Here the damage is either repaired or the cells are forced to undergo senescence or

apoptosis (Fragkos et al., 2009). Consequently, senescence acts as a tumour suppressor mechanism, which needs to be circumvented by cells in order for them to become malignant (Shay & Wright, 2005). In fact, our previous research has shown that p53 plays a significant role in decreasing telomerase activity. After metformin treatment of oesophageal cancer cells, it was thought that the AMPK pathway was activated, which in turn activated p53, and suppressed hTERT promoter activity by repressing hTERT expression through the binding of the hTERT promoter SP1 binding sites (Bernert et al., (unpublished); Kanaya et al., 2000). The binding activity of p53 is activated through the ATM-dependent phosphorylation of serine 15 due to telomere loss. It is important to note, however, that this is not necessarily the only reason for this activation, age-related oxidative damage can also cause this phosphorylation (Kim et al., 2014). This suggests that mutations in the p53 tumour suppressor could directly increase telomerase activity and drive cancer cell immortality. Taking this into consideration, DNA damage response pathways and telomere dynamics can play a vital role in the progression of diseases such as cancer, due to its characteristic uncontrolled cell proliferation (Figure 1.6). This means that if cells lack sufficient DNA damage responses, such as in the case of mutated p53 or phosphorylated retinoblastoma protein (pRb), the cells could bypass senescence and become genetically unstable. This second checkpoint is known as “cellular crisis” (Figure 1.6 and Figure 1.5). “Cellular crisis” is characterised by critically short telomeres and chromosome instability, which can lead to telomere fusions (Capper et al., 2007). In order for cancer cells to continue proliferating at this stage, telomeres must either be maintained by the upregulation of telomerase (and therefore increased telomerase activity), or through alternative lengthening of telomeres (ALT) (Cesare & Reddel, 2010). ALT is recombination based and is utilised by approximately 10% of cancers, whereas telomerase upregulation can be found in up to 90% of cancers. ALT is utilised by cancers to avoid being recognised as DNA damage/ breaks, which could lead to chromosome end-fusions and further genomic instability. It uses homologous recombination (where chromosomes exchange telomeric material between one another) to maintain telomeres. This rare form of telomere maintenance is able to evade senescence and lead to cell immortalisation (Cesare & Reddel, 2010). This makes targeting telomeres and telomerase activity an interesting prospect for anticancer treatment.

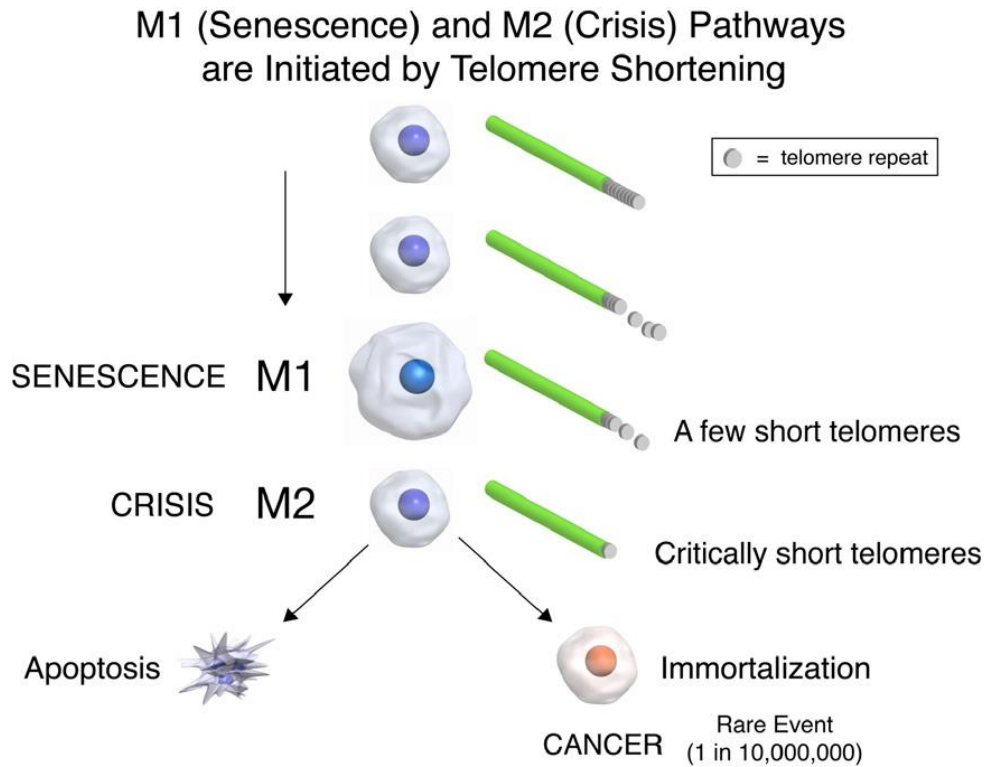


Figure 1.5: The relationship between telomere shortening and cancer generation

As the telomeres shorten after successive cell divisions, cells can either enter a senescent state or, by bypassing this, enter cellular crisis. At this point, if DNA damage response mechanisms are still active, the cell will undergo apoptosis. However, cell immortalisation may occur if these mechanisms are suppressed, potentially leading to cancer.

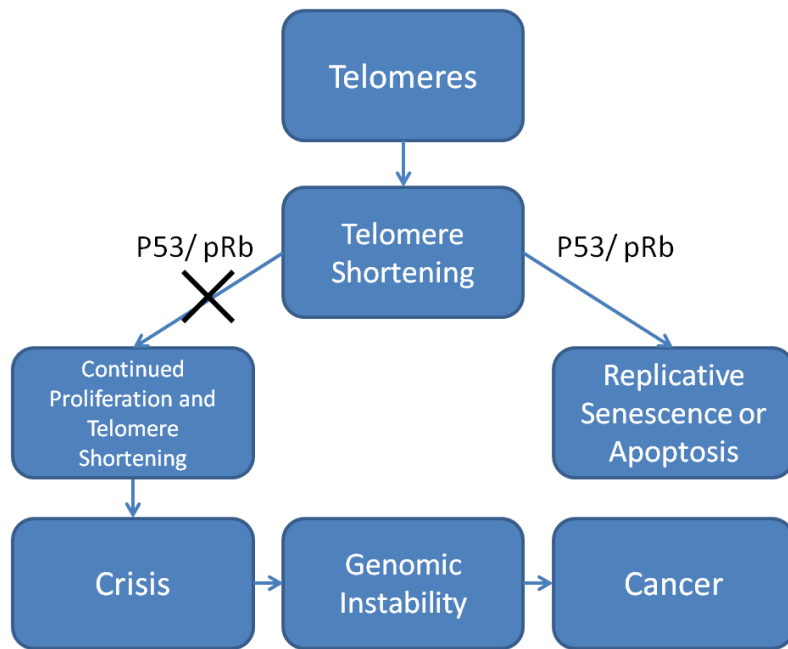


Figure 1.6: Flow diagram of cellular crisis

This diagram shows the relationship of telomere shortening in the presence and absence of functional DNA repair mechanisms (phosphorylated retinoblastoma protein (pRb) and p53). In the presence of functional mechanisms, the cell will undergo apoptosis or replicative senescence, whereas without these mechanisms, telomere shortening can progress to cellular crisis. This can subsequently lead to genomic instability and even cancer.

1.2.1.1. Oesophageal cancer

A cancer that has previously been shown to have high levels of telomerase is oesophageal cancer. Oesophageal cancer caused over 540,000 deaths, making it the 6th most deadly cancer in 2020 (GLOBOCAN 2020). Southern Africa has been shown to have a high rate of oesophageal cancer, with South Africa having one of the highest in the world (Arnold et al., 2015). In South Africa, oesophageal cancer is the 13th and 11th most diagnosed cancer for woman and men respectively, however, is the 5th and 4th most deadly cancer respectively (GLOBOCAN 2020). This is thought to mainly be caused by the high amount of tobacco and alcohol use in the country, as well as poor diet (Alaouna et al., 2019). The two most prevalent types of oesophageal cancer are oesophageal

adenocarcinoma and oesophageal squamous carcinoma. Oesophageal adenocarcinoma is commonly found in developed countries where it makes up to 30-50% of the oesophageal cancer diagnoses in these regions (Alaouna et al., 2019). This cancer mainly affects the lower third of the oesophagus. Oesophageal squamous carcinoma is found in the upper oesophagus and is more commonly found in developing countries where it makes up over 95% of all oesophageal cancer diagnoses (Alaouna et al., 2019). The largest risk factors for these cancers are environmental which include consuming alcohol, smoking cigarettes and inhaling or ingesting carcinogenic pollutants (Alaouna et al., 2019; Arnal et al., 2015; Brown et al., 2001). Most of these seem to be due to single nucleotide polymorphisms (SNPs) which cause these detrimental genetic issues (Alaouna et al., 2019).

Late-stage oesophageal cancer is also prone to metastasis and treatment can therefore be very difficult if it is not detected at an early stage. Metastasis is the process in which cancer cells migrate and invade distant tissue sites, most commonly through blood vessels or the lymphatic system. The cells can accomplish this by overexpressing certain cell signalling and adhesion proteins, such as cadherins, integrins, CD44 and the 37-kDa/67-kDa laminin receptor precursor/laminin receptor (LRP/LR) (Berno et al., 2005; Geiger & Peeper, 2009). These proteins allow the cells to adhere to different tissues through cell-cell interactions. In the case of LRP/LR the modification of laminin-1 and subsequent proteolytic enzyme activity results in the invasion of new tissue types through the breakdown of the extra cellular matrix (Berno et al., 2005). This marks late-stage cancer (stage 4) and unfortunately, like most cancers, there are no-currently available, dedicated treatment options and therefore conventional treatments must be used. These include chemotherapy, surgery, and radiation therapy. These treatment options, however, come with their own risks and severe side effects. These side effects can include vomiting, diarrhoea, nausea, and immune system suppression. Although chemotherapy disproportionately affects cancer cell mechanisms, such as high proliferation rate and metastasis-enhancing proteins, it's non-specific nature results in a dose limiting toxicity which limits its overall effectiveness (Malhotra & Perry, 2003). Furthermore, due to its limited oral bioavailability, it is mostly administered intravenously. This is a very non-specific treatment route and can therefore reach and affect more healthy cells. For example, antimetabolites are S-phase specific drugs

which interfere in the synthesis of DNA and RNA, whereas DNA intercalating agents such as bleomycin result in DNA strand disruption via oxidative damage. Alkylating agents on the other hand, such as platinum complexes, reduce cell proliferation by creating DNA crosslinks, which prevent the synthesis of RNA and subsequently proteins (Malhotra & Perry, 2003). Chemotherapeutic agents such as these all affect healthy cells and are often used in combination to improve therapy efficacy; however, this can therefore also broadly affect healthy cells in the same way (Corrie, 2007; Lawenda et al., 2008; Malhotra & Perry, 2003). The difficulty in treating cancer, as well as the inadequate current treatment options, makes finding alternative therapies very important, one possible target, due to its interaction with LRP/LR and its involvement in cancer and a variety of age-related disorders could be the enzyme telomerase.

1.2.2. The role of telomeres in age related disorders

Cardiovascular Disease (CVD) is a very common age-related disease that resulted in the deaths of approximately 18.6 million in 2019 (Roth et al., 2020). This makes CVD one of the world's leading causes of death. CVD is a major concern in the developed world as well as the developing world, where health care facilities may not be able to address the issue due in part to the cost involved (Bentzon et al., 2014). CVD refers to a group of progressive diseases that are characterised by high blood pressure, atherosclerosis and myocardial infarctions (Roth et al., 2020). These symptoms are primarily caused by the occlusion (either total or partial) of major and minor blood vessels. This can be brought on by both genetic and lifestyle factors such as suffering from diabetes, obesity as well as eating and exercising habits (Roth et al., 2020). Due to these conditions, the body can experience an increase in ROS, which is one of the principle driving factors of atherosclerosis. Atherosclerosis is the formation of plaques within blood vessels. These plaques can lead to the partial or total blockage of the vessels. Further, the plaques may break apart, creating clots that could migrate to other parts of the body, most notable the brain and heart (Bentzon et al., 2014). These plaques are the result of an increase in ROS which in turn oxidises low density lipoproteins (LDL) causing the formation of oxidised low-density lipoprotein

(oxLDL). This causes an increase in the inflammatory process which recruits monocytes (Mallat & Tedgui, 2000). These then differentiate into macrophages which upregulate LOX-1 in an attempt to remove the oxLDL (Li et al., 2004; Pirillo et al., 2013). This leads to the shortening of telomeres and the subsequent activation of apoptosis, which creates foam cells. These foam cells then accumulate and are covered by fibrous tissue from the blood vessel, forming plaques. The plaques subsequently lead to blood vessel occlusion and high blood pressure due to the heart pumping harder to compensate for the blood vessel occlusion (Mallat & Tedgui, 2000). Additionally, it has been shown that telomere shortening leads to the weakening and degradation of vascular beds by causing endothelial dysfunction, leading to increased cellular turnover and vascular wall stress (Serrano & Andrés, 2004).

1.2.3. The role of telomeres in neurodegenerative disorders

Telomeres have also recently been implicated in Alzheimer's disease pathology (Bignoux et al., 2019; Franco et al., 2006; Wang et al., 2015). It has been found that Alzheimer's disease patients have shorter neuronal telomeres than their health counterparts (Franco et al., 2006). Additionally, further interaction with key Alzheimer's disease related proteins such as Amyloid-Beta ($A\beta$)₄₂, shows that telomerase is part of the disease pathology. This is clear, as $A\beta$ ₄₂ has been shown to inhibit the functioning of telomerase through the blocking of TERC, the RNA template component (Wang et al., 2015). This would lead to shortening of telomeres and increase tissue deterioration. Furthermore, LRP::FLAG overexpression in HEK-293 and SH-SY5Y cells has also been shown to decrease $A\beta$ shedding and concomitantly intracellular $A\beta$ levels, which may be due to LRP::FLAG promoting TERT expression, as LRP::FLAG overexpression also resulted in an increase in telomerase, which in turn serves a protective role against Alzheimer's disease pathology by protecting neuronal cells against $A\beta$ induced apoptosis (Bignoux et al., 2019).

1.3. Telomerase modulators

There are multiple compounds and proteins that are able to modulate telomerase activity, including inhibitors such as metformin and MST-312 and enhancers such as TA-65. These are an interesting target for research, as they may help treat a variety of age-related diseases by either increasing or decreasing telomerase activity.

1.3.1. Metformin inhibits telomerase activity

Metformin is an interesting case-study in potential repurposing of existing drugs to combat diseases outside of its original scope. Metformin (1,1-dimethylbiguanide hydrochloride) is an antidiabetic drug for type-2 diabetes sufferers. Although the exact mode of action is not entirely known, the drug is known to activate the AMP-activated protein kinase (AMPK) pathway in conjunction with the protein kinase: liver kinase B1 (LKB1). This leads to an increase in glucose uptake in muscle cells through the phosphorylation of target of rapamycin complex 2 (TORC2) and the subsequent blocking of gluconeogenesis (Vallianou et al., 2013). This helps mitigate insulin resistance in type-2 diabetes sufferers (Zakikhani et al., 2006). Studies have shown that diabetic patients using metformin seem to have lower incidences of hepatocellular, prostate, ovarian, breast, pancreatic and lung cancer (Evans et al., 2005; Vallianou et al., 2013). Additionally, it is known that LKB1 has a tumour suppressor function, as the activation of AMPK by metformin causes a signal cascade, which leads to the suppression of the electron transport chain. Cells therefore compensate by activating p53 in order to arrest cell proliferation to await the restoration of normal glucose levels (Buzzai et al., 2007). This has multiple possible implications, for one it causes p53 negative tumour cells to be unable to resist glucose deprivation, severely affecting cell viability (Buzzai et al., 2007) and therefore for p53 positive tumour cells, it may aid in the activation of the p53 DNA damage pathway. This could indicate

that the drug may be able to decrease cell proliferation and therefore potentially reduce the risk of cancer. Indeed, studies have shown that individuals using metformin displayed reduced cancer risk (Evans et al., 2005; Tseng, 2019; Vallianou et al., 2013).

Additionally, it has been shown that cell proliferation in oesophageal squamous carcinoma cell lines is significantly reduced in the presence of metformin (Damelin et al., 2014). Furthermore, it was demonstrated that if mice were treated with metformin in conjunction with conventional chemotherapy, they experienced longer remission times compared to the untreated mice (Hirsch et al., 2009). Metformin treatment also resulted in a decreased recurrence for gastric cancer patients after surgery (Lee et al., 2015). Previous research has shown that metformin not only seems to have an anti-proliferative effect on cancer cells, but it seems to affect telomere dynamics, including telomerase activity, which is involved in cancer progression (Bernert et al., (unpublished)). Moreover, hTERT mRNA levels have been shown to be reduced by metformin in endometrial cancer, however, the mechanism is not yet understood (Hanna et al., 2012).

Our previous research showed a significant reduction in telomerase activity after metformin treatment in an oesophageal cancer cell line expressing wild type p53 (Bernert et al., (unpublished) supplementary Figure 7.1). Telomerase activity was assessed using the TRAPeze RT telomerase activity assay (as described by Bignoux et al., 2023 and in section 3.1.8.1). One possible explanation put forward by Kanaya et al. is that p53 represses hTERT expression by acting as a transcription factor and binding the SP1 binding sites found in the hTERT promoter. This was shown by overexpressing p53 in SiHa (cervical carcinoma) cells via adenoviral infection, resulting in a decrease in hTERT expression and a subsequent decrease in telomerase activity (Kanaya et al., 2000). Since the telomerase component, hTERT, is known to be transported to the mitochondria via its mitochondrial leader sequence, and that metformin acts within the mitochondria (Buzzai et al., 2007), there may be a direct interaction between the drug, hTERT and p53 which affects cancer progression.

1.3.1. The MST-312 telomerase inhibitor

Epigallocatechin gallate (EGCG), a tea derived catechin/antioxidant, was found to inhibit telomerase directly (Seimiya et al., 2002). However, the fact that this compound is a natural product and is therefore difficult to synthesise and produce in large quantities, lead to the creation of simpler synthetic derivatives including MST-312 ([N,N'-bis(2,3-dihydroxy-benzoyl)-1,2-phenylenediamine]) (Seimiya et al., 2002). MST-312 was especially effective at inhibiting telomerase activity, with a determined IC₅₀ (50% inhibitory concentration) of only 0.67 µM and an effective dose of 1-2 µM, however, the mechanism by which it accomplishes this is so far unknown (Seimiya et al., 2002). MST-312 proved to be easily synthesised in large quantities and may be an interesting candidate as a novel chemotherapeutic agent.

1.3.2. The TA-65 telomerase enhancer

TA-65 is a compound isolated from the root of *Astragalus membranaceus*, a plant used in traditional Chinese medicine (de Jesus et al., 2011; Harley et al., 2011). This compound has been studied in humans as a dietary supplement and has been found to significantly decrease the percentage of cells with short telomeres (<4 kbp) without negative side effects (Harley et al., 2011). This was confirmed in mice, where significant telomere lengthening was seen without a concomitant incidence of cancer (de Jesus et al., 2011), as well as in cell culture, where TA-65 increased telomerase activity in foetal fibroblasts and neonatal keratinocytes two- to threefold at a 30 nM concentration (Harley et al., 2011).

Telomerase activity plays an integral part in various diseases, which make telomerase modulators an interesting prospect for the treatment of these diseases in conjunction with traditional

treatment options. One such telomerase modulator, which has been shown to enhance telomeres activity is LRP/LR.

1.4. 37 kDa laminin receptor precursor/67 kDa high affinity laminin receptor

1.4.1. Structure and function

The 37 kDa Laminin Receptor Precursor/67 kDa High Affinity Laminin Receptor (LRP/LR) has recently been shown to influence telomerase activity (Naidoo et al., 2015; Otgaar et al., 2017). LRP/LR is a highly conserved non-integrin transmembrane receptor, which is able to bind a variety of molecules such as prion proteins, elastin and laminin (Gauczynski et al., 2001, 2006; Mercurio, 1995) and is implicated in a variety of disorders (Figure 1.7). Although it performs its major functions on the cell surface, such as cell migration and invasion of foreign tissues, LRP/LR has been found in the cytosolic domain as well as the perinuclear compartment, suggesting that it may play a role in many additional processes, such as cell proliferation and growth (Gauczynski et al., 2001; Naidoo et al., 2015). Similar to TERT, LRP/LR has been shown to influence cell survivability and proliferation, particularly in cancer cells. This can be seen by the fact that LRP/LR is not only involved in tissue differentiation, but in adhesion and invasion of cancer cells through the binding of laminin-1 (Chetty et al., 2014; Jovanovic et al., 2015; Mercurio, 1995). Since LRP/LR is so widespread within the cell, some additional functions of the receptor are nuclear structure maintenance as well as translational functions (Jovanovic et al., 2015).

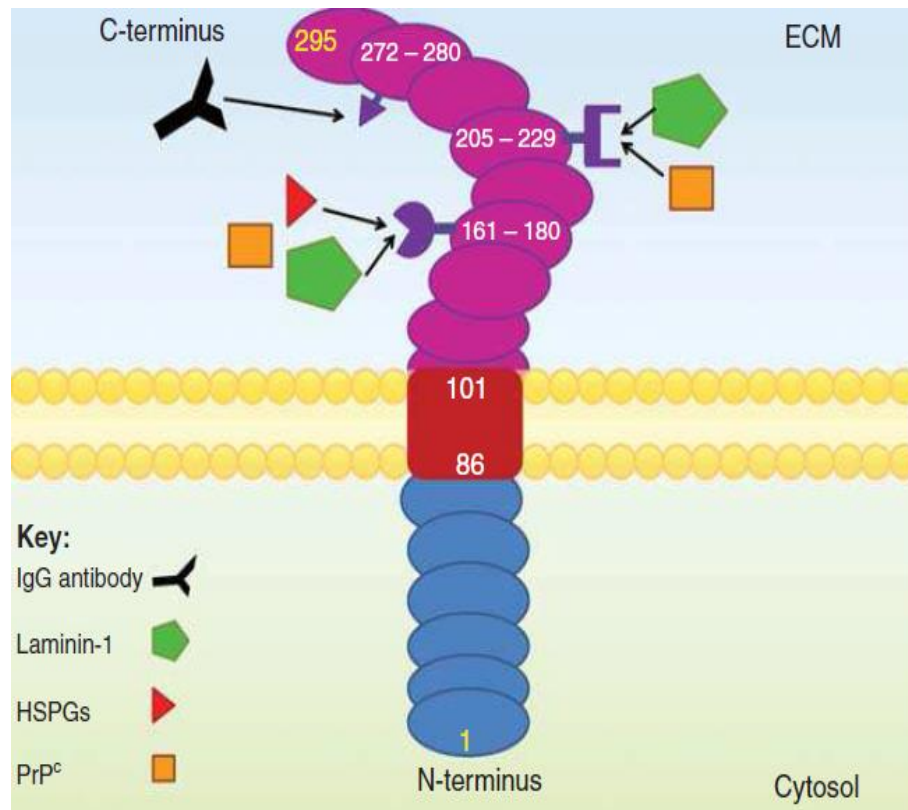


Figure 1.7: Schematic representation of the LRP/LR transmembrane receptor, binding various biomolecules

The function of LRP/LR as a as well as common binding targets are depicted with the N-terminus of the receptor found in the cytosol. This is then connected to the short transmembrane domain. The C-terminus is shown outside of the cell in the extra cellular matrix, where molecules bind to the active sites of the receptor to elicit various cellular responses, including IgG antibody binding at the 272-280 binding site. LRP/LR has been shown to bind primarily laminin-1 and heparin sulphate proteoglycans (HSPs) in the 205-229 binding site Laminin-1, HSPs and cellular prion proteins (PrP^c) in the 161-180 binding site. (Jovanovic et al., 2015).

1.4.2. LRP/LR and telomerase

This proximity to the nucleus puts LRP/LR in very similar locations to TERT and these proteins may therefore have an interaction. This is indeed the case, as it has been shown that LRP/LR

increases telomerase activity to promote cell viability and prevent cellular senescence as shown by the reduction of gamma H2AX (which marks sites of DNA damage and DNA breaks) and the senescence biomarker β -galactosidase (Bodnar et al., 1998; Otgaar et al., 2017). Further evidence shows that hTERT protein levels, telomerase activity and subsequently telomere length were increased after the overexpression of LRP::FLAG within both the MRC5 and HEK-293 cell lines. This may suggest that LRP/LR or LRP::FLAG aids in the formation of the active telomerase enzyme from its major hTERT and hTERC components. This is evidenced by their co-localisation as well as telomerase activity increasing with increased LRP levels (Bignoux et al., 2019; Bodnar et al., 1998; Cuttler et al., 2020; Otgaar et al., 2017). This interaction has potential applications for the treatment of various diseases including cancer and neurodegenerative diseases.

1.4.3. The role of LRP/LR in cancer

Due to the highly conserved nature of LRP/LR across a multitude of species, it has become a common component in disease pathogenesis. Most notably for cancer and neurodegenerative diseases. As previously mentioned, LRP/LR is involved in cell proliferation, survivability, and migration. This has led LRP/LR to be overexpressed in tumourigenic cells, in order to overcome their replication limit and become metastatic (Chetty et al., 2014; Jovanovic et al., 2015). In addition to this, the receptor has been found to be involved in the promotion of angiogenesis and causes a reduction in apoptosis (Chetty et al., 2013, 2014, 2015). Angiogenesis relies heavily on the prior degradation of the basement membrane before the restructuring of the endothelial cells into vascular structures. It is theorised that LRP/LR helps facilitate this process through its laminin-1 interactions, by activating metalloproteases such as collagenase (Chetty et al., 2013). Additionally, LRP/LR is thought to bind chromatin and the nuclear envelope to one another during interphase of the cell cycle. This is thought to result in increased chromosomal stability and cell viability, leading to a bypassing of apoptosis (Chetty et al., 2015). Consequently, it was also shown that when LRP/LR was blocked using an anti-LRP/LR specific antibody (IgG1-iS18) or downregulated by the LRP-targeting siRNA, that adhesion, invasion, angiogenesis, and cell

viability were decreased in cancerous cells (Chetty et al., 2013, 2015; Jovanovic et al., 2015; Naidoo et al., 2015). The newly discovered link between LRP/LR and telomerase also supports this trend, as it was shown that by overexpressing LRP::FLAG, hTERT levels increased and telomerase activity increased, which could lead to cell immortalisation and increase cell viability (Bignoux et al., 2019; Naidoo et al., 2015; Otgaar et al., 2017). These interesting interactions with LRP/LR could lead to the development of novel anti-cancer treatments in the future through the downregulation or blocking of the receptor protein.

1.4.4. The role of LRP/LR in neurodegenerative disease

Similarly, LRP/LR has been shown to play a significant role in neurodegenerative diseases such as Alzheimer's disease and prion disorders. In prion diseases, LRP/LR has been shown to be a receptor for the scrapie prion protein (PrP^{Sc}), which facilitates the internalisation of the prion, leading to aggregation and an eventual toxic build-up resulting in cell death termed spongiform encephalitis (Gauczynski et al., 2006; Leucht et al., 2003). In Alzheimer's disease, LRP/LR has been shown to promote A β shedding and internalisation. This can lead to aggregation and cytotoxicity within neuronal cells, driving the formation of amyloid plaques (da Costa Dias et al., 2013, 2014; Jovanovic et al., 2015). Similarly, to cancer, the blockage or downregulation of LRP/LR by IgG1-iS18 and LRP-targeting siRNA, respectively, has been shown to improve the disease state via reducing cytotoxicity, by decreasing A β aggregation as well as improving cell viability (da Costa Dias et al., 2013, 2014; Jovanovic et al., 2015; Leucht et al., 2003).

Additionally, LRP::FLAG has been shown to have a positive effect on the Alzheimer's disease state. After the transfection and subsequent overexpression of LRP::FLAG in HEK-293 and SH-SY5Y cells, LRP::FLAG was shown to directly interact with the tau protein (Cuttler et al., 2020). This overexpression further showed a decrease in PrP^c levels as well as phosphorylated tau. Briefly, the tau protein is associated with and helps stabilise the assembled microtubules. In Alzheimer's disease, however, the tau protein is hyperphosphorylated and dissociates from the microtubules. These loose tau proteins then associate with one another and eventually form neurofibrillary

tangles that lead to cell death (Haass & Mandelkow, 2010). Furthermore, LRP::FLAG overexpression in HEK-293 and SH-SY5Y cells has also been shown to decrease A β shedding and concomitantly intracellular A β levels (Bignoux et al., 2019), similar to what was observed after downregulating LRP/LR. This may be due to LRP::FLAG promoting TERT which in turn serves a protective role against Alzheimer's disease pathology (Bignoux et al., 2019).

This further shows that anti-LRP/LR drugs could be very useful in combating neurodegenerative diseases, however, transfection is not a viable treatment option, as it might cause off-target effects, and so a different approach is needed. Using the LRP protein alongside a non-toxic drug delivery system would mitigate these issues.

1.5. Applications of nanoparticles in drug delivery and research

Polymer and metallic nanoparticles have become an interesting prospect for both the delivery of therapeutic agents, due to their low toxicity and biocompatibility, as well as for the use as a research tool, due to their interesting optical properties.

1.5.1. PLGA nano-capsules as drug delivery agents

Nano-capsules, such as those synthesised using Poly(lactic-co-glycolic acid) (PLGA), are able to contain the active compound of a drug. They can contain anything from small chemical molecules, nucleic acids and plasmids to proteins (Danhier et al., 2012; Gholizadeh et al., 2022). The molecules contained within the nanoparticles also gain the benefit of having increased stability compared to those that are not protected, allowing them to have longer active periods compared to when unprotected (Sharma et al., 2016). PLGA nanoparticles are also biodegradable, as natural processes are able to hydrolyse the polymer into its constituent monomers: lactic acid and glycolic acid, which are easily metabolised (Danhier et al., 2012;

Sharma et al., 2016). This makes it more useful than functionalised metallic nanoparticles, as these could build up within a system to toxic levels due to them not being able to be metabolised. In the case of PLGA, this polymer has previously been used in medical procedures as biodegradable (dissolvable) sutures (Mccall & Sirianni, 2013), making PLGA a safe and tested compound in medical applications. PLGA nanoparticles enter the cell by endocytosis, after which they leave the endo-lysosome and are released into the cell (Vasir & Labhasetwar, 2007). PLGA nano-capsules can also be further modified to target specific regions of the body or even specific cell types. This can be done through PEGylation, where polyethylene glycol (PEG) is added to the surface of the nano-capsule (Danhier et al., 2012). PEG is a widely used polymer which can bind a variety of molecules such as proteins and antibodies. Specific cell surface receptors could be targeted via surface antibody functionalisation, increasing the uptake of the therapeutic in desired tissues. This is very beneficial to the treatment of specific disorders, as there would be an increase in drug availability for these tissue sites and at the same time, there would be less off-target effects due to less uptake of the therapeutic in non-targeted tissues. This has potential applications in many different diseases, for example, by bypassing obstacles such as the blood brain barrier they can be used to treat neurodegenerative diseases (Hoyos-Ceballos et al., 2020). In cancer treatment on the other hand, it would be beneficial if the drug specifically affected only the cancer cells, unlike chemotherapy, which affects healthy cells as well (Lawenda et al., 2008). This would improve the quality of life for patients suffering from severe chemotherapy-related side-effects.

1.5.2. Nanoparticles in telomerase activity assays

Telomerase is an important target for cancer research, and therefore many different telomerase activity assays have been developed. These are often based on the telomeric repeat amplification protocol (TRAP). A TRAP protocol consists of a DNA telomerase substrate which is amplified by the telomerase enzyme in the presence of dNTPs (reviewed in Zhou & Xing, 2012). After a whole protein extraction process, the active telomerase enzyme extends the telomeric repeats on the

DNA substrate, which can be quantified by a quantitative polymerase chain reaction (qPCR) (as described in section 3.1.8.2) or conventional PCR. The number of repeats added is directly proportional to the signal obtained, which is then an accurate, relative measurement of telomerase activity. TRAP based telomerase activity assays are usually reliable, however, they can present many different problems. These protocols require whole protein extract from tissues or cells, which can leave impurities behind. Due to the sensitivity of the DNA binding dyes and fluorescent probes utilised by these protocols, any impurities, including cell debris, genetic material and trace RNases can adversely affect the experiment. This could cause interference with the RNA component of telomerase, or DNA contamination, non-specific binding and the formation of primer dimers could lead to false positives. This particularly affects telomerase activity assays, as they mainly quantify the extension of DNA (reviewed in Zhou & Xing, 2012). qPCR based techniques are also often expensive and time consuming. Therefore, creating a need for alternative, more cost-effective assays with fewer obstacles.

Metallic nanoparticles, for example gold nanoparticles (AuNPs) are another type of nanoparticle that have very interesting optical properties. AuNPs change the colour of the nanoparticle colloid solution based on their size and proximity to one another (Yarbakht & Nikkhah, 2016). The larger the AuNPs are in solution (20-90 nm in diameter), the greater the wavelength of the peak absorbance of the nanoparticle solution (>600 nm absorbance, more blue). On the other hand, the smaller the AuNPs in the solution (10-20 nm in diameter), the lower the wavelength of the peak absorbance of the nanoparticle solution (500-600 nm absorbance, more red). If AuNPs become more aggregated, the colour of the solution also shifts towards blue as they are mimicking larger nanoparticle sizes. This colour shift will continue until the gold aggregates become macro in scale. This aggregation can be achieved by adding salt to the AuNP solution, which causes the AuNPs to stop repelling each other and begin to interact with one another. This occurs due to a change in surface charge, which can be exploited to surface modify the nanoparticles. Due to these properties, one could very easily detect changes to the surface of the nanoparticle, as even a small change could result in an observable and therefore easily spectrophotometrically measurable, colour change (Yarbakht & Nikkhah, 2016). This sensitivity as well as their ability to be easily functionalised to many different molecules, including the

covalent bonding of thiolated DNA to the surface of the AuNP, could make AuNPs a very useful biosensor in detecting telomerase activity. If AuNPs could be coupled to a telomerase substrate (thiolated DNA), and salt is added to the solution, the colour of the solution would shift towards blue due to the close association of the particles. However, once telomerase is allowed to elongate the substrate, the steric hindrance caused by the elongated DNA, and possible secondary structure formation, will prevent the nanoparticle from closely associating. These secondary structures are caused by the extended telomerase substrate folding in on itself and subsequently preventing the close association of the AuNPs. Since the modified AuNPs now resist aggregation, this would cause the colour of the solution to shift from a blue to a more red colour (Wang et al., 2012) (Figure 1.8). This colour change could then be measured using UV-visual spectrophotometry (Wang et al., 2012).

Detecting telomerase activity using nanoparticles could prove very beneficial, as many steps found in conventional qPCR-based methods could be eliminated. This includes the use of fluorescent probes and dyes, which can easily degrade, be quenched, auto-fluorescence and show false positives due to primer dimers, resulting in differing results from one experiment to another. This would also mitigate signal bleed through in 96-well plates, which can result in false positive results. Nanoparticles can reduce the time and cost involved in performing telomerase activity assays, due to the reduced need for specialised equipment. In addition, the simplicity of the reaction lends itself to shorter preparation times, while still maintaining the sensitivity of the assay. Indeed, telomere extension has been detected in the protein extract of only 10 HeLa cells using AuNPs (Wang et al., 2012). Here, Wang et. al successfully confirmed a reduction in telomerase activity, using the TMPyP4 telomerase inhibitor, with their gold nanoparticle assay (Wang et al., 2012). If this concept could be adapted for rapid telomerase activity analysis, it would become a valuable tool for the research of age-related diseases which heavily involve telomerase.

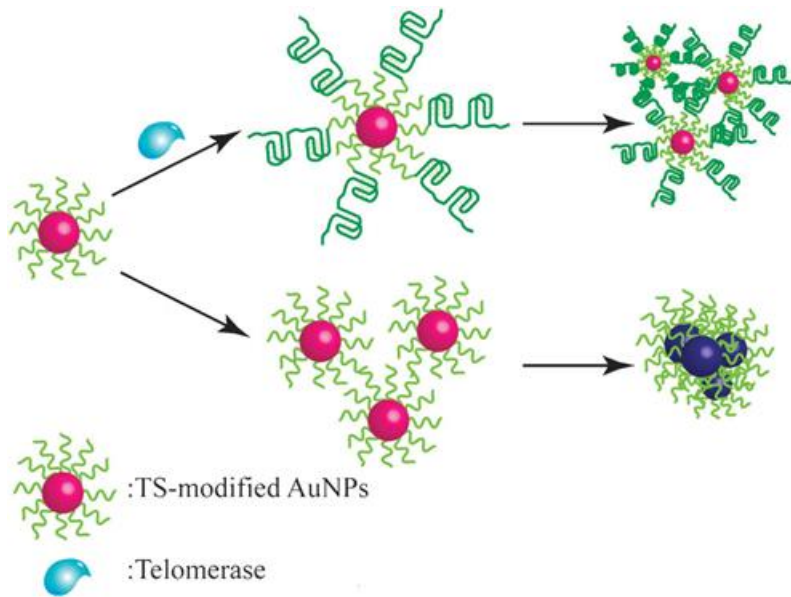


Figure 1.8: Principles of a AuNP-based telomerase activity assay

Thiolated DNA (telomerase substrate) is functionalised to AuNPs. After functional telomerase is introduced to the nanoparticle solution, the substrate is elongated in a PCR-like reaction. This causes steric hindrance between the particles, causing them to disperse and causes a red shift in colour. The nanoparticle solution with the non-elongated substrate turns a blue colour due to the close association of the nanoparticles (Wang et al., 2012).

1.6. Research rationale

Telomere dynamics, specifically telomerase activity, have become a vitally important factor when studying a variety of age-related diseases, such as CVD and cancer. This makes the accurate detection of telomerase activity within cell cultures and tissue samples a necessity. Conventional techniques have many drawbacks, including their very high cost. This project, therefore, aimed to develop a AuNP based assay to determine telomerase activity. This would fulfil the need for an accurate, cost-effective tool to determining telomerase activity in a research capacity. This assay could be used for the research of a variety of diseases, such as cancer. It is important to

note, however, that this assay would not be limited to cancer but can easily be used in any age-related disease field or as a general telomerase activity assay. As stated above, previous research has shown that telomerase activity is directly affected by the LRP protein, which has been shown to have therapeutic effects in Alzheimer's disease models. The AuNP-based telomerase activity assay could be used to assess this effect on telomerase activity by an LRP-based drug while telomerase inhibitors, such as MST-312, can be used to test its sensitivity. The development of an LRP-based drug could therefore be very beneficial, since the nano-capsule would protect the therapeutic agent from degradation and can facilitate the safe uptake into cells without being degraded via natural immune responses. Additionally, as LRP is a natural protein found in the body and that no additional non-degradable or cytotoxic substances are taken in by the cells, the elevation of LRP levels in this manner should not adversely affect cell viability. Due to the wide range of applications elevating LRP levels has in the treatment of different disorders, this could represent a safer alternative to plasmid transfection treatment and could potentially be used for the treatment of age-related diseases, including Alzheimer's disease, through its ability to increase telomerase activity.

2. Aims and Objectives

2.1. Aim 1: Optimise the gold nanoparticle telomerase activity assay and improve the stability of the functionalised AuNPs by redesigning separate linker and extension strands.

1. Synthesise AuNPs using the chemical hydrothermal method.
2. Improve DNA functionalisation by employing pH-dependent binding methods.
3. Improve signal acquisition by optimising sample volume and utilising spectrum analysis to determine the optimal acquisition wavelengths.
4. Treat oesophageal cancer cells with metformin and the MST-312 telomerase inhibitor to detect changes in telomerase activity.
5. Compare conventional telomerase activity assays to the AuNP-based telomerase activity assay.

2.2. Aim 2: Create an LRP based nanoparticle drug.

1. Optimise PLGA nano-capsule synthesis by the emulsion solvent evaporation technique.
 - a. Test various synthesis protocols, solvents, and emulsifiers.
 - b. Optimise purification of the nano-capsules while retaining high yields.
2. Characterize PLGA nano-capsules using UV-visual spectrophotometry, dynamic light scattering and scanning electron microscopy.
3. Determine cytotoxicity profile of empty PLGA nano-capsules on HEK-293 cells.
4. Synthesise and purify the therapeutic protein LRP.
5. Encapsulate the LRP protein using PLGA.
6. Confirm encapsulation and cytotoxicity profile of the LRP-encapsulated PLGA nano-capsules on HEK-293 cells.
7. Assess the effect on telomerase activity of both empty and LRP-encapsulated PLGA nano-capsules on HEK-293 cells.

3. Materials and Methods

3.1. Cell culture

3.1.1. Cell culture protocol

Oesophageal carcinoma cell line; WHCO-5 (Veale & Thornley, 1989), and human embryonic kidney cells; HEK-293 (ATCC, USA) (Graham et al., 1977), were cultured for this project. The HEK-293 cells have previously been used to optimise procedures involving telomerase activity and TERT expression, as these cells are known to display relatively high levels of TERT and telomerase activity (Letsolo et al., 2010). Ethics approval for these cell lines was obtained from the Human Research Ethics Committee (Medical): reference number W-CJ-140804-1.

Each of the cell lines were cultured in Dulbecco's Modified Eagle's Medium (DMEM) (Hyclone, GE Life Sciences, Massachusetts, USA) containing 10% Foetal Bovine Serum (FBS) (Biowest, Nuaille, France) and 1% Penicillin-Streptomycin (Thermo Fisher Scientific, Massachusetts, USA). The cells were kept in a 5% CO₂, 37 °C humidified atmosphere to ensure that the pH of the system remained constant through the CO₂/HCO₃⁻ buffering system and that the cells experienced maximum cell growth by mimicking *in vivo* like conditions.

3.1.2. Passaging of cells

Each cell culture flask was viewed under an inverted light microscope (Zeiss Primovert) to monitor cell growth, cell detachment and to determine the level of confluency. After the cells reached approximately 80% confluency, they were harvested and passaged to prevent contact inhibition and therefore allow the cells to continue growing. To passage the cells, the cells were first detached from the flask using trypsin-EDTA treatment. The trypsin-EDTA (Biowest, Nuaille, France) was then inactivated by adding an equal volume of supplemented cell culture medium.

The cells were evenly passaged into multiple T25 culture flasks (NeST Technology, Virginia, USA) at a density of 0.7×10^6 cells/ml.

3.1.3. Cryo-preservation of cells

After harvesting, cell samples were cryopreserved to be re-cultured at a later stage. After trypsinisation the cells were harvested and centrifuged at low speed (± 200 - 400 g) for 10 minutes. The excess media was then removed, and the pellet resuspended in a cryopreserving solution (15% Glycerol (Associate chemical enterprise, Southdale, South Africa), 20% FBS, 65% DMEM). The vials were then kept at -20 °C overnight and transferred to -80 °C or liquid nitrogen storage. When thawing the frozen cells, an initial high FBS concentration of 20% was used to provide extra nutrients for the cells. This was then stepped down to 10% once the cells stabilised.

3.1.4. Cell quantification

To accurately quantify the number of cells in each flask once they reached confluency, a Neubauer haemocytometer or the TC 20™ automated cell counter was used. The cells needed to be quantified to ensure subsequent experiments and subcultures utilise consistent numbers of cells for reliable results. To distinguish between dead and live cells, the trypan blue stain was used. This stain is only taken up by dead cells due to their porous/permeable cell membrane and is excluded by live cells due to their intact membrane. This leads to dead cells being stained blue under the microscope (Tran et al., 2011). This allows for easy quantification of unstained, live cells. The cell suspension (20 μ l) was mixed with 20 μ l trypan blue for a 2x dilution and a small sample added to the Neubauer haemocytometer. Live cells were then quantified, using the 16-square region of the haemocytometer, while utilising a light microscope (Zeiss Primovert). Thereafter, cell concentration, total number of cells as well as cell viability were calculated using the following formulas:

Total number of cells = Cell concentration $\left(\frac{\text{cells}}{\text{ml}}\right) \times \text{total volume of suspension}$

Cell concentration $\left(\frac{\text{cells}}{\text{ml}}\right) = \text{cells per 16 squares} \times 10^4 \times \text{dilution factor}$

Cell viability (%) = $\left(\frac{\text{number of viable cells}}{\text{total number of cells}}\right) \times 100$

3.1.5. Metformin and MST-312 Treatments

Metformin treatment: A 250mM filter sterilised metformin stock solution was created using the above-mentioned culture medium. Thereafter flasks were seeded with newly passaged cells. The cells were allowed to attach for 24 hours before they were treated with metformin (Merck, Darmstadt, Germany). Each flask was then treated with 10 mM metformin and incubated for 48 hours alongside the untreated controls. The cells were then harvested as mentioned above and utilised in subsequent downstream procedures.

MST-312 Telomerase inhibitor treatment: A 10 mM filter sterilised MST-312 (Thermo Fisher Scientific, Massachusetts, USA) stock solution was created using the above-mentioned culture medium. Thereafter flasks were seeded with newly passaged cells. The cells were allowed to attach for 24 hours before they were treated with the inhibitor. Each flask was then treated with a final concentration of 4 μM MST-312 and incubated for 48 hours alongside the untreated controls. The cells were then harvested as mentioned above and utilised in subsequent downstream procedures.

3.1.6. MTT cell viability assay

The MTT (3-(4,5-dimethylthiazol-2-yl)-2,5-diphenyltetrazolium bromide) (Thermo Fisher Scientific, Massachusetts, USA) assay was used to determine cell viability of the treated cells. A 5 mg/ml MTT stock solution was created using serum free cell culture media. The MTT stock solution was then filter-sterilised and added to the cells (in serum free culture media) to a final concentration of 0.5 mg/ml. Only viable cells reduce the reagent through cellular NAD(P)H-dependent oxido-reductases, as these enzymes are involved in metabolic activity. This reaction is carried out for 4 hours as the viable cells reduce the yellow MTT reagent into an insoluble formazan product, which is purple in colour. This is a reflection of cell viability. The precipitate is then treated with a detergent such as DMSO (Associate chemical enterprise, Southdale, South Africa) and mixed until fully dissolved. After the formazan crystals are dissolved, the absorbance is measured at 570 nm, using a spectrophotometer (VICTOR® Nivo™ Multimode Microplate Reader - PerkinElmer). The more viable cells that are present (the more active enzyme), the higher the amount of dissolved product and therefore the higher the absorbance reading.

This assay was performed in 96-well plates (NeST Technology, Virginia, USA) to a final volume of 200 µl, where each well was seeded with 5000 cells. The cells were then allowed to attach overnight, and treatment commenced the following day. Each treatment as well as each control was performed in biological and technical triplicates. The controls included the no-cell control, no-MTT control, 100% dead cells (treated with 1% triton x-100 - Biorad Hercules, CA, USA) as well as the untreated cell control. The absorbance readings of the treated samples were then compared to those of the controls which were set to 100% cell viability to more easily compare.

3.1.7. DNA quantification - agarose gel electrophoresis

DNA was resolved on 1.5% TBE agarose gels (Thermo Fisher Scientific, Massachusetts, USA) at 90V for 45-60 minutes for the DNA to adequately separate. This method utilises the negative

charge of the DNA as well as the pore size of the agarose gel to separate DNA fragments according to their size. Each sample was resolved alongside a 1 kbp DNA ladder (New England Biolabs, Ipswich, MA, USA) containing known fragment lengths. Through the application of an external electric field, the negatively charged DNA is repelled by the negatively charged electrode and is forced through the pores of the gel. The shorter the fragment, the more quickly it travels, leading to a separation of size. After the addition of GR-Green (Inqaba Biotechnical Industries, South Africa), this separation can be seen under UV light as bands in the gel. The integrity of the DNA was determined by observing the streaking patterns on the gel. The less streaking, the more intact the DNA.

3.1.8. Telomerase activity

3.1.8.1. *TRAPeze Assay*

The TRAPeze[®] RT Telomerase Detection Kit (Merck, Darmstadt, Germany) was used to determine telomerase activity for all cell lines. This assay represents a common, accurate telomerase activity assay which was used to compare to the novel AuNP-based telomerase activity assay. qPCR amplifies a target DNA strand like conventional PCR but is also able to simultaneously quantify the synthesis of the DNA strand. With the TRAPeze kit, this was achieved using a sequence specific primer/DNA probe containing a fluorescent reporter as well as a quencher molecule. These reporter molecules fluoresce; however, due to the proximity of the quencher molecule, the fluorescent signal is suppressed. After the telomerase extraction from mammalian cells, the enzyme elongates the telomerase substrate, and the probe causes a complimentary strand to be synthesised by hot start taq polymerase. The incorporation of the probe causes the distance between the quencher and the fluorescent reporter molecule to increase, creating a fluorescent signal. Therefore, the fluorescent signal is proportional to the amount of added telomeric repeats.

Protein, including telomerase, was extracted from cell pellets using 3-[(3-Cholamidopropyl)dimethylammonio]-1-propanesulfonate (CHAPS) (Merck, Darmstadt, Germany) lysis buffer as it is non-denaturing and therefore capable of extracting active enzymes.

Cells are first harvested via trypsinisation, washed in PBS and the resulting cell pellets are each lysed in 200 μ l CHAPS lysis buffer for 30 minutes on ice. The cell lysate is then centrifuged at 12 000 xg for 20 minutes at 4 °C. The protein-containing supernatant was harvested, and the amount of protein being used was standardised to 0.5 mg/ml (final concentration of 50 ng/ μ l). The HEK-293 cells were used as a positive control for telomerase activity as they display elevated telomerase activity (Letsolo et al., 2010). Additionally, heat treated HEK-293 cells were used as negative telomerase controls, as the heat treatment inactivated the enzyme. CHAPS and no-template-controls were also prepared to account for possible buffer effects. The following thermal cycle was used on the Roche LightCycler LC480 (Roche, Basel, Switzerland): Pre-incubation consisted of one cycle of 37 °C for 30 minutes and 95 °C for 2 minutes. Amplification consisted of 45 cycles of 95 °C for 30 seconds, 59 °C for 1 minute and 45 °C for 10 seconds (where a single acquisition, fluorescent data acquisition, was performed). The readings were compared to TSR8 standard curve (20-0.2 amoles/ μ l) and analysed using Agilent Aria Software (v1.5) and expression fold change calculated using the $\Delta\Delta$ Ct method:

$$\Delta Ct = Ct (\textit{gene of interest}) - Ct (\textit{housekeeping gene})$$

$$\Delta\Delta Ct = \Delta Ct (\textit{treated sample}) - \Delta Ct (\textit{untreated sample})$$

$$\textit{Expression fold change} = 2^{(-\Delta\Delta Ct)}$$

3.1.8.2. Modified TRAP assay

In addition to the TRAPeze assay, a modified TRAP assay was used to determine telomerase activity. Protein extraction and sample preparation was done as previously described in the above TRAPeze assay section 3.1.8.1. Samples were mixed with a TRAP reaction buffer, consisting of ultra-pure BSA (which acts as a PCR enhancer) (Merck, Darmstadt, Germany), EGTA (Merck, Darmstadt, Germany) (which inhibits RNAses that could interfere with TERC), Luna[®] Universal qPCR Mastermix (New England Biolabs, Massachusetts, USA), RNase free water, ACX primer (Inqaba Biotechnical Industries, South Africa) (an anchor that prevents primer dimer formation and therefore self-amplification) and the TS primer (Inqaba Biotechnical Industries, South Africa)

(which acts as a telomerase substrate) (Table 3.1). The assay was performed with the following thermal cycle: Pre-incubation consisted of one cycle of 37 °C for 1h and 95 °C for 2 minutes. Amplification consisted of 45 cycles of 95 °C for 30 seconds, 59 °C for 1 minute and 45 °C for 10 seconds (where a single acquisition, fluorescent data acquisition, was performed). The readings were compared to TSR8 standard curve (20-0.2 amoles/ μ l) and analysed using Agilent Aria Software (v1.5) on the Roche LightCycler LC480 (Roche, Basel, Switzerland) as stated above.

Table 3.1: Telomerase activity primers

Name	Primers (5'-3')		Annealing Temp (°C)	Reference
TS	Forward	AATCCGTCGAGCAGAGTT	58	Kim et al., 1997
ACX	Reverse	GCGCGGCTTACCCTTACCCTTACCCTA		

3.2. Section 1: Gold nanoparticle telomerase activity assay

Telomere dynamics, specifically telomerase activity, have become a vitally important factor in a variety of age-related diseases, such as CVD, Alzheimer's disease, and cancer. Thus, this technology presents a potential research kit utilizing gold nanoparticles to determine the activity of the telomerase enzyme. Through the addition of telomeric repeats and therefore the elongation of the synthetic telomeres attached to the AuNPs, the extracted telomerase leads to a colour change in the gold nanoparticle solution. This colour change is detectable using spectrophotometric readings and represents telomerase activity. This would be useful as an alternative to expensive existing telomerase activity kits for the use in cancer, ageing and age-related disease research.

3.2.1. AuNP synthesis

A concentrated 3:1 mixture of HCl:HNO₃ (aqua regia) (HCl and HNO₃ acquired from Associate chemical enterprise, Southdale, South Africa) was used to treat glassware. This prevents nanoparticles from attaching themselves to the sides of the glassware, which prevents unwanted nucleation points that would otherwise result in aggregation and the formation of gold macroparticles. The gold nanoparticles were synthesized using the chemical hydrothermal method using sodium citrate (Merck, Darmstadt, Germany) as the reducing agent, where a rapidly stirring 50 ml solution of 0.5 mM gold chloride (Merck, Darmstadt, Germany) is first brought to a boil before 2 ml of 10 mg/ml sodium citrate is rapidly added. Through this reaction sodium citrate reduces the gold chloride to atomic gold. The reaction completes after 5 minutes to form gold nanoparticles (AuNPs) with a diameter of 13-16 nm with a solution colour of red. The solution was then removed from the heat source and allowed to settle for a further 20 minutes with gentle stirring at RT. The AuNP solution was then kept in 0.02 % sodium azide (Merck, Darmstadt, Germany) to prevent contamination and then stored at room temperature in the dark. This technique was adapted from Kimling et al., 2006, however, all volumes and times were optimised to suit our specific laboratory conditions. The AuNPs were characterized using transmission electron microscopy (TEM) and UV-Vis spectrophotometry as described in section 3.2.4.

3.2.2. AuNP DNA functionalisation

After synthesis, the nanoparticles were attached to synthetic thiolated DNA which, in this case, acts as a substrate for the extracted telomerase to extend.

All glassware was treated with aqua regia and washed with deionised water to prevent AuNPs from strongly attaching to the glass. This ensured that the nanoparticles could be easily

recovered, as they occasionally adhere to untreated glassware. Thiolated Telomerase substrate DNA (1 mM) (Inqaba Biotechnical Industries, South Africa) (Table 3.2) was bound to gold nanoparticles using a pH dependant sodium citrate method. This method was chosen to reduce the number of nanoparticle purification steps and subsequently reduce loss in nanoparticle yield. Since the synthesis method already utilised sodium citrate as a reducing agent, it does not need to be removed before the functionalisation step. This was to improve on the method put forward by Wang et. al 2012, as the salt-ageing functionalisation reaction is labour intensive and time consuming, requiring constant adjustment and taking up to 40h to complete. Briefly, the salt ageing method involves lengthy incubations (6-8h) with increasing salt concentrations to cause the thiol-groups present on the DNA to bind to the AuNPs. The pH dependant method involves reducing the pH of the solution from pH7 to pH2-4. This helps to facilitate the adsorption of the thiol groups, attached to the DNA, to the AuNPs. This can be achieved using an HCl sodium citrate solution. This was convenient, as it requires less purification steps after synthesis due to the use of sodium citrate as the reducing agent as well as potentially increasing the speed at which the nanoparticles become functionalised.

An improved version of AuNP-based telomerase activity assay was also performed in a similar manner with the following differences: Before nanoparticle functionalisation, 90 μ l of 0.1 mM Thiol-DNA (linker strand) (Inqaba Biotechnical Industries, South Africa) was added to 90 μ l of 0.1 mM extension strand and was allowed to anneal at 60 °C for 1 minute with gentle agitation. The resultant DNA solution was then added to 3 ml of sterile AuNP solution and was mixed for 2 minutes with gentle agitation. This change was made to improve the stability of the nanoparticles by introducing a dsDNA region as well as a potential additional quantitative test in the form of a STELA-like assay. This would be achieved by detaching the extension strand, amplifying it via PCR and resolving it on an agarose gel (Figure 3.1). To facilitate the rapid DNA functionalisation, 100 μ l of 10 mM sodium citrate (pH 1) is then added to reduce the overall pH of the solution to pH 3. The solution was gently stirred for 10 minutes before centrifugation at 6000 xg for 10 minutes to gently pellet out the functionalised nanoparticles. The supernatant was discarded, and the pellet was resuspended in dH₂O to remove the excess sodium citrate and return the nanoparticle solution to a more neutral pH. The solution was then characterized using TEM and UV-Vis

spectrophotometry as described in section 3.2.4. The absorbance spectra (200 nm to 1000 nm) of the functionalised particles were then read on the UV-vis spectrophotometer (VICTOR® Nivo™ Multimode Microplate Reader - PerkinElmer) along with a control solution containing no DNA.

Table 3.2: Oligo sequences for the improved AuNP-based telomerase activity assay.

(bold denotes complementarity)

Name	Sequence 5'→ 3'
Telomerase Substrate (Wang et al., 2012)	(5' Thiol)-TTTTTTTTTTAATCCGTCGAGCAGAGTT-3'
Extension Strand	CTTAGGTGCCTAACGAAACACATGAATCCGAATCCGAATCCGAATCCGAATCCG
Thiolated Linker Strand	CATGTGTTTCGTTAGGCACCTAAGGCTAGCTTTTTTTTTT -(3' Thiol)
Extension Strand PCR Primer	GAATCCACGGATTGCTTTGTGTAC

3.2.3. AuNP based telomerase activity assay

The telomerase activity assay was originally based on the procedure by Wang et. al 2012, with the aim of increasing the speed at which the assay was performed as well as the ease of reading the results. In addition, Wang et. al 2012 performed their experiment on Cervical cancer (HeLa), liver carcinoma (HepG2), breast cancer (MCF7), and leukaemia (K562) cell lines. The assay could

potentially become a rapid, easy to use test which could measure telomerase activity in a variety of cell lines. Therefore, it was first tested on human embryonic kidney and oesophageal cancer cells. The AuNP based telomerase activity assay was designed to be similar to a PCR reaction. A buffer is added to the DNA functionalised nanoparticle solution containing essential components needed by the telomerase enzyme to elongate the telomeric DNA substrate (20mM Tris-HCL at pH8.3, 6.3 mM KCL, 1 mM EGTA, 0.005% Tween-20, 0.1 mg/ml BSA, 1.5 mM MgCl₂, 1 mM dNTPs) (Wang et al., 2012). Protein extract (extracted using CHAPS lysis buffer as described in 3.1.8.1), from HEK-293 cells, was then added to the solution to a final concentration of 50 ng/μl, to keep it consistent with the qPCR telomerase activity assay and a final volume of 50 μl. The solution was then incubated at 45 °C for up to 2h. This differed from the protocol designed by Wang et. al 2012; to ensure that the DNA was significantly elongated, 2h incubation was used instead of the 1h incubation and the temperature was changed from 30 °C to 45 °C to keep it in line with the temperatures used in the qPCR-based telomeres activity assay. After the extension reaction, the solution was transferred directly to a 96-well plate and the absorbance was measured with the VICTOR® Nivo™ Multimode Microplate Reader (PerkinElmer) at 520 nm and 610 nm. These wavelengths were chosen as it was determined to be the peak absorbance for the AuNP solution as well as the DNA functionalised AuNP solution used in this experiment. This was an attempt to decrease the time and steps required to measure the absorbance compared to the method described by Wang et. al 2012, where they utilised a 400–750 nm spectra. The assay was then performed on the metformin and MST-312 telomerase inhibitor treated HEK-293, and WHCO-5 cell lines. Changes in the absorbance of the samples were then compared to the results obtained from the qPCR telomerase activity assay. A decrease in absorbance ratio should indicate a decreased telomerase activity, as the nanoparticles associate closer together (Yarbakht & Nikkhah, 2016). This could then be compared to the results obtained with the TRAPeze qPCR kit. The telomerase activity results over time are expected to resemble those of a standard enzymatic activity assay (Figure 3.1).

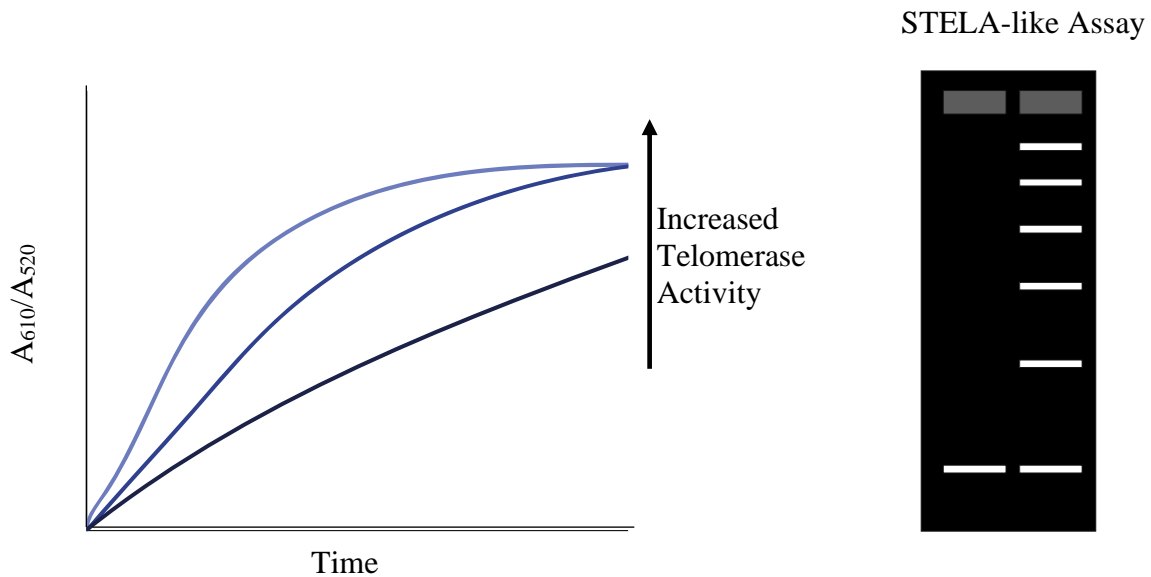


Figure 3.1: Predicted results when using the improved AuNP-based telomerase activity assay

The expected UV-Vis spectrophotometry results (left) would indicate an increasing telomerase activity over time from low (black) to high telomeres activity (light blue), with a concomitant increase in the A610/A520 absorbance ratio. This assay could potentially also produce additional STELA-like results (right). A PCR amplification of the detached and elongated extension strand, resolved on an agarose gel, could produce a STELA-like pattern which could be analysed as a separate result.

3.2.4. Electron microscopy (SEM and TEM) and spectrophotometry

Scanning electron microscopy using the FEI Quanta FEG-SEM (University of the Witwatersrand, Microscopy and Microanalysis Unit - Wits MMU) and the TESCAN MIRA3 FEG-SEM (University of Cape Town, Centre for Imaging and Analysis - UCT CIA) and transmission electron microscopy using the FEI Spirit 120 kV TEM (Wits MMU) was used to determine the shape and size of the

nanoparticles. Sample preparation for the SEM included adding liquid Poly(lactic-co-glycolic acid) (PLGA) nanoparticle solution (approximately 50 μ l) to a carbon film attached to a metallic sample stub. The samples were then left to dry at room temperature overnight to ensure that no liquid remains, as this could adversely affect the vacuum within the microscope as well as image clarity.

Sample preparation for the TEM included adding liquid AuNP nanoparticle solution (approximately 10 μ l) to a 3 mm diameter copper grid which was previously coated with lacey carbon. The sample was then dried under a heat lamp for 30 minutes until no moisture remained. The nanoparticles would then remain trapped on the lacey carbon and could then be viewed.

Spectrophotometric readings were also taken of the functionalised and non-functionalised nanoparticle solutions using the VICTOR[®] Nivo[™] Multimode Microplate Reader (PerkinElmer). Full spectra (from 400 to 700 nm) were taken, and these were compared to one another as well as readings at specific wavelengths. Distilled water and gold chloride solution were used as controls for the AuNP work.

3.3. Section 2: LRP-based PLGA nanoparticle drug design

3.3.1. Nanoparticle drug design

3.3.1.1. *Synthesis, purification, and characterisation of PLGA Nano-capsules*

Poly(lactic-co-glycolic acid) (PLGA) nano-capsules, which are capable of encapsulating proteins, can be synthesised using a relatively simple double emulsification-solvent evaporation technique (Mccall & Sirianni, 2013). This was done by dissolving 100 mg of PLGA polymer (Merck, Darmstadt, Germany) in 2 ml of a solvent, such as dichloromethane (DCM) or ethyl acetate (EA) (Associate chemical enterprise, Southdale, South Africa), overnight for a 50 mg/ml initial solution. While optimisation experiments were performed for both solvents, it was found that EA was the better option for a protein based therapeutic DCM can lead to protein aggregation and is more cytotoxic to cells (Olvera-Bello et al., 2010). Protein encapsulation was first optimised using 0.2

mg green fluorescent protein (GFP) (28 kDa - Merck, Darmstadt, Germany) and 1 mg bovine serum albumin (BSA) (68 kDa- Merck, Darmstadt, Germany) per encapsulation, as it was affordable and as they are slightly smaller and larger in size than the LRP protein (37 kDa) respectively, making them ideal to test the effects of protein size on nano-capsule morphology. Thereafter purified LRP was encapsulated. The protein, in a water suspension, was added to the PLGA solution using a glass Pasteur pipette. The protein solution was then repeatedly aspirated to create the first emulsion.

Thereafter, 4 ml of the vitamin-E (TPGS) (Merck, Darmstadt, Germany) or polyvinyl alcohol (PVA) (Associate chemical enterprise, Southdale, South Africa) emulsifier, was separately vortexed while the first emulsion was added to the vortexing vitamin-E (TPGS) or PVA in a rapid, but dropwise manner to aid in the creation of a uniform solution. The solution was then vortexed for an additional 15 seconds. The resulting solution was rapidly transferred onto ice and then sonicated for five cycles of 10 seconds on and 10 seconds off at a 40% amplitude to form the nano-capsules by cavitation. This created the second emulsion. The nano-capsule solution (second emulsion) was then transferred to 45 ml vitamin-E (TPGS) or PVA solution, while rapidly stirring for 3 hours, to facilitate the evaporation of the solvent and the subsequent hardening of the nano-capsules (Mccall & Sirianni, 2013). Vitamin-E (TPGS) was found to be the better option, as PVA led to inconsistent synthesis.

The nano-capsules were then collected in the supernatant by centrifugation at 500 xg for 1 minute. This removed any large microparticles while leaving the majority of desired nano-capsules behind. The nano-capsules were then further purified by centrifugation at 14000 xg for 1 minute and the pellet was resuspended in RNase free dH₂O, as the vitamin-E (TPGS) was found to adversely affect cell viability. This purification step was performed three times, and the resultant nanoparticle solution was retained for eventual lyophilisation. The nano-capsules were then characterised using dynamic light scattering (DLS) and SEM and TEM as described in section 3.2.4, with the amendment that the nanoparticle samples were coated with carbon or gold-palladium to facilitate with conductivity.

3.3.1.2. *PLGA Nano-capsule Cytotoxicity*

HEK-293 cells were treated with various concentrations of the nanoparticles to determine if the nanoparticles are toxic to the cells. An MTT assay was performed as described in 3.1.6. The 48h treatments consisted of 1, 5 and 10 % (v/v) of the PLGA-nano-capsules to the supplied growth media.

3.3.2. BCA/ micro-BCA assay

BCA assays (Thermo Fisher Scientific, Massachusetts, USA) were performed to determine if the protein encapsulation was successful. Empty, purified LRP and BSA encapsulated PLGA nano-capsules were tested. Samples and controls (empty nano-capsules) were first prepared in a 96-well plate by resuspending nano-capsules in radioimmunoprecipitation assay (RIPA) buffer (Merck, Darmstadt, Germany) or DMSO for 10 minutes to disrupt the polymer shell. A BSA standard curve (0, 0.2, 0.4, 0.6, 0.8 and 1 mg/ml) was prepared in order to compare the protein readings. A BCA working solution was created by mixing copper sulphate and bicinchoninic acid with a ratio of 1:50, and 200 µl of working solution was added to 10 µl of the extracted sample and was mixed by aspiration. The samples were then incubated for 30 minutes at 37 °C until a colour change was achieved. The absorbance was measured at 562 nm using a VICTOR® Nivo™ Multimode Microplate Reader (PerkinElmer). A standard curve was used to determine the amount of protein present.

3.3.3. Western blot

After the HEK-293 cells were treated with both the empty and LRP encapsulated PLGA nano-capsules, Western blot analysis was performed to determine if the LRP was successfully delivered to the cells.

Cell pellets were incubated in RIPA buffer for 20 min to lyse the cells. The resultant solution was resuspended vigorously and thereafter centrifugation at 10000 xg for 20 min. This pelleted the cell debris and allowed for the isolation of the protein found in the supernatant. The protein concentration of each sample was then standardised using the BCA assay (section 3.3.2). After cell lysis, protein extracts were resolved on a 10% Sodium dodecyl sulphate - polyacrylamide gel electrophoresis (SDS-PAGE) gel to separate proteins according to size/charge. This procedure disrupts disulphide bonds within proteins, changing their conformation, using beta mercaptoethanol, while SDS gives the proteins an overall negative charge. Since the proteins will have a negative charge, they will be separated based on charge by electrophoresis. The gel was resolved at 120 V in a 1x electrophoresis tank buffer (25 mM Tris, 192 mM glycine - Merck, Darmstadt, Germany) until the dye front reached the bottom of the gel. Alongside the samples, a molecular weight marker was added to estimate the size of the bands (Laemmli, 1970).

The SDS-PAGE gel was placed on a nitrocellulose membrane which was then be sandwiched between layers of blotting paper. The proteins were electro-transferred from the gel to the membrane in the presence of a 1x transfer buffer (25 mM Tris, 192 mM glycine, 20 % (v/v) methanol - Associate chemical enterprise, Southdale, South Africa) using the Trans-Blot® Turbo™ Transfer System (Biorad).

After the proteins were transferred, the membrane was blocked using 5% BSA to prevent non-specific protein binding (Towbin et al., 1979). The membrane was then incubated in the primary anti-LRP antibody (IgG1-iS18). Thereafter the membrane was incubated in the horse radish peroxidase (HRP) linked secondary antibody (anti-human IgG-HRP) which binds to the primary antibody. A chemiluminescent reaction was then created after incubation in Clarity™ Western ECL Blotting Substrate (Bio- Rad, California, USA) which reacts with HRP, revealing the LRP. The blot was visualised using the ChemiDoc (Biorad) imager with the Image Lab (v5.1) software.

3.3.4. Telomerase activity

After it was shown that there was an increase in LRP after the nanoparticle treatment of the HEK-293 cells with the LRP-encapsulated PLGA nano-capsules compared to the empty nano-capsules, telomerase activity was assessed as discussed in section 3.1.8.

3.4. Data analysis and statistical evaluation

Data analysis was performed in Microsoft Excel 365 Pro (Microsoft Corporation), whereas the statistical analysis was performed in GraphPad Prism (v6.05), using student t-tests and ordinary one-way ANOVA at 95% confidence level, using Dunnett's and Newman-Keuls multiple comparisons post hoc analysis.

4. Results

Telomere dynamics, specifically telomerase activity, play a significant role in a multitude of diseases and have therefore become a vitally important component when investigating possible therapeutics for these diseases. Additionally, previous work investigating LRP upregulation as a potential therapeutic for ageing, CVD and neurodegenerative disease has shown that LRP upregulation through LRP::FLAG overexpression, causes an increase in telomerase activity (Otgaar et al., 2017). This makes it necessary to have a means of accurately determining telomerase activity, however, current assay options are costly and not easily accessible. Therefore, this study aimed to design a new, more cost-effective assay to test telomerase activity by utilising DNA-functionalised AuNPs in a colorimetric assay. Furthermore, since the upregulation of LRP has proven to be an effective therapeutic option in *in vitro* ageing, neurodegenerative disease, and CVD cell culture models, it was necessary to design a suitable vehicle replacement for plasmid transfection to further test the potential therapeutic *in vivo*. This was accomplished in the form of a polymer-based drug delivery system, whereby the therapeutic LRP protein was encapsulated into PLGA nano-capsules and further tested in a cell culture model to compare the efficacy.

4.1. Section 1: AuNP-based telomerase activity assay

AuNPs were successfully synthesised, characterised, and functionalised using a synthetic telomerase substrate. The telomerase activity assay was then optimised and tested on HEK-293 and WHCO-5 cells.

4.1.1. Metallic nanoparticle synthesis

Spherical nanoparticles synthesis was optimised using the chemical hydrothermal method by metal salt reduction. The reaction temperature as well as the reducing agent concentration and method of addition were varied in an attempt to produce AuNPs of the desired size range. Chloroauric acid was reduced using sodium citrate to synthesise gold nanoparticles. Size and morphology of the nanoparticles were determined using scanning and transmission electron microscopy (SEM and TEM). All synthesis reactions were successful (Figure 4.1). Once the correct parameters had been determined, chloroauric acid concentration (0.5 mM) and reaction temperature (rapid boiling) were kept constant. Sodium citrate was then added as the reducing agent and the concentration was increased from 10 mg/ml (as described in section 3.2.1) to 100 mg/ml, to produce larger nanoparticles. It was found that as the nanoparticle size decreases and approaches 14 nm (Figure 4.1, E), there is a red shift in solution colour, compared to the larger nanoparticles, presenting a more blue shift (Figure 4.1, A). It is evident that in the more blue shifted solutions (Figure 4.1, A-C) there are significant size and morphological variations, including nano rods, triangles and larger micro particles. Due to the multiple morphologies present in Figure 4.1 C, the UV-vis peaks would contain shoulders, whereas the slight aggregation present in Figure 4.1 D would result in a shifted peak (towards the right) compared to non-aggregated samples (Figure 4.1 E). Furthermore, it was seen that as the nanoparticle size decreased (Figure 4.1, D-E), the size and morphology became more consistent, although more size variation was still apparent in Figure 4.1 D compared to E.

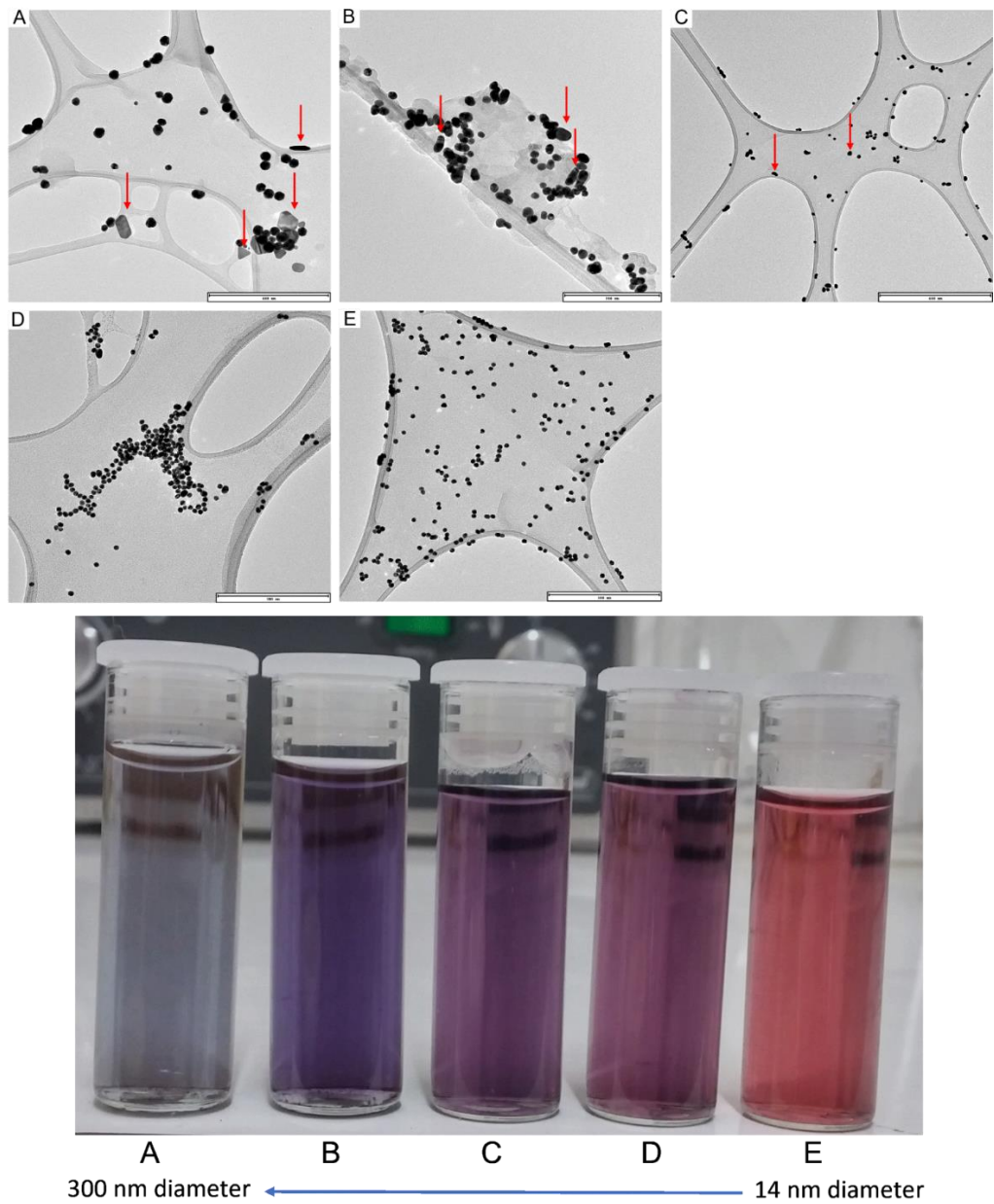


Figure 4.1: Optimisation of AuNP synthesis parameters

Multiple syntheses reactions were performed to determine the parameters necessary to create AuNPs at the desired size and morphology. This image shows early attempts to synthesise spherical AuNPs at the desired size of 14 nm in diameter. Batch A-E represent AuNP samples synthesised using different parameters. Each TEM image is accompanied by the solution colour for each batch. Nano rods and triangles are shown by red arrows. Scale bars represent: A-400 nm, B-200 nm, C-600 nm, D-300 nm, E-300 nm.

4.1.2. AuNP characterisation

Once the parameters to synthesise 14 nm diameter AuNPs were successfully optimised, multiple synthesis reactions were performed and their absorbance spectrum (400 – 700 nm) was measured in order to obtain standard absorbance peaks of the desired AuNP size range. This would allow for the rapid identification of successful synthesis reactions as well as failed ones, as successful reactions would closely resemble each other. Three separate synthesis reactions were chosen as a representative sample for subsequent experiments (Figure 4.2). It can be seen that the spectra are closely aligned across all three syntheses, indicating that there was negligible batch to batch variation, which suggests that a successful, consistent and repeatable protocol for larger scale production was optimised. Furthermore, the peak observed at 520 nm indicates that there was minimal polydispersity, which suggests minimal size variation, among the nanoparticle solutions and between each batch.

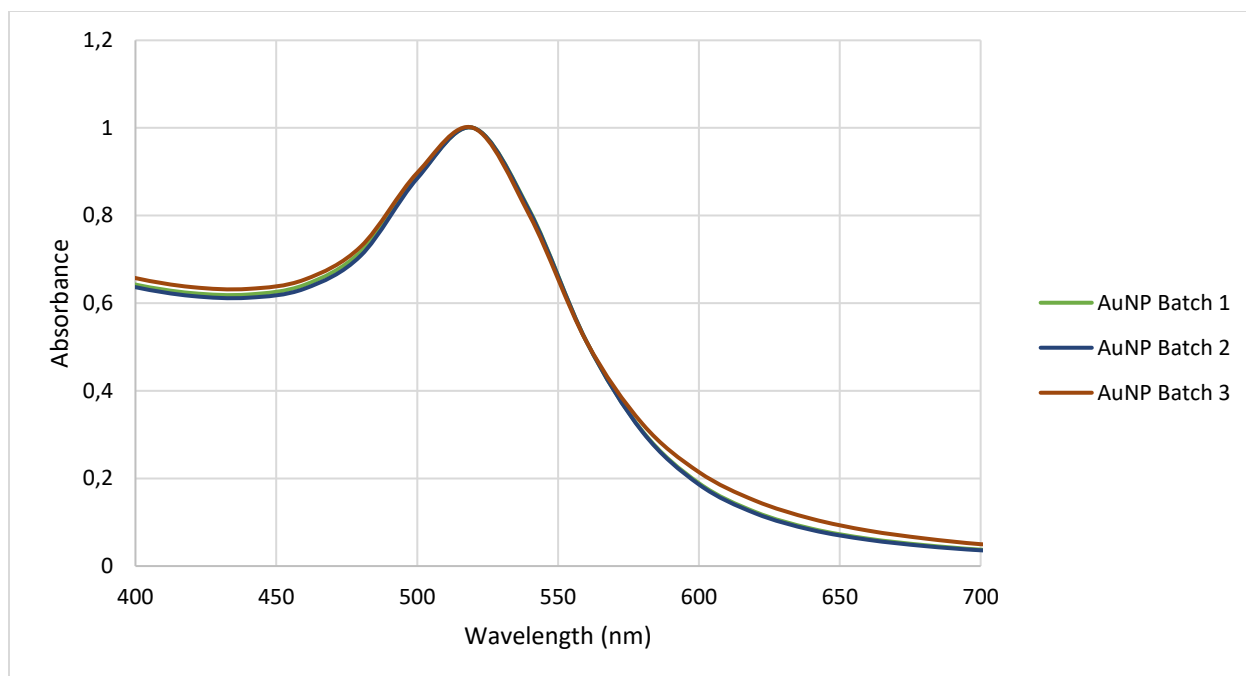


Figure 4.2: Spectrophotometric analysis of AuNP synthesis reactions

UV-Vis spectra (400 nm – 700 nm) was obtained for three separate batches of AuNP solutions, Batch 1 (green), 2 (blue) and 3 (red) showed peaks at 520 nm.

In order to confirm the low polydispersity within and among the three batches, the $A_{610/520}$ ratio was recorded for each sample. Sample solutions which contain a large proportion of AuNPs with increased size would shift the peak towards the 600 nm range, therefore, using a ratio between 610 and 520 nm would provide more information on the size distribution of the nanoparticles in the solution. The 520 nm absorbance value was used as it is the peak absorbance of AuNPs at the desired size range and the 610 nm peak represents the peak of DNA-functionalised AuNPs. It was found that the $A_{610/520}$ ratio was between 0.144 and 0.173 for all three batches, which indicates that the nanoparticle sizes within and among the three batches were reasonably monodisperse and uniform across the three batches. This, therefore, further suggests the reproducibility of the optimised protocol.

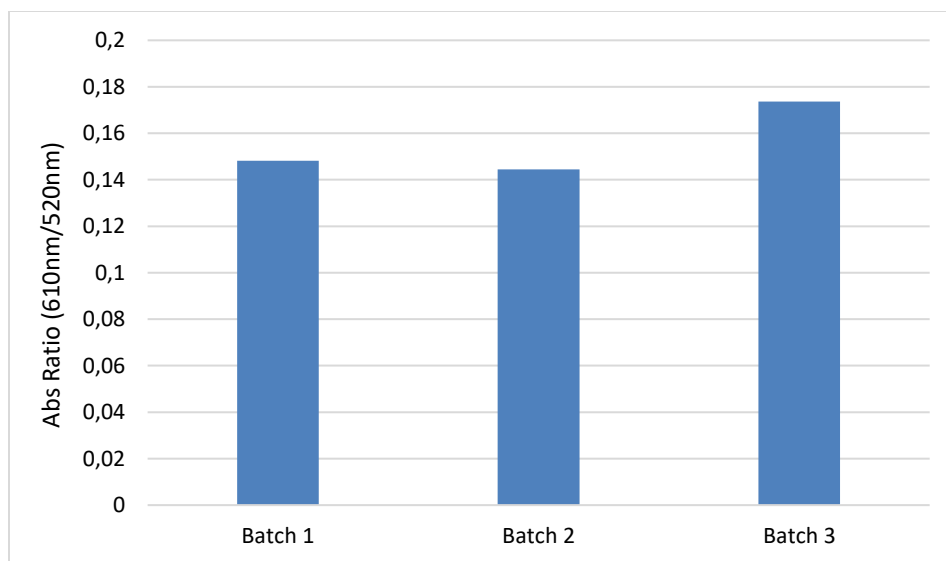


Figure 4.3: $A_{610/520}$ ratio confirms the consistency of the AuNP synthesis reactions

The ratio of the absorbance at two wavelengths (610 nm and 520 nm) of AuNP batch 1, batch 2 and batch 3 were recorded as 0.148, 0.144 and 0.173 respectively.

Once the spectra and $A_{610/520}$ ratios were determined, a size analysis was performed using ImageJ software (National Institutes of Health and LOCI, University of Wisconsin) on particles from representative TEM images (Figure 4.3). The morphology of the nanoparticles was assessed visually based on the TEM images obtained, and it was found that the nanoparticles were predominantly circular. The size distribution of the nanoparticles was obtained by measuring the diameter of the nanoparticles in the images (Figure 4.4, A-C), and an average diameter of 14 nm was calculated, with a standard deviation of 0.936 nm. This 14 nm diameter is optimal for downstream colorimetric applications for the telomerase activity assay, as these nanoparticles produce a red-coloured solution.

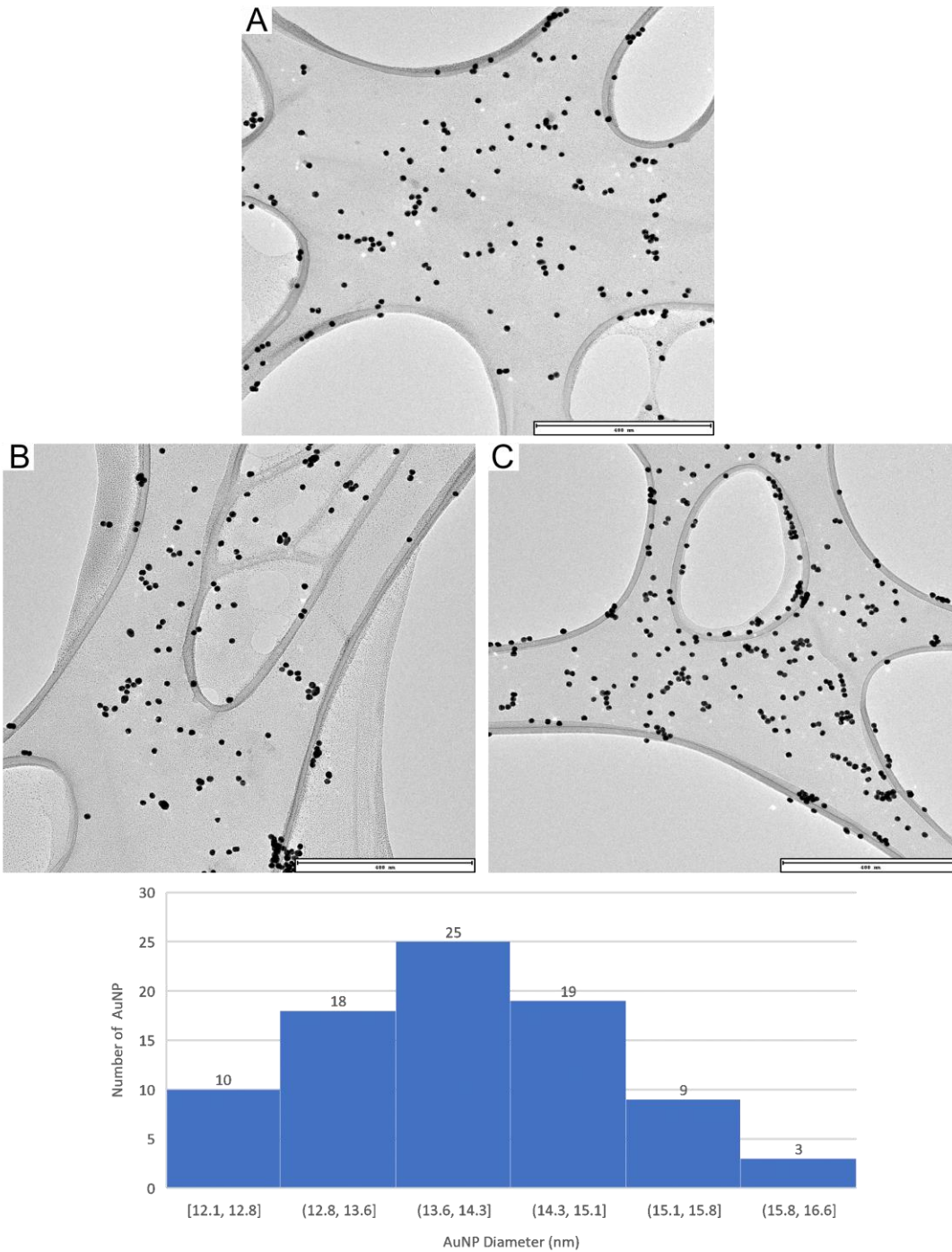


Figure 4.4: AuNP size distribution determined by TEM and ImageJ analysis

TEM images of the three batches of AuNPs (A-C) Figure 4.2 and Figure 4.3 were taken. In addition, a size analysis was performed using the ImageJ software (National Institutes of Health and LOCI, University of Wisconsin) on particles from all three TEM images. The diameter and size distribution of the spherical

nanoparticles was obtained, and they were found to have an average diameter of 14 nm with a standard deviation of 0.936 nm. Scale bars represent 400 nm.

4.1.3. Thiol-DNA Functionalisation of gold nanoparticles

Subsequent to optimisation of AuNP synthesis, thiolated DNA was functionalised to the nanoparticles using the pH-dependent method (section 3.2.2) to provide a telomeric substrate strand for the telomerase protein to extend. After multiple optimisations, the initial AuNP-based telomerase activity assay was revised and improved to reduce nanoparticle aggregation.

4.1.3.1. AuNP-based telomerase activity assay concept:

Once the synthesis of the AuNPs was successfully optimised for size and shape uniformity, a thiolated DNA strand (telomerase substrate) consisting of 28 bases (Table 3.2), was successfully attached to the AuNPs using the pH-dependent method (Figure 4.5). This represents the initial attempts at creating a AuNP-based telomerase activity assay.

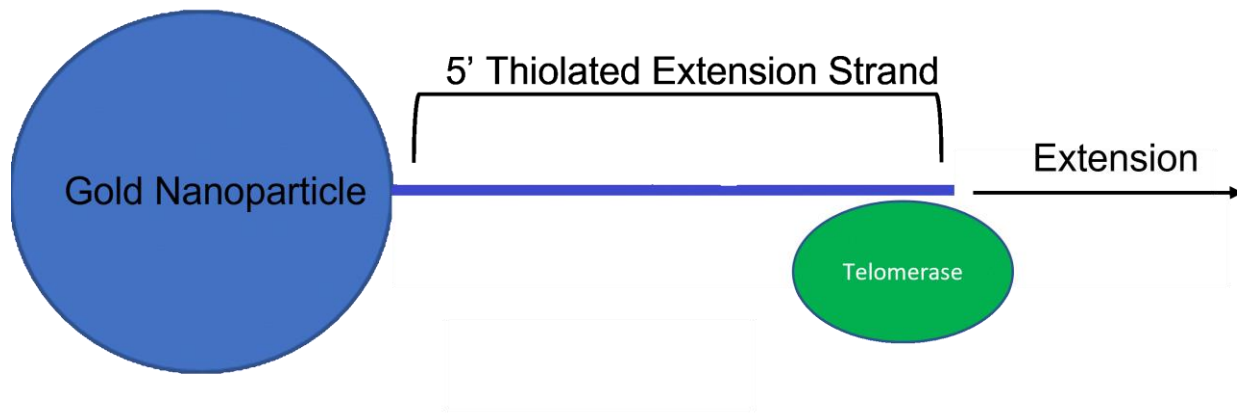


Figure 4.5: Schematic representation of the first iteration of the AuNP-based telomerase activity assay

A AuNP is coupled to a 5' thiolated extension strand (See Telomerase Substrate Table 3.2) which is elongated by the telomerase enzyme. This elongation can be detected using UV-Visual spectrophotometry, as the colour of the AuNP solution shifts.

Once the initial concept was determined, the AuNPs were functionalised and exposed to telomerase extracted from HEK-293 cells. In order to determine if the nanoparticles were functionalised, TEM was performed alongside non-functionalised controls. A clear halo is present around the NP's, suggesting that the DNA was present (Figure 4.6, B). However, the nanoparticles aggregated when in the presence of the protein extract (Figure 4.6, C). This meant that the synthesis had to be modified, as aggregated nanoparticles cannot be used for the detection of telomerase activity.

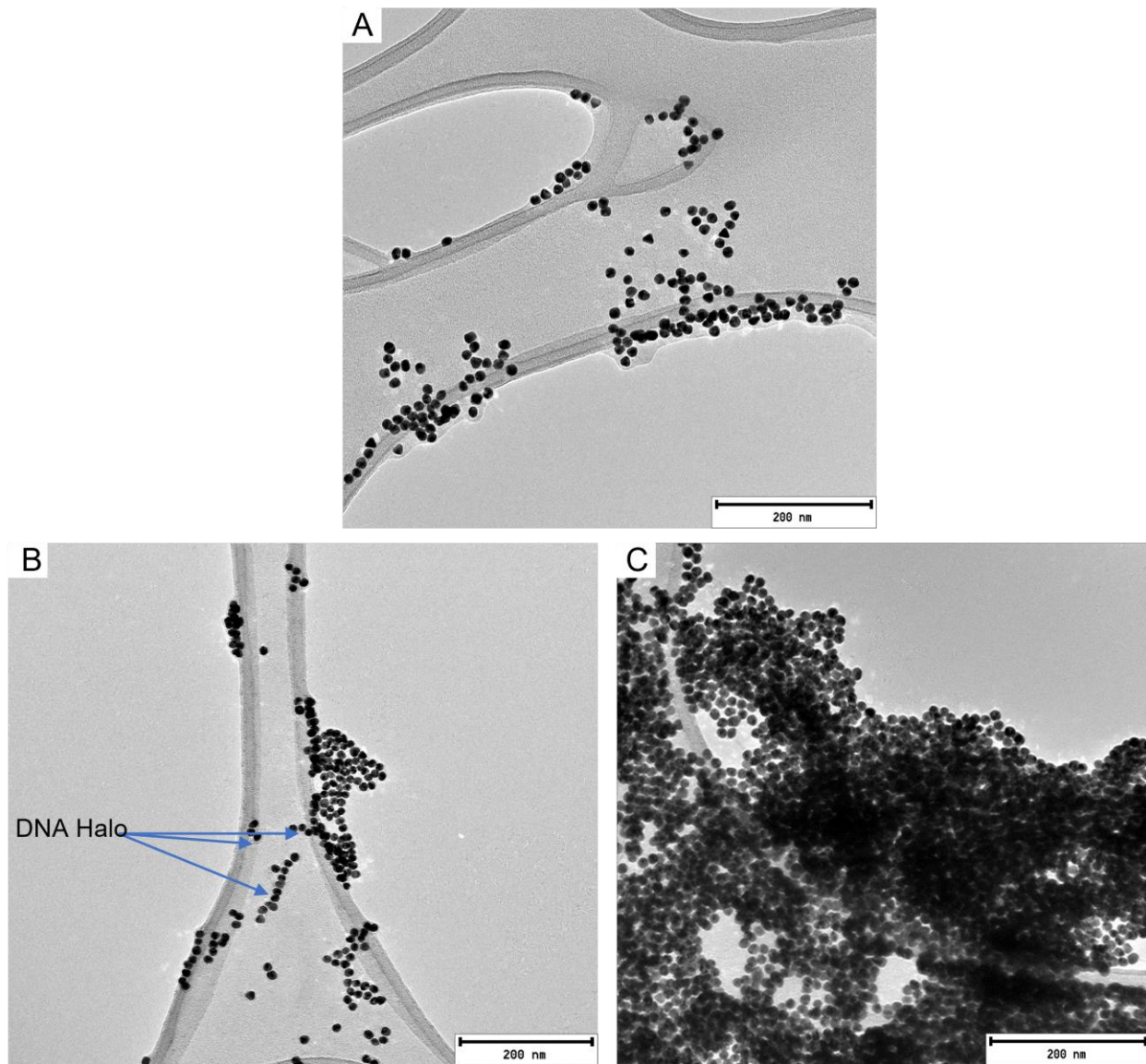


Figure 4.6: Transmission electron microscopy analysis of 5' extension strand functionalised AuNPs

(A) TEM images of non-functionalised AuNP control and (B) 5' extension strand functionalised AuNPs. A clear halo was present around DNA modified AuNPs (B- arrows), however, the functionalisation caused aggregation in the AuNP solution (C). Scale bars represent 200 nm.

4.1.3.2. Improved AuNP-based telomerase activity assay concept

Due to the aggregation seen after functionalisation (Figure 4.6, C), the assay was redesigned to improve on stability. This new concept included the addition of an extension strand, whereby the gold nanoparticles were coupled to the 3' thiolated strand as in the first iteration but which now serves as a linker strand that contains a complimentary sequence for the additional extension strand. In this way, the linker strand is coupled to the nanoparticles by the pH- dependant sodium citrate method as described in 3.2.2 and the extension strand can then be added to the linker strand through DNA annealing, via the complimentary DNA sequence. The extension strand (synthetic telomere) can then be elongated by the telomerase enzyme within the samples (Figure 4.7). This extension process causes the functionalised nanoparticles to increase their relative size and causes them to resist aggregation, as the particles can no longer directly interact with one another. This results in a colour change of the nanoparticle solution, which can be detected at 610 nm and 520 nm using a standard spectrophotometer. The more the enzyme elongates the attached DNA, the greater the ratio of 610/ 520 nm becomes. This ratio can therefore be used to determine telomerase activity within tissue samples or cell culture models.

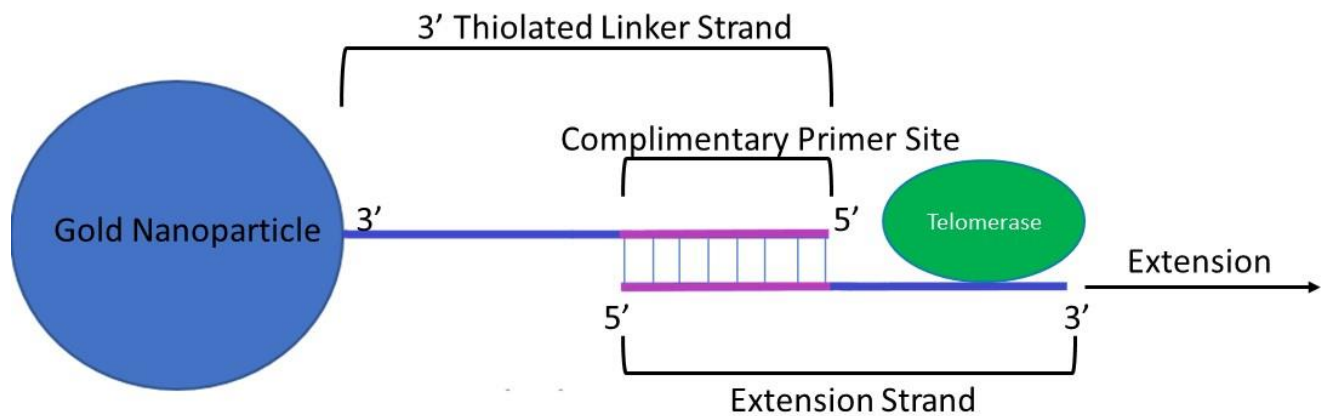


Figure 4.7: Schematic diagram of the Improved AuNP telomerase activity assay

A gold nanoparticle (AuNP) is coupled to a 3' thiolated "linker" strand which contains a complimentary sequence for the "extension" strand that is elongated by telomerase. This elongation can be detected using

UV-Vis spectrophotometry. Compared to a single oligo setup, this concept was predicted to be more stable due to the ss-DNA spacer and the ds-DNA section, leading to less aggregation.

4.1.4. DNA functionalisation - pH dependent method

Prior to the AuNP-DNA functionalisation reaction, the thiolated linker and the extension strand were first annealed at 60 °C for 1 minute. Annealing was confirmed by agarose gel electrophoresis. It was seen that after the annealing process, a band was observed at approximately 200bp (Figure 4.8; Lane 4) when compared to the linker (Figure 4.8; Lane 2) and extension (Figure 4.8; Lane 3) strands, each observed at under 100bp. Furthermore, only one band was observed (Figure 4.8; Lane 4). This therefore confirmed that the annealing between the linker and extension strands was successful.

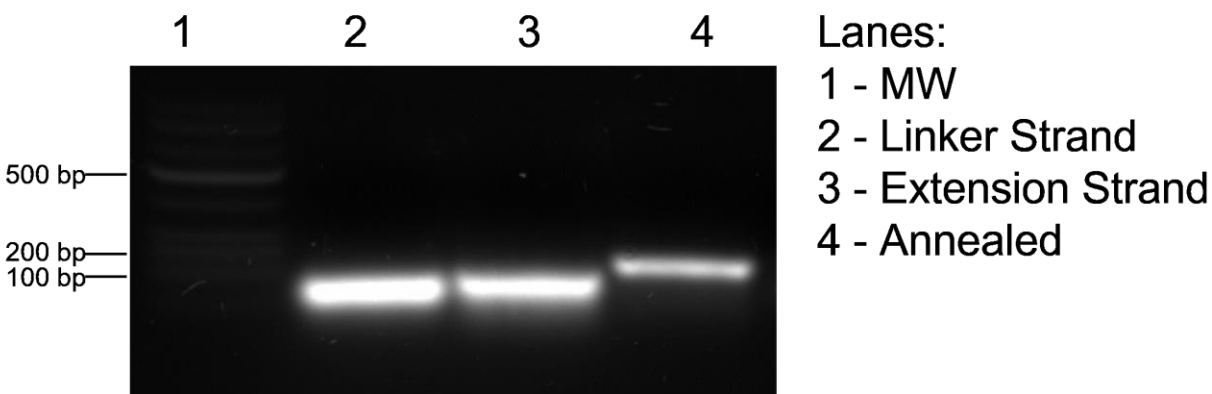


Figure 4.8: Annealing of telomerase extension strand and thiolated linker DNA

This figure shows the annealing of two DNA components of the improved AuNP-based telomerase activity assay on a 1.5% agarose gel. The linker strand – 40 bases (lane 2) was resolved alongside the extension strand – 54 bases (lane 3). Lane 4 shows the annealed construct. No additional bands were seen in lane 4.

Subsequent to the annealing step, the AuNPs were functionalised using the pH-dependant method as described in section 3.2.2. In order to confirm that the functionalisation was successful, spectrophotometry was used and the absorbance of the non-functionalised AuNPs and thiol-DNA functionalised AuNPs was measured across an absorbance spectrum of 400 – 1000 nm. There was a large shift in the peak absorbance wavelength from 520 nm to 650 nm observed between the non-functionalised AuNPs and functionalised AuNP's respectively (Figure 4.9), suggesting that the functionalisation was indeed successful. Furthermore, the small shoulder in the DNA functionalised sample at 520 nm indicates that some AuNPs were not functionalised, however, the large peak at 650 nm indicates the majority of the AuNPs were indeed functionalised.

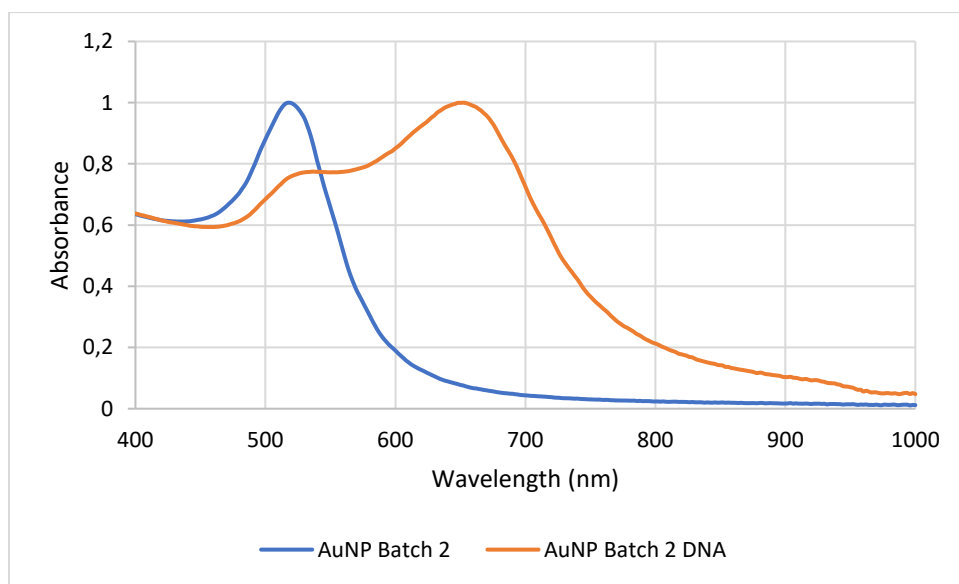


Figure 4.9: Spectrophotometric comparison between thiol-DNA functionalised and non-functionalised AuNPs

This figure shows a continuous spectrophotometric reading, from 400 nm to 1000 nm, for functionalised AuNPs (orange) and a non-functionalised AuNP control (blue).

The absorbance ratio of 610/520 nm was consequently determined, and it was observed that there was a clear increase in the ratio from 0.151 to 0.528 after the addition of the thiol-DNA (Figure 4.10). This method can therefore be used to measure the levels of telomerase activity within samples as the extension of the thiol-DNA by telomerase would increase the 610/520 nm value proportionally to the levels of telomerase activity in the samples.

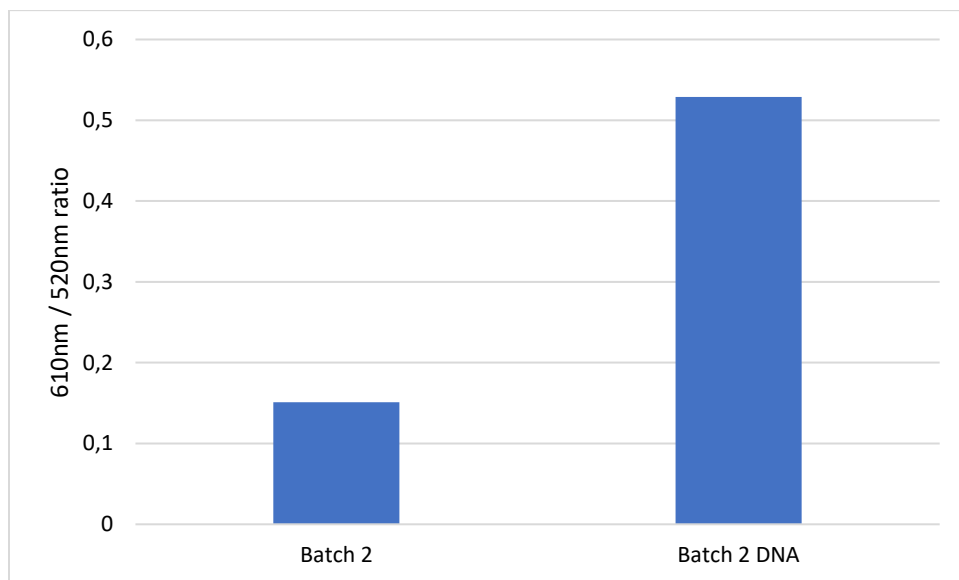


Figure 4.10: Comparison of DNA-functionalised and non-functionalised AuNP, using the $A_{610/520}$ ratio

The ratio of the absorbance at two wavelengths (610 nm and 520 nm) of both unfunctionalized (Batch 2) and functionalized (Batch 2 DNA) AuNPs was calculated. It is shown that the addition of the DNA to the surface of the AuNPs causes a distinct increase in the $A_{610/520}$ ratio.

TEM images were subsequently taken to determine if the addition of the linker strand prevented aggregation of the AuNPs and to further confirm successful functionalisation. A distinct halo of thiol-DNA was observed after functionalisation (Figure 4.11 B vs A) with a marked decrease in

aggregation. This method of AuNP production and functionalisation was therefore used for subsequent experiments.

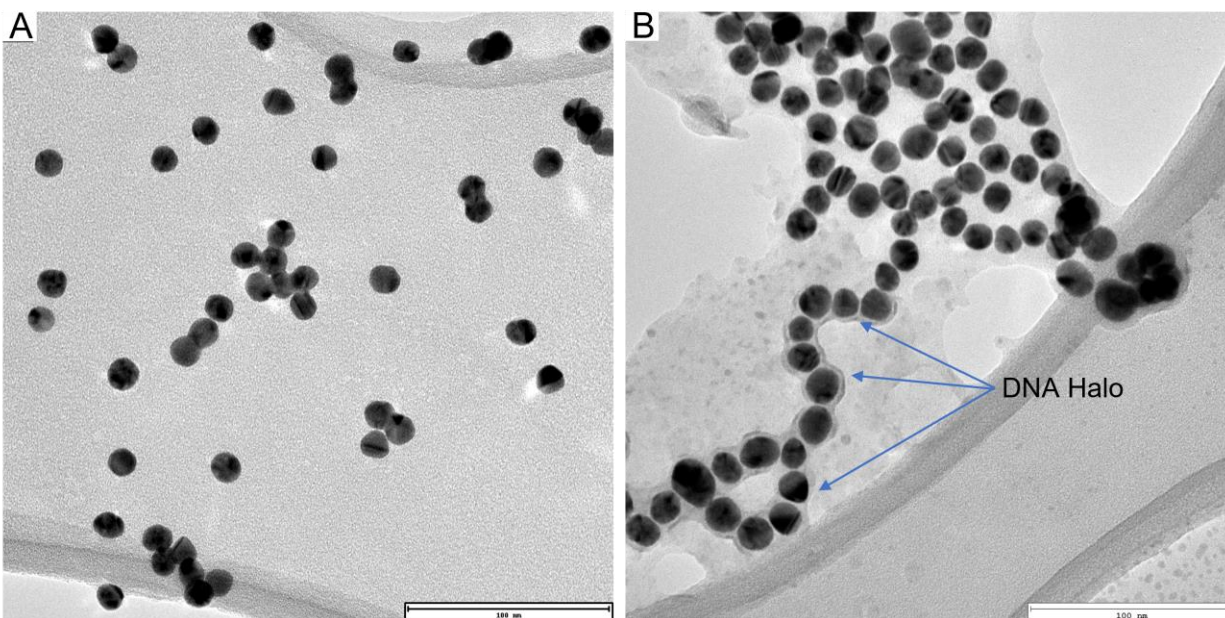


Figure 4.11: Transmission electron micrograph of DNA functionalized AuNPs

TEM images of the (A) AuNP control and (B) DNA functionalized AuNPs. A distinct halo around many of the particles from the functionalised sample is observed (arrows), which is absent in the unmodified particles. Scale bars represent 100 nm.

4.1.5. AuNP-based telomerase activity assay

Since the AuNP production and functionalisation was optimised, the AuNP assay was then ready to be tested to determine if telomerase extracted from cells would indeed extend the thiolated DNA extension strand. HEK-293 cell lysates (described in section 3.2.3) were incubated with the functionalised AuNPs and absorbance was measured at 610 nm and 520 nm, every 5 minutes for a 70-minute period, whereafter the 610 nm/520 nm ratio was calculated for each timepoint (Figure 4.12). There was a clear increase in the $A_{610/520}$ ratio over time, suggesting the extension

of the telomerase substrate, therefore indicating the activity of the telomerase enzyme. In addition, when comparing the HEK293 samples to the HEK293 heat-treated control samples, there is a clear and consistently higher ratio, resembling that of an enzyme activity profile, which coincides with the predicted results (Figure 3.1).

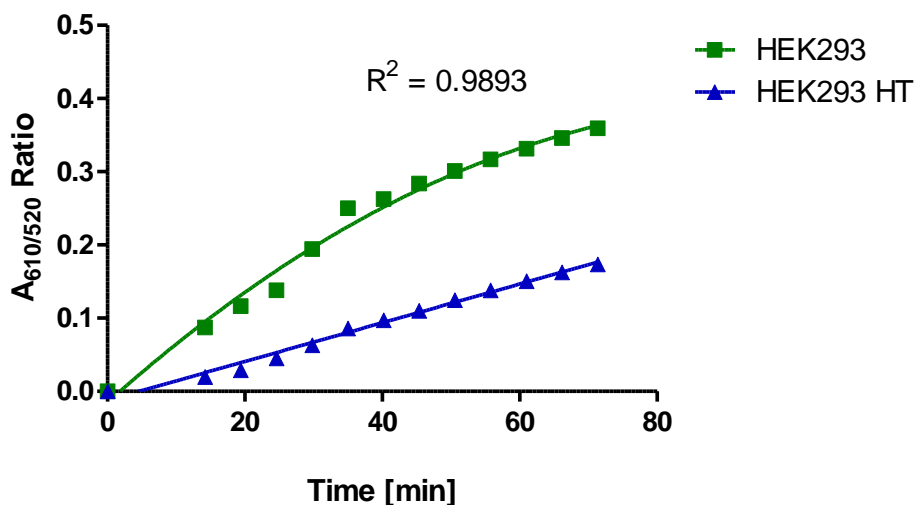


Figure 4.12: Successful detection of telomerase activity using the improved AuNP based telomerase activity assay

The telomerase activity assay was performed on HEK-293 cells (green), known to have high levels of telomerase activity, as well as a heat-treated (telomerase inactivated) sample (blue). The assay was performed over a 70-minute period and the absorbance ratio (610 nm/ 520 nm) was measured every 5 minutes. The results resemble an enzyme activity profile, where the HEK-293 sample showed a consistently higher ratio than that of the heat-treated control, closely resembling the predicted results (Figure 3.1). The results were fitted to a curve using non-linear regression, resulting in a good fit ($R^2=0.9893$).

Since the ability of the assay to detect telomerase activity was confirmed, HEK-293 and WHCO-5 cells were treated with the telomerase inhibitors, MST-312 and metformin for 48 hours. This was done to decrease telomerase activity, in order to assess the sensitivity of the AuNP-based

telomerase activity assay. First however, these samples were assessed using a commercially available telomerase activity kit. Using the TRAPeZe® RT Telomerase Detection Kit (Merck, Darmstadt, Germany). with the heat-treated samples as controls, it was found that the MST312 telomerase inhibitor caused a significant 80% and 55% reduction in telomerase activity in the HEK293 and WHCO5 cells, respectively (Figure 4.13, A). In addition, there was a significant 62% and 52% decrease in telomerase activity observed in the HEK293 and WHCO5 cells, respectively, when treated with metformin (Figure 4.13, B).

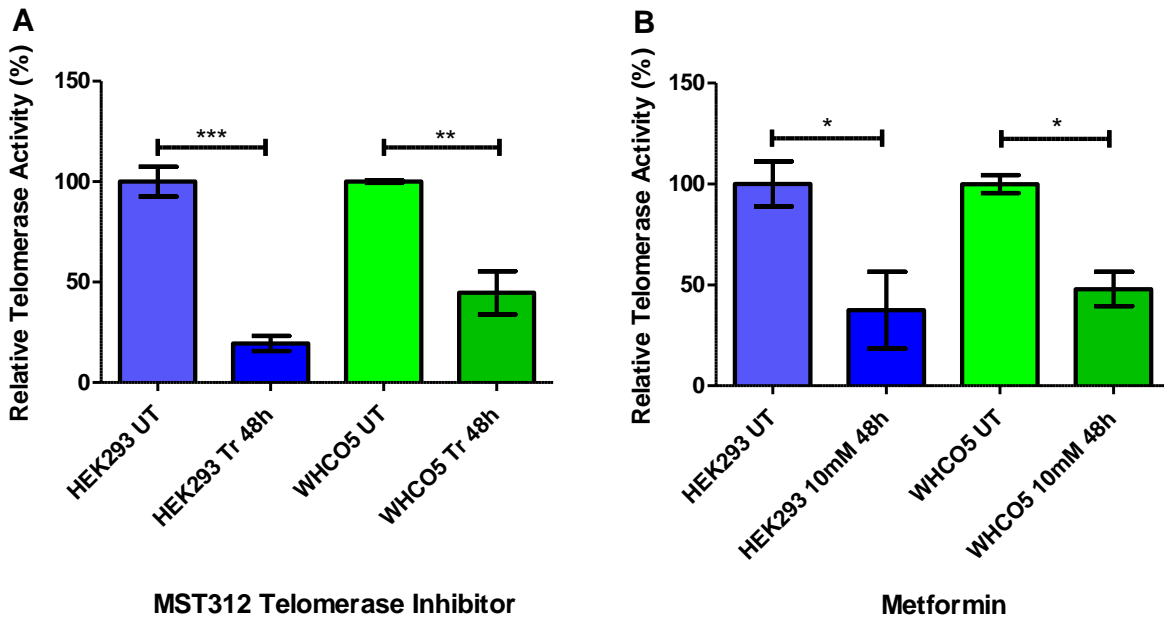


Figure 4.13: Relative telomerase activity of HEK-293 and WHCO-5 cells after MST-312 telomerase inhibitor and metformin treatment (TRAPeZe® RT Telomerase Detection Kit)

The relative telomerase activity for both HEK-293 and WHCO-5 cells, treated for 48h with 4 µM of the MST-312 telomerase inhibitor and 10 mM metformin, was obtained using the TRAPeZe® RT Telomerase Detection Kit (Merck, Darmstadt, Germany) via RT qPCR (section 3.1.8.1). (A) MST-312 treatment caused a significant decrease in telomerase activity for both cell lines, where HEK-293 cells experienced a decrease of 80 % ($\leq p, 0.001$) and WHCO-5 cell a decrease of 55 % ($\leq p, 0.01$). (B) Similarly, the metformin treatment

*caused a 62 % decrease ($\leq p, 0.05$) in the treated HEK-293 cells and a decrease of 52 % ($\leq p, 0.05$) in the treated WHCO-5 cells. Error bars represent standard deviation; N=3 biological replicates; ns $p > 0.05$, * $p \leq 0.05$, ** $p \leq 0.01$, *** $p \leq 0.001$.*

Once the telomerase activity of the HEK-293 and WHCO-5 cell samples was established using an existing commercialised kit, the telomerase activity in these samples was then tested using the AuNP-based telomerase activity assay and the results were compared. The treated cell samples were compared to the heat-treated controls. A significant decrease was detected for the MST-312 treatment (9 %, 40 % and 43 % respectively), between each sample and its respective heat-treated controls (besides the 48h HEK-293 sample), for both the HEK-293 and WHCO-5 cell lines (Figure 4.14, A). Furthermore, a significant decrease (24 %, 13 %, 26 % and 34 % respectively) in telomerase activity was observed between each metformin treated sample and the respective heat-treated controls, as well as a significant decrease of 18 % between the untreated and treated HEK-293 samples (Figure 4.14, B). This therefore indicates that the AuNP-based telomerase activity assay is unable to detect differences between treated and untreated samples but is able to distinguish between functional and heat inactivated telomerase samples.

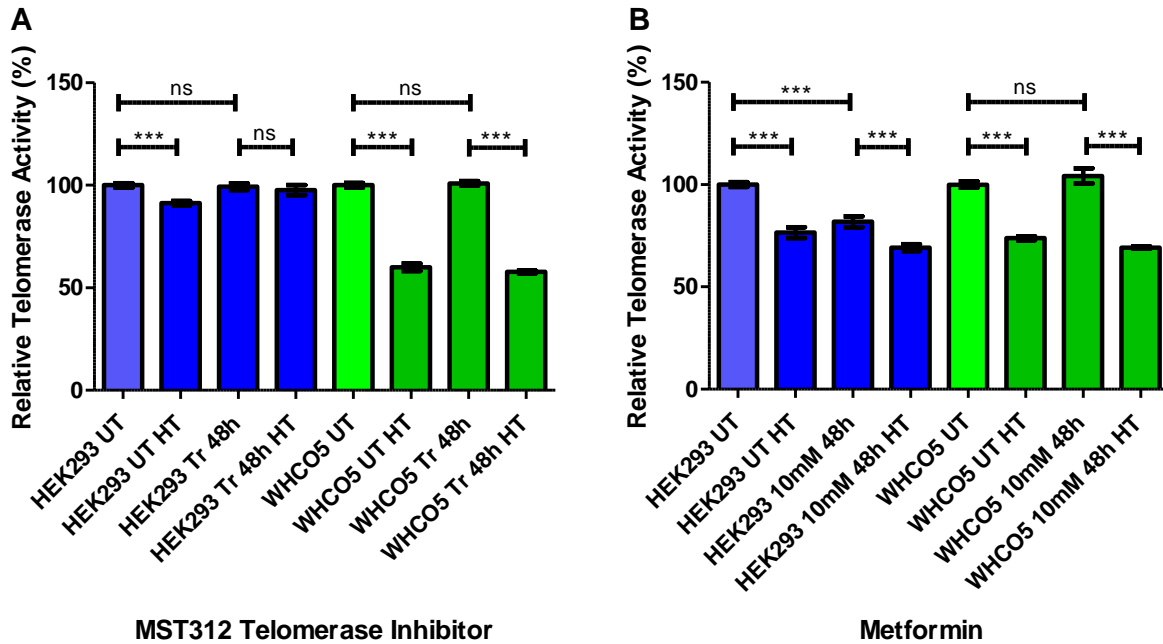


Figure 4.14: Relative telomerase activity of HEK-293 and WHCO-5 cells after MST-312 telomerase inhibitor and metformin treatment (AuNP-based telomerase activity assay)

The relative telomerase activity for both HEK-293 and WHCO-5 cells treated for 48h with 4 μ M of the MST-312 telomerase inhibitor and 10 mM metformin was obtained using the AuNP-based telomerase activity assay (section 3.2.3). For the MST-312 treatment (A), a significant difference ($p < 0.001$) was seen between each sample and the respective heat-treated controls, for both the HEK-293 and WHCO-5 cell lines. Similarly, the metformin treatment (B) showed significant decreases ($p < 0.001$) between the samples and their heat-treated controls as well as a significant decrease of 18 % ($p < 0.001$) between the untreated and treated HEK-293 cells. Error bars represent standard deviation; $N=3$ biological replicates; ns $p > 0.05$, * $p \leq 0.05$, ** $p \leq 0.01$, *** $p \leq 0.001$.

Altogether, the AuNP based telomerase activity assay was optimised and compared to the commercial TRAPeze telomerase activity kit using an embryonic/normal cell line (HEK-293), as well as a cancer cell line (WHCO-5). It was found that the assay was not sensitive enough to consistently distinguish between positive controls and the reduced telomerase activity samples.

Despite there being room for improvement in the sensitivity of the assay, that the assay was able to detect differences in telomerase activity compared to heat-inactivated samples.

4.1. Section 2: Encapsulated-LRP PLGA nano-capsules

Since we have previously shown that LRP overexpression increases telomerase activity and provides a rescuing effect in Alzheimer's disease models *in vitro* (Bignoux et al., 2019), we planned to translate this research to *in vivo* models, however, using plasmid transfection *in vivo* is not an effective strategy. The correct delivery method for a potential therapeutic molecule is crucial, as unprotected molecules may be degraded by the body, leading to reduced efficacy or non-specific side effects. Therefore, in order to use the LRP protein as a therapeutic molecule *in vivo*, an effective delivery method is needed. One such method is by using the PLGA polymer to encapsulate the protein, conferring this protection. This method is useful, as PLGA is biodegradable and non-toxic, theoretically leading to a slow, longer lasting release of the therapeutic LRP. In this study, the double emulsion solvent evaporation technique was optimized using various conditions to produce a high yield of uniform PLGA nano-capsules within the desired size range of 200-450 nm in diameter. The nano-capsule solution was then lyophilised and resuspended in a variety of buffers including distilled water and PBS. Thereafter, HEK-293 cells were treated with various concentrations of empty nanoparticles to determine the maximum concentration at which the nanoparticles can be used and not be cytotoxic. Moreover, cells were further treated with LRP encapsulated in the PLGA nanoparticles to compare the efficacy of this treatment to previously established results.

4.1.1. Optimisation of PLGA nano-capsule synthesis

Poly(lactic-co-glycolic acid) (PLGA) nano-capsule synthesis was optimised using the double emulsion, solvent evaporation method (McCall & Sirianni, 2013) with EA or DCM as the solvent and vitamin-E (TPGS) or PVA, as the emulsifier. After each synthesis, the shape and size of the nano-capsules were determined using various microscopy methods (section 3.2.4). Images were initially taken of the large fraction (pelleted by centrifugation at 500xg) using light microscopy (Figure 4.15, A), to determine if the nano-capsule synthesis method yielded spherical particles before committing to electron microscopy. It was found that indeed the synthesis method produced spherical nanoparticles. Furthermore, the small fraction (supernatant) was then imaged using TEM, to determine the size of the nanoparticles, and it was confirmed the nanoparticles were within the 200-450 nm size range (Figure 4.15, B). However, due to the difficulty in visualizing these nano-capsules under TEM, as the uncoated capsules were cracking and bursting under the intensity of the electron beam, additional characterization was done by SEM as well as DLS.

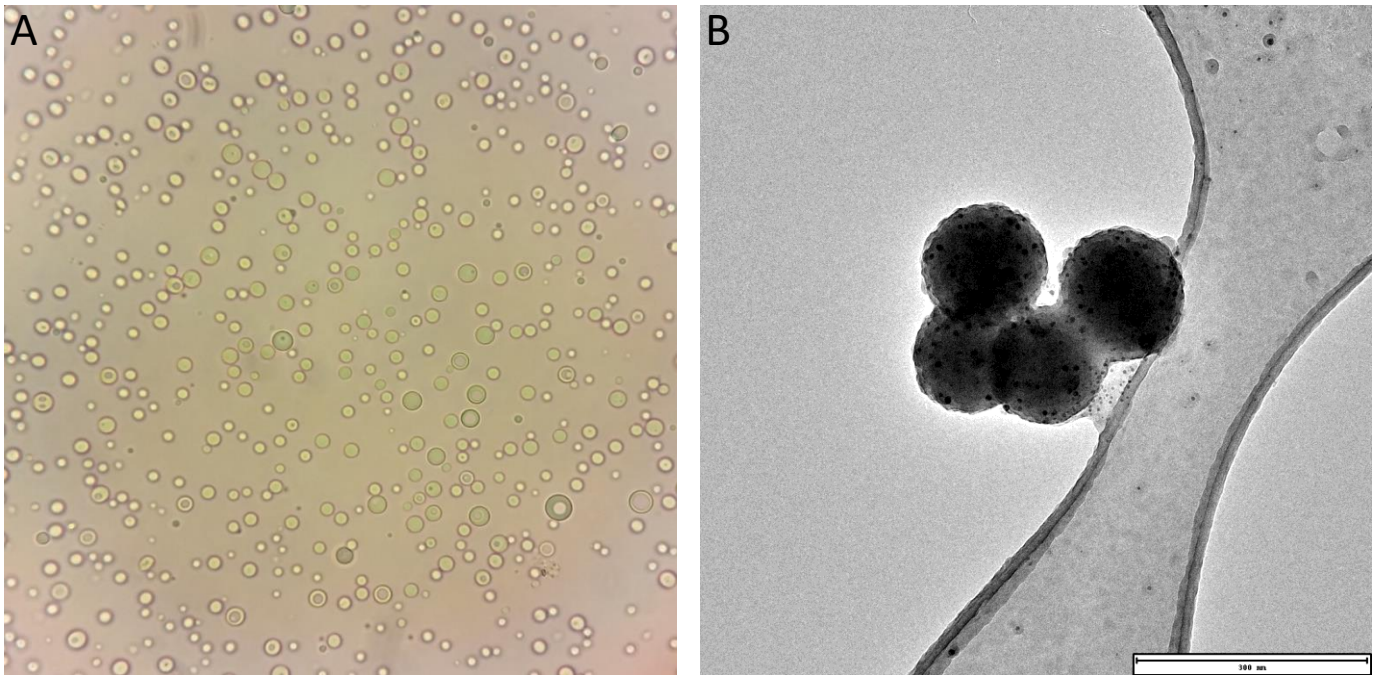


Figure 4.15: Light microscope and TEM images of PLGA nano-capsules

(A) shows a light micrograph (100x magnification - Zeiss Primovert) of hollow PLGA micro-capsules. These micro-capsules represent the larger particles that were removed during the purification process (pelleted out by centrifugation at 500 xg) and confirm spherical nano-capsules were formed. (B) A transmission electron micrograph (FEI Spirit 120 kV TEM – Wits MMU) of the small fraction (supernatant) of PLGA nano-capsules. This confirmed that the PLGA nano-capsules were within the desired size range of 200-450 nm in diameter. Scale bar represents 300 nm.

Further characterisation of this sample (Figure 4.15) was therefore, carried out using scanning electron microscopy (SEM) with both gold-palladium and carbon sputter-coated samples and uncoated samples (Figure 4.16). Coating the samples allowed for better conductivity and therefore, better images and resolution. It was found that a thin double coat of gold-palladium or a double coat of carbon resulted in the best conductivity while retaining the most visible surface structures. However, it was found that these samples resuspended in PBS exhibited a

large amount of crystal formation when viewed under SEM. Since the sample was dried as described in section 3.2.4, this could have led to the concentration of the salts in the PBS, leading to crystal formation as observed (Figure 4.16).

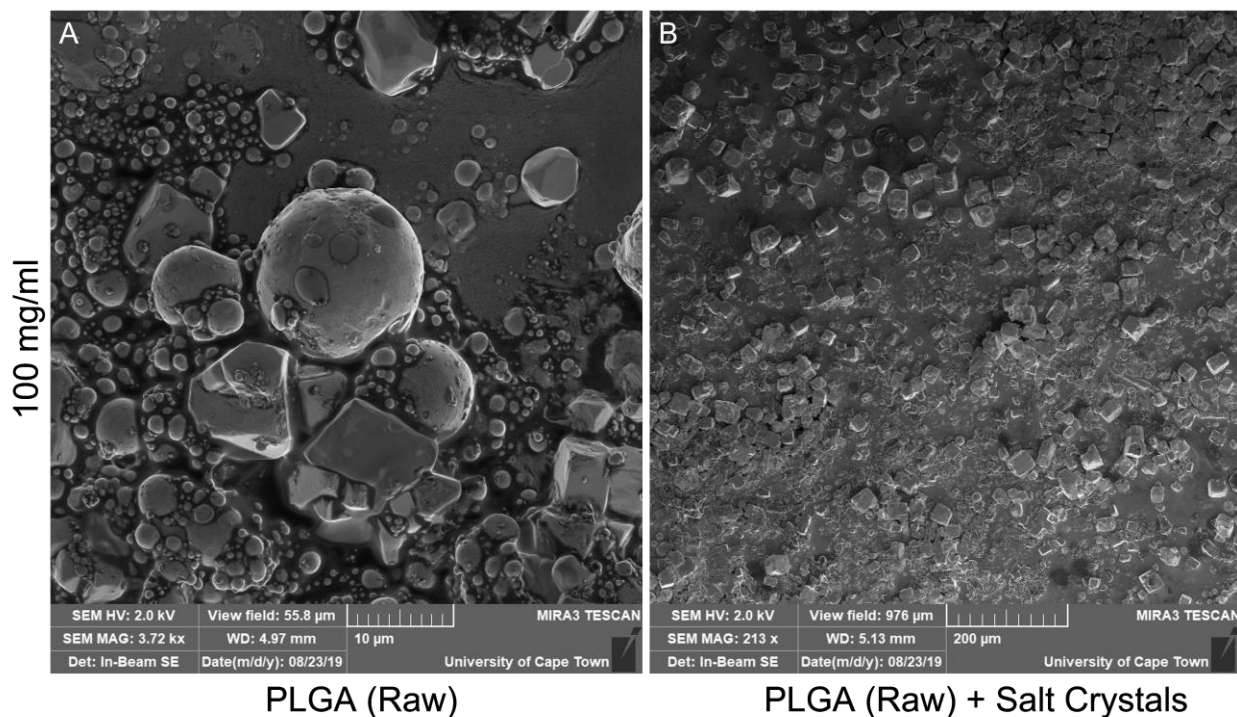


Figure 4.16: Initial PLGA nano-capsule synthesis

SEM images of gold-palladium coated PLGA nano-capsules from the initial nano-capsule synthesis reaction, using DCM as the solvent and PVA as the emulsifier (TESCAN MIRA3 FEG-SEM - UCT CIA). The resulting nanoparticle suspension was centrifuged at 14 000 xg for 10 minutes and resuspended in PBS. (A) Raw, unprocessed nanoparticles had a high polydispersity and (B) samples resuspended in PBS were found with high numbers of crystals. Scale bars represent A- 10 μ m, B- 200 μ m.

Due to the crystal formation suspected to be caused by PBS, the nanoparticles were resuspended in deionised, RNase-free water in all subsequent experiments. Next, PLGA nano-capsule synthesis

was optimised in order to obtain capsules within the 200-450 nm diameter range. Multiple reactions using PVA were performed, however, it was found that PVA led to inconsistent synthesis, as the PLGA frequently “spiderwebbed” during sonication. This created long PLGA filaments instead of forming spherical nano-capsules. Therefore, PVA was eliminated as an emulsifier for future experiments.

Two different initial concentrations of PLGA were tested for the synthesis reactions and consequent nanoparticle batches were characterised using SEM. It was postulated that the initial concentration would influence the uniformity of the synthesised nano-capsules, due to the drop-wise addition of the solubilised PLGA. It was expected that a higher concentration would not be efficiently sonicated, leading to increased polydispersity. Indeed, it was found that the nano-capsules produced using the 50 mg/ml initial concentration of PLGA exhibited lower polydispersity and smaller nano-capsules overall (Figure 4.17, D-F) in comparison to those produced using a 100 mg/ml initial dilution of PLGA (Figure 4.17, A-C). Furthermore, the nanoparticles were confirmed to be hollow, and thus we confirmed that nano-capsules were being produced. Therefore, the 50 mg/ml initial dilution of PLGA was used for all subsequent syntheses.

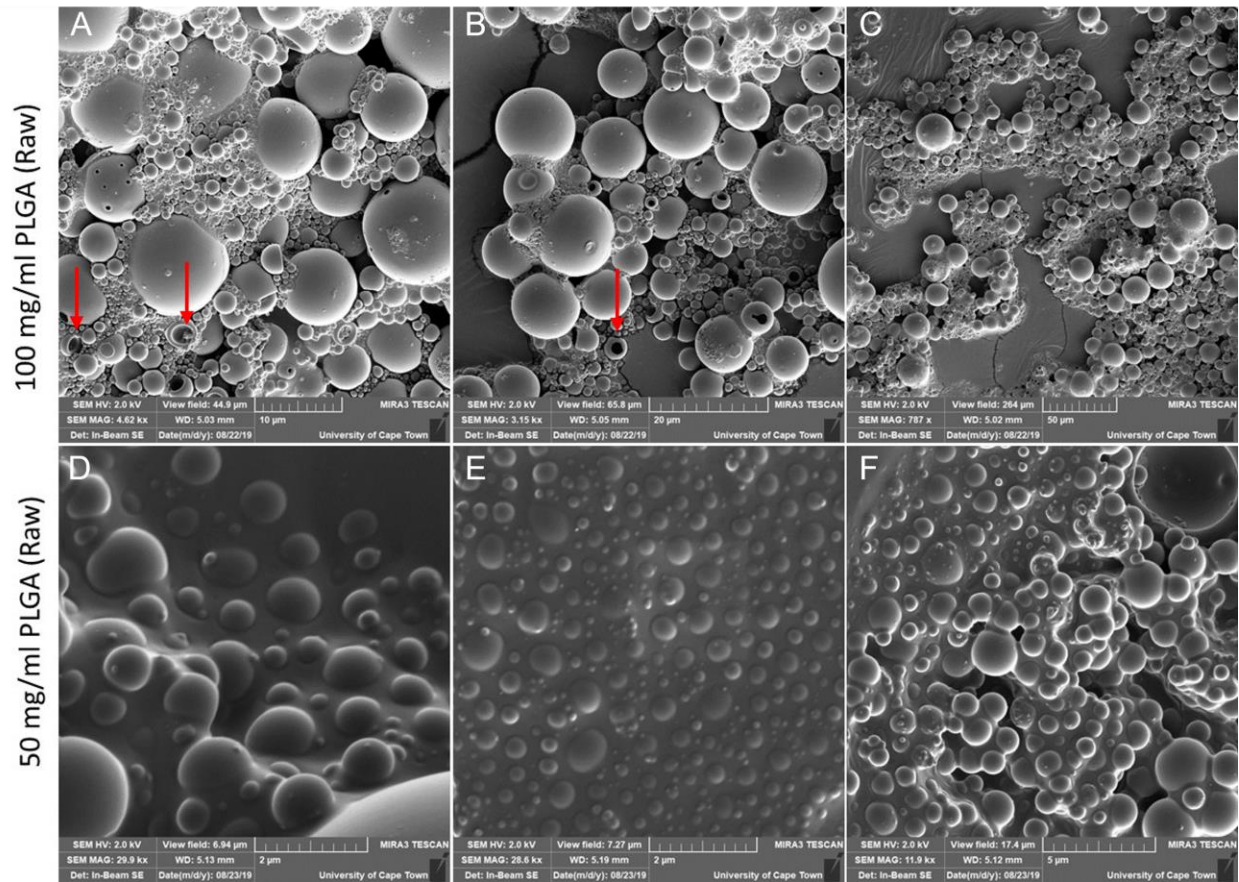


Figure 4.17: The effect of initial PLGA (in solvent) concentration on nano-capsule polydispersity

SEM micrographs depicting un-purified (raw) PLGA nano-capsules, synthesised using DCM and vitamin-E (TPGS) at both 50 and 100 mg/ml initial concentration, (gold-palladium coated - TESCAN MIRA3 FEG-SEM - UCT CIA). Red arrows show hollow nano-capsules, this confirmed that the nano-capsules formed correctly. Scale bars are represented on each panel.

In addition, various centrifugation parameters (8000 xg, 10000 xg, 12000 xg, 14000 xg, and 500 xg) as well as syringe filtration (0.45 µm) were tested to determine the best parameters to isolate and purify nano-capsules of the desirable size for cell culture experiments (under 450 nm). It was proposed that at these centrifugation parameters, the larger, unwanted nano-capsules would pellet out, leaving behind only the desired size range. After centrifugation for 5 minutes, the supernatant of each PLGA nano-capsule sample was isolated and prepared for SEM analysis as described in 3.2.4. However, the trend of the nanoparticles produced using the 50 mg/ml initial

PLGA dilution being more uniform and smaller in size compared to the 100 mg/ml solution was once again confirmed.

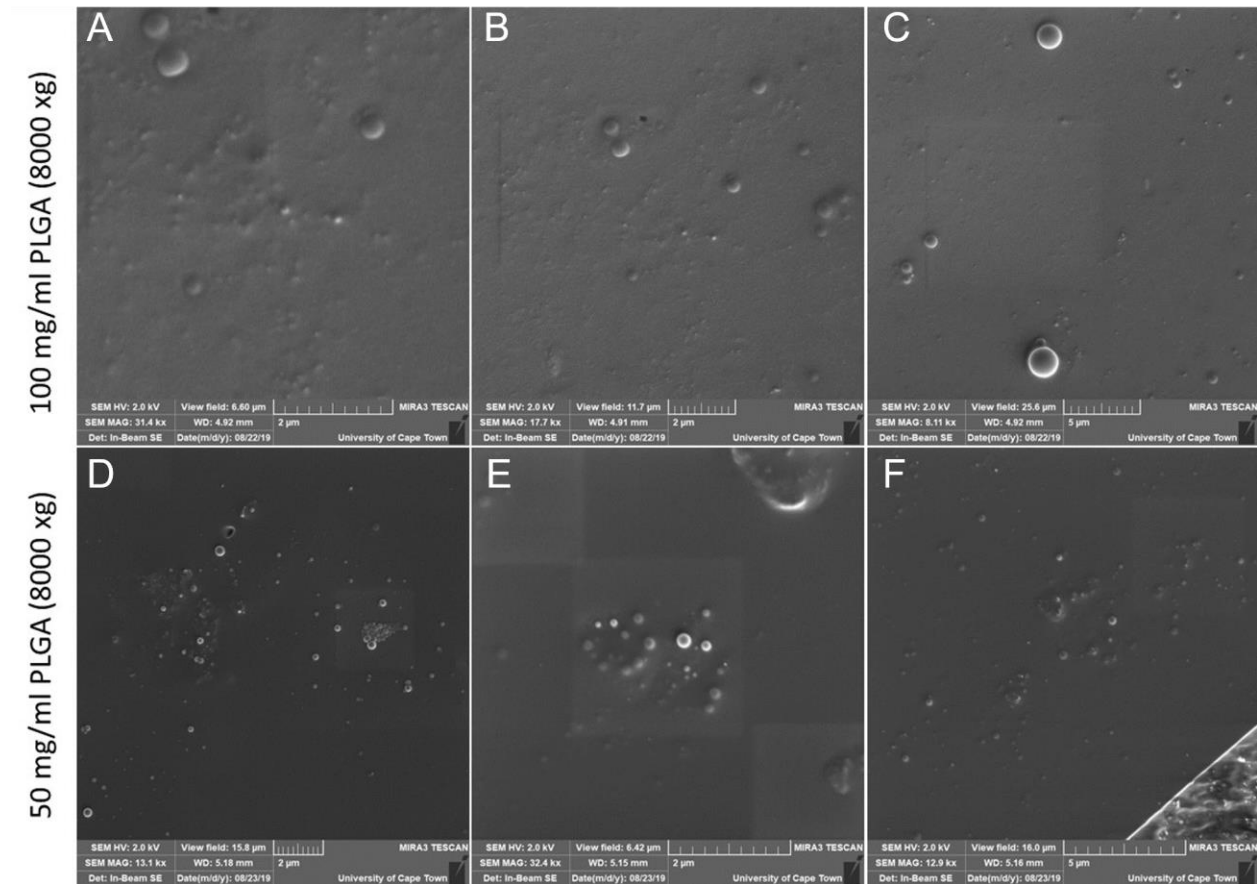


Figure 4.18: PLGA nano-capsules purification by centrifugation at 8000 xg

These SEM micrographs depict 8000 xg isolated PLGA nano-capsules, synthesised using DCM and vitamin-E (TPGS) at both 50 and 100 mg/ml initial concentration, (gold-palladium coated - TESCAN MIRA3 FEG-SEM - UCT CIA). Scale bars are represented on each panel.

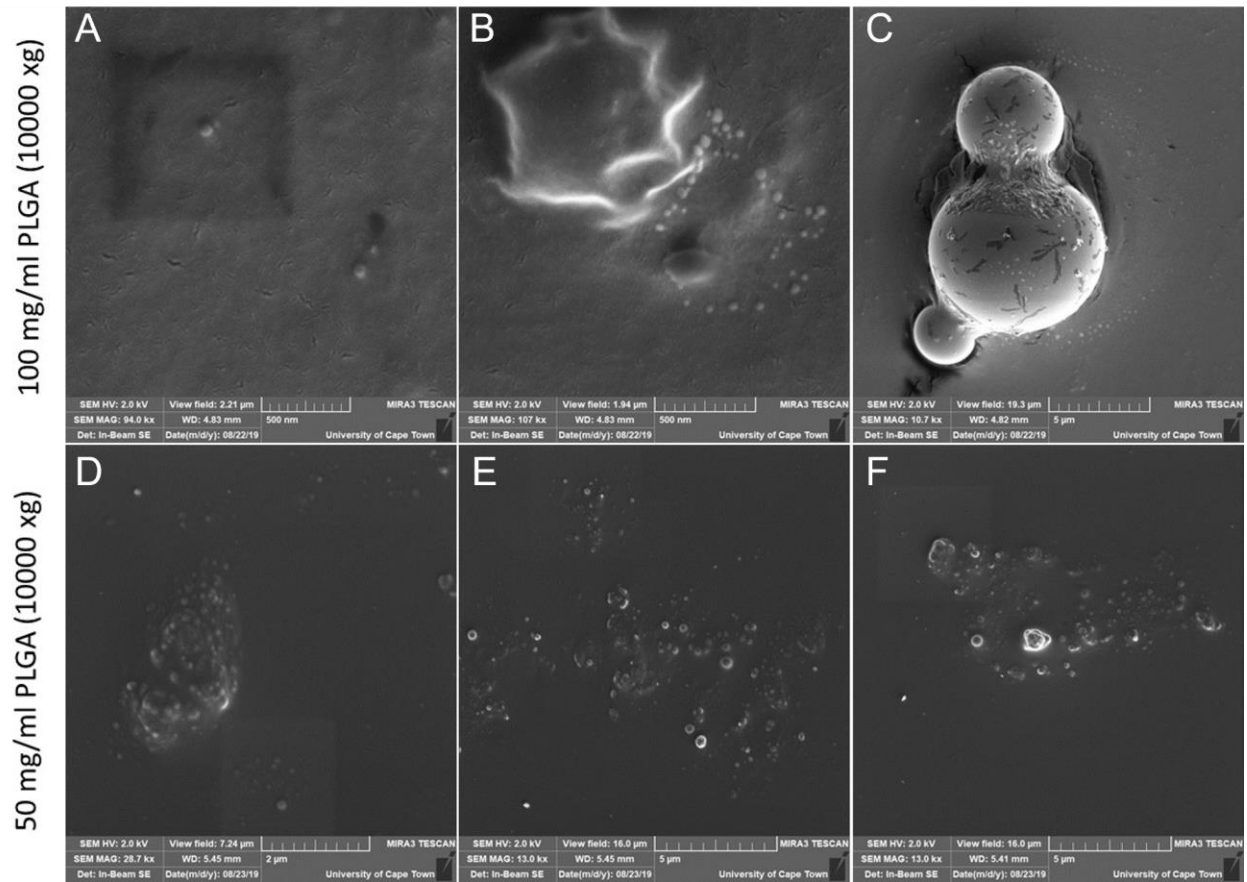


Figure 4.19: PLGA nano-capsules purification by centrifugation at 10 000 xg

This figure shows SEM micrographs depicting 10000 xg isolated PLGA nano-capsules, synthesised using DCM and vitamin-E (TPGS) at both 50 and 100 mg/ml initial concentration, (gold-palladium coated - TESCAN MIRA3 FEG-SEM - UCT CIA). Scale bars are represented on each panel.

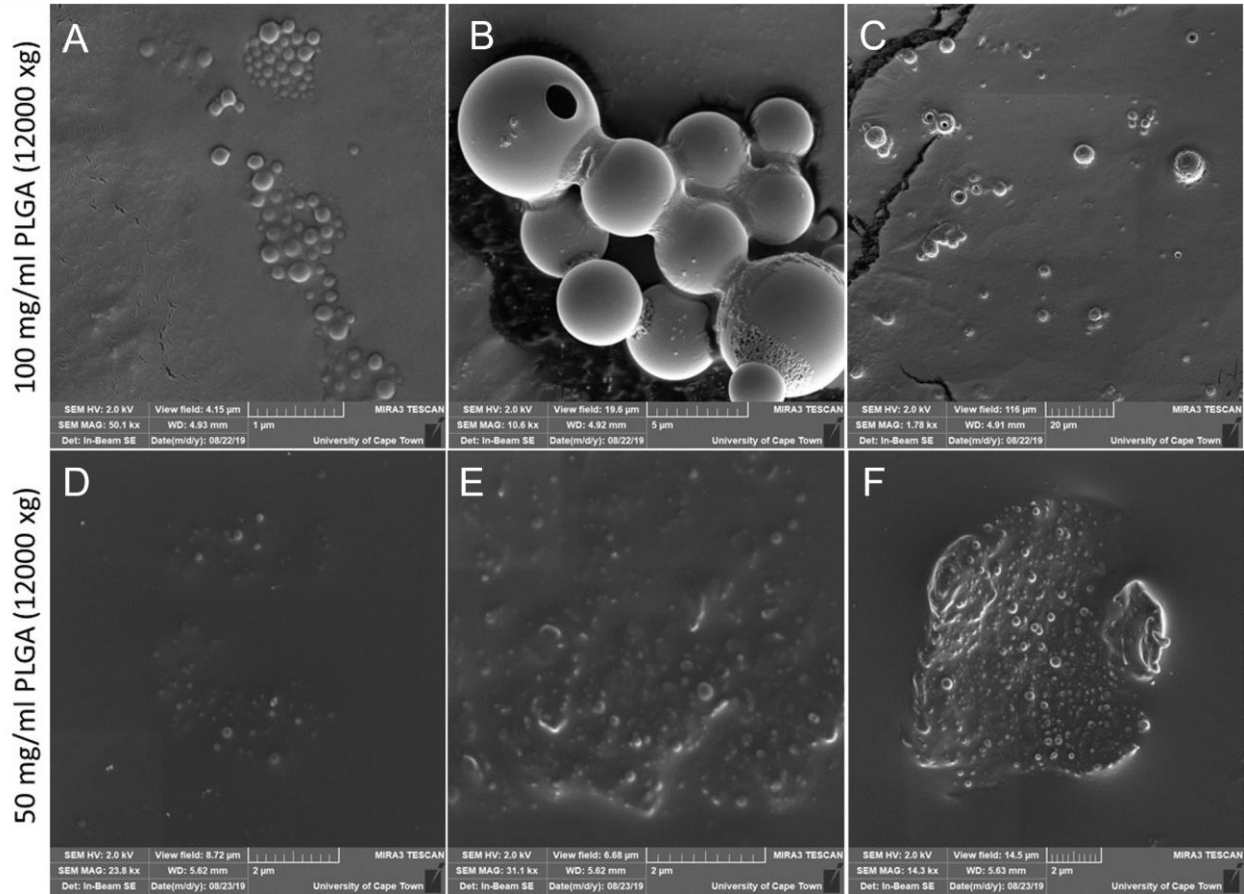


Figure 4.20: PLGA nano-capsules purification by centrifugation at 12 000 xg

In this figure, SEM micrographs show 12000 xg isolated PLGA nano-capsules, synthesised using DCM and vitamin-E (TPGS) at both 50 and 100 mg/ml initial concentration, (gold-palladium coated - TESCAN MIRA3 FEG-SEM - UCT CIA). Scale bars are represented on each panel.

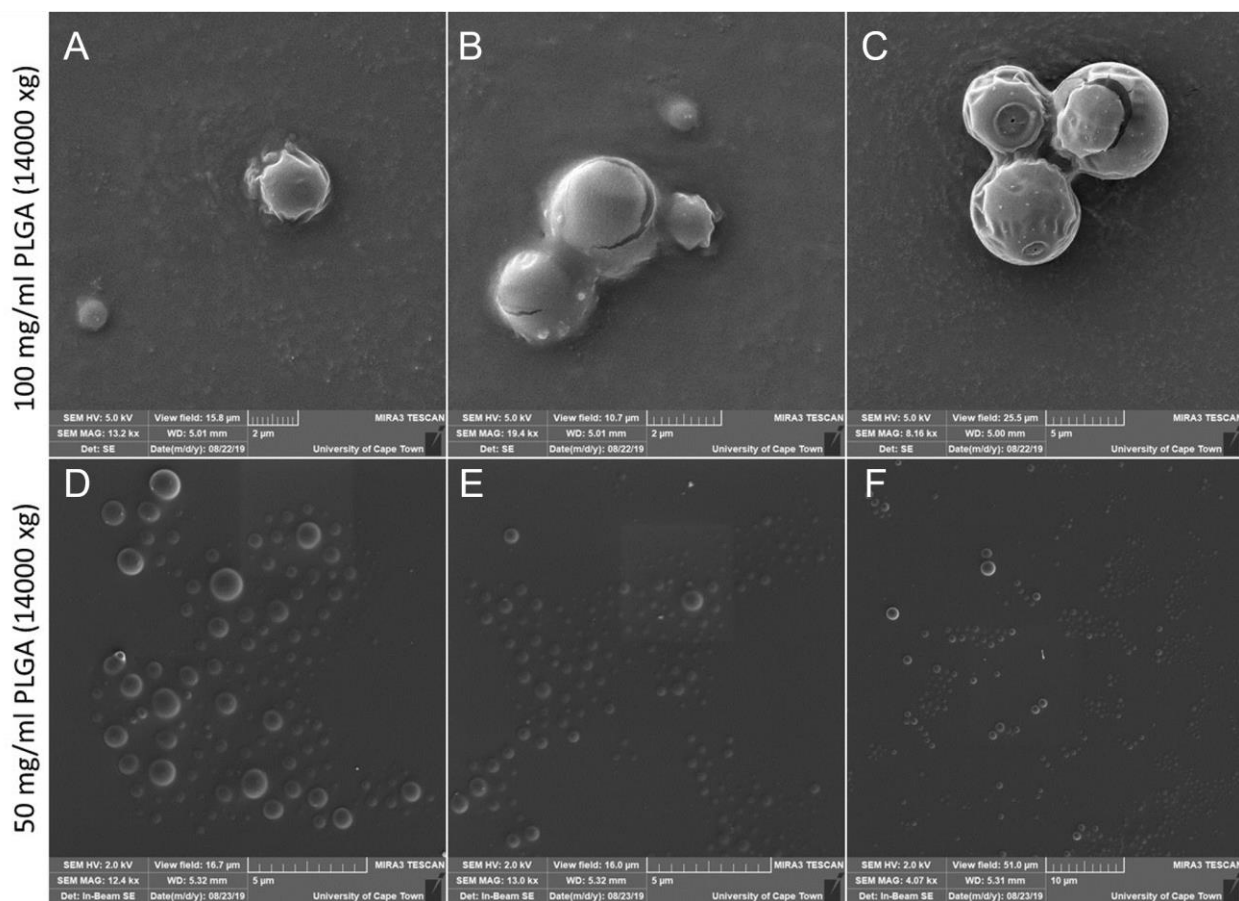


Figure 4.21: PLGA nano-capsules purification by centrifugation at 14 000 xg

SEM micrographs depicting 14000 xg isolated PLGA nano-capsules, synthesised using DCM and vitamin-E (TPGS) at both 50 and 100 mg/ml initial concentration, (gold-palladium coated - TESCAN MIRA3 FEG-SEM - UCT CIA). Scale bars are represented on each panel.

Since the lower initial PLGA (in solvent) concentration (50 mg/ml) consistently produced less polydisperse nano-capsules than the higher concentration (100 mg/ml, as observed in Figure 4.18 - Figure 4.21 all future syntheses were therefore performed using the lower initial in solvent concentration. Additionally, although the desired PLGA nano-capsule size range was successfully isolated using high centrifugation parameters, there was a significant loss of nanoparticles. It was thus decided to attempt low centrifugation isolation, where samples would be centrifuged at 500

xg for 1 minute as well as syringe filtration (0.45 μ l) (Figure 4.22). DCM was also exchanged for EA in the initial PLGA synthesis. This was done, as EA and DCM both produced identical nano-capsules as well as the fact that DCM can lead to protein aggregation and is more cytotoxic to cells (Olvera-Bello et al., 2010). This would be detrimental to the development of a protein-based therapeutic.

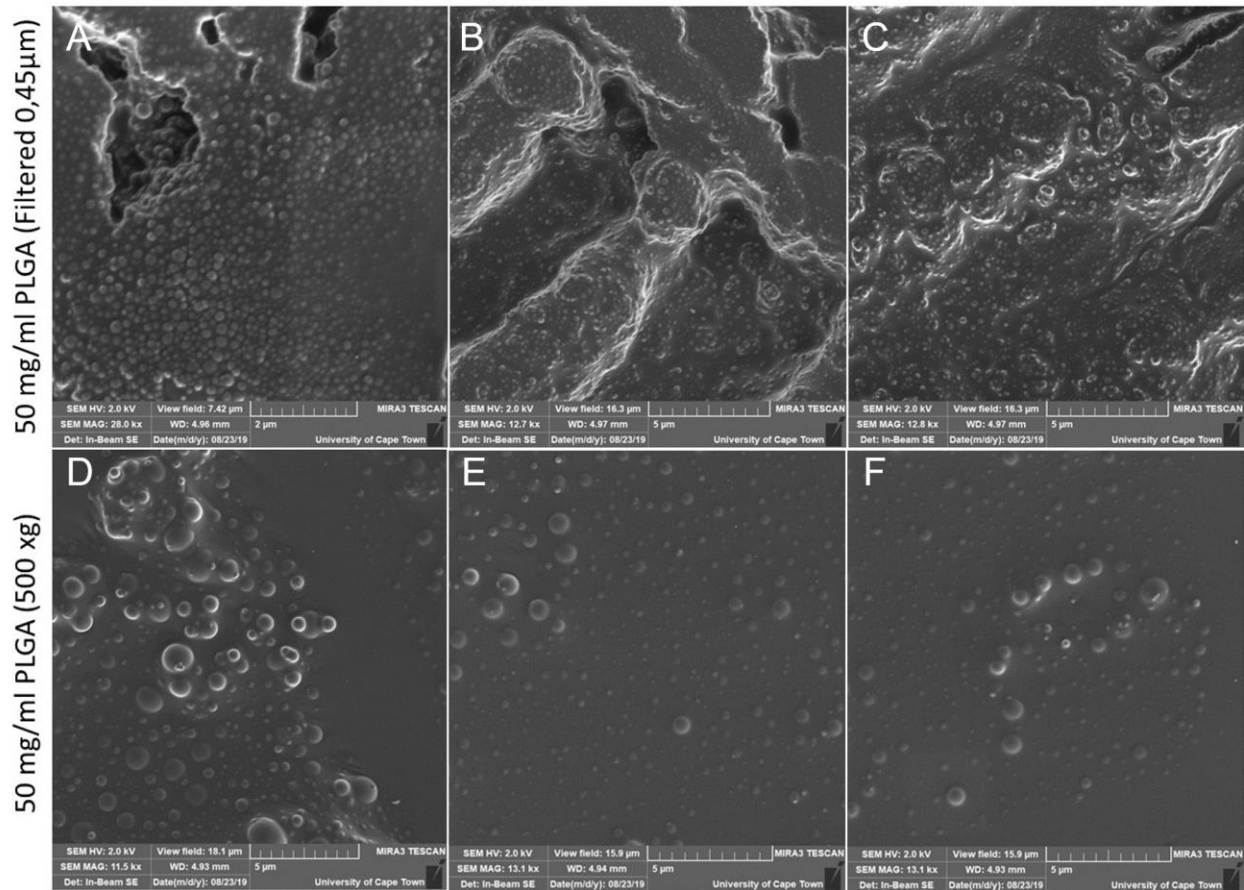


Figure 4.22: PLGA nano-capsules purification by 0.45 μ l filtration and centrifugation at 500 xg

SEM micrographs depicting 0.45 μ l filtered (A-C) and 500 xg isolated (D-F) PLGA nano-capsules, synthesised using EA and vitamin-E (TPGS) at 50 mg/ml initial concentration, (gold-palladium coated - TESCAN MIRA3 FEG-SEM - UCT CIA). Scale bars are represented on each panel.

The 0.45 μ l filtration and 500 xg isolation technique both produced the desired PLGA nano-capsule size range and uniformity. The 500 xg isolation technique, however, resulted in a higher yield than the filtration technique. This resulted due to the filters rapidly becoming clogged and was evident by the reduced opacity of the filtered nanoparticle solution. Therefore, the 500 xg isolation technique was used for future experiments.

The average diameter as well as the polydispersity index (PDI) of the PLGA nano-capsules was determined by dynamic light scattering (Table 4.1). The PDI describes the uniformity of particle size distribution, where values greater than 0.7 indicate a broad size distribution and values below 0.05 are considered monodisperse. This means that, after isolation at 500 xg and PBS purification, the particles do not significantly differ from one another in terms of size as the PDI = 0.38. DLS determines the hydrodynamic size (actual size of the particle in addition to an associated aqueous layer) of the nanoparticles therefore, the reported size would be slightly larger than the actual size. The PDI of the purified PLGA nanoparticles is far lower than that of the un-purified and raw samples which indicates that the size distribution of the nanoparticles is far more uniform after the purification step (nanoparticles resuspended in distilled, RNase-free water).

Table 4.1: DLS results of PLGA nano-capsules

PLGA Sample	Average diameter (nm)	Polydispersity Index
Raw Vit-E TPGS	324.87	0.71
500 xg Vit-E TPGS	200.27	0.79
500 xg PBS Purified	502.80	0.38

Next, a size distribution analysis was performed using the SEM images of raw, 500 xg isolated and PBS washed/purified samples to further confirm the results obtained using DLS (Figure 4.22). The analysis was done using the ImageJ software (National Institutes of Health and LOCI, University

of Wisconsin), and it was found that the nanoparticles had an average diameter of 390 nm, with a standard deviation of 88.5 nm. This therefore confirmed the nanoparticles produced and purified in this way were indeed within the desired size range of 200 – 450 nm.

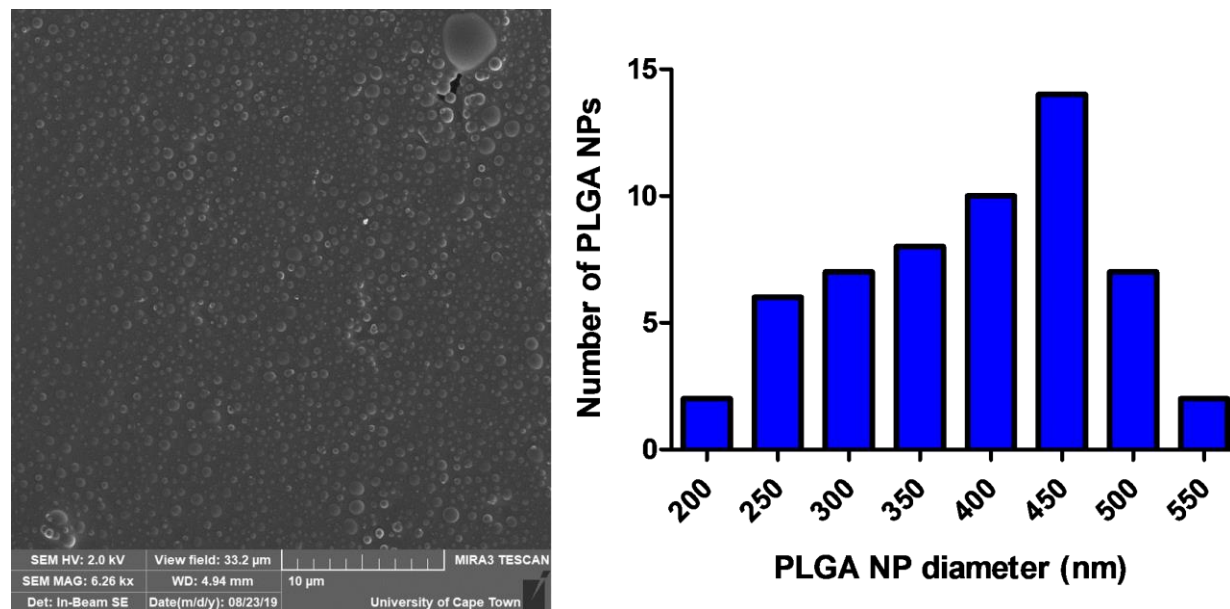


Figure 4.23: Evaluation of the size distribution of PLGA nano-capsules

SEM micrograph of 500 xg isolated PLGA nano-capsules, synthesised using EA and vitamin-E (TPGS) at 50 mg/ml initial concentration (gold-palladium coated - TESCAN MIRA3 FEG-SEM - UCT CIA) was analysed using ImageJ (National Institutes of Health and LOCI, University of Wisconsin) to determine the size distribution. Scale bar represents 10 µm.

4.1.2. The effects of empty PLGA nano-capsules on cell viability

Once the isolation and purification method were optimised, HEK-293 cells were treated with empty PLGA nano-capsules to determine the cytotoxicity of the polymer nanoparticles. Cells were treated with 1, 5 and 10 % (v/v) PLGA nano-capsules, which represents percentage

nanoparticles to total blood volume. Protocatechuic acid (PCA) was used as a negative cell viability control. There was no significant decrease ($p > 0.05$) in cell viability observed in the cells treated with 1 and 5% PLGA, however, a significant decrease ($p \leq 0.05$) of 30.41 % was observed in the cells treated with 10% PLGA. This, therefore, confirms that despite the very high concentrations of the treatments, PLGA nano-capsules have minimal effect on cell viability in the HEK293 cells.

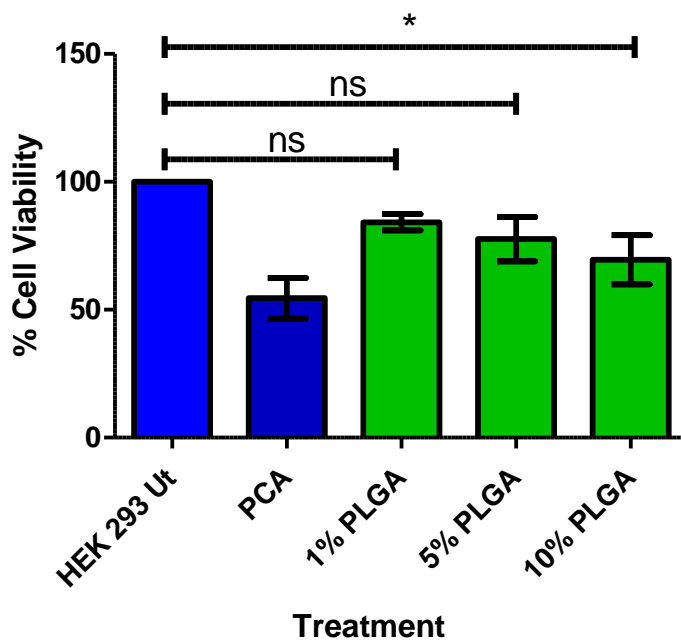


Figure 4.24: HEK-293 cell viability after PLGA nano-capsule treatment

*HEK-293 cells were treated with 1%, 5% and 10% (v/v) by volume of empty PLGA nano-capsules. Although there was some loss of cell viability for the 1 and 5 % treatments, it was non-significant compared to the untreated control with a mean decrease of 15.77 and 22.34 % respectively. At the highest concentration (10 %) there was a significant decrease in cell viability of 30.41 % ($p \leq 0.05$). Error bars represent standard deviation; N=3 biological replicates; ns $p > 0.05$, * $p \leq 0.05$.*

4.1.3. Protein encapsulation using PLGA nano-capsules

Before encapsulating LRP, as the protein was in short supply, GFP (28 kDa - Merck, Darmstadt, Germany) and BSA (68 kDa- Merck, Darmstadt, Germany) were used to optimize the encapsulation procedure. These proteins were ideal for testing, as they are slightly smaller and larger in size to the LRP protein (37 kDa) respectively. This would show the effect of the size of the encapsulated protein on the morphology of the PLGA nano-capsules. The addition of the protein to the PLGA nano-capsules should, however, not impact their size, as the protein is added during the synthesis step and is far smaller (< 20 nm in height (A. K. Wright & Thompson, 1975)) than the nano-capsules (\pm 450 nm). It was observed that the encapsulation of GFP (Figure 4.25, B) and BSA (Figure 4.25, C) within the PLGA nano-capsules produced using the optimised method, was successful and that this did not affect the size or morphology of the nano-capsules in comparison to the empty nano-capsules produced simultaneously (Figure 4.25, A).

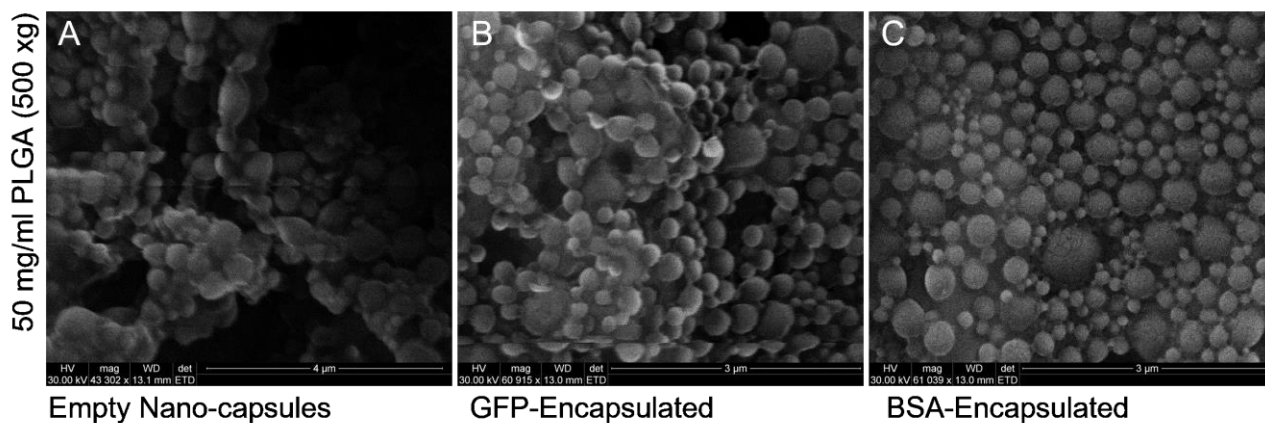


Figure 4.25: Scanning electron micrograph of protein encapsulated PLGA nanoparticles

SEM micrographs depicting 500 xg isolated empty and protein encapsulated PLGA nano-capsules, synthesised using EA and vitamin-E (TPGS) at 50 mg/ml initial PLGA concentration, (carbon coated - FEI Quanta FEG-SEM - Wits MMU). The morphology of an empty nanoparticle control (A) was compared to successfully encapsulated GFP (B) and BSA (C)). Scale bars are represented on each panel.

To confirm successful protein encapsulation, a micro-BCA assay was utilized to confirm the presence of BSA (1 mg) (Figure 4.26) and GFP (0.2 mg) (Figure 4.27). Empty and encapsulated-protein PLGA nano-capsules were concentrated down to 1 ml by centrifugation and then treated with DMSO. This treatment disrupts the polymer shell to release the protein within. Multiple parameters were explored, including DMSO incubation time and wash steps. However, due to protein losses, displayed results were obtained by a 10-minute DMSO incubation. The PLGA encapsulated BSA solution showed a significant 2-fold increase in absorbance compared to the empty nanoparticle solution when measured via the BCA assay (Figure 4.26). This indicates that BSA was successfully encapsulated in the PLGA nanoparticles.

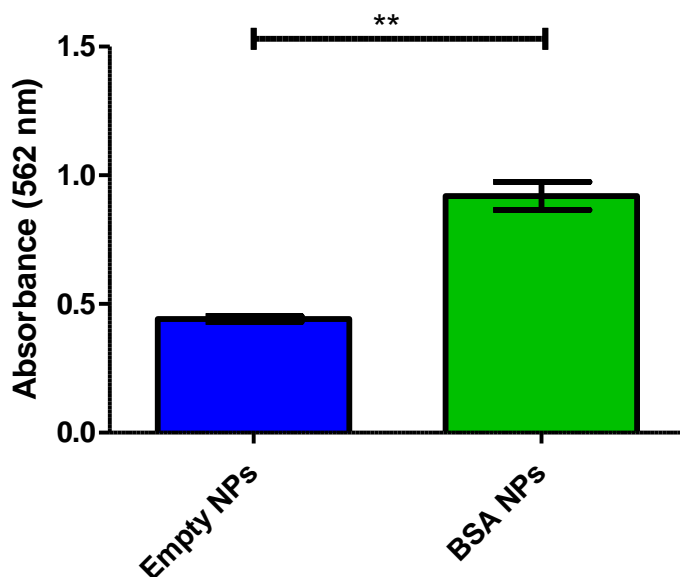


Figure 4.26: BCA assay results of encapsulated-BSA PLGA nanoparticles

A BCA assay was performed on both the empty nanoparticle control as well as the encapsulated-BSA nanoparticles and was analysed using a student's t-test at 95% confidence. A significant difference ($p \leq$

*0.01) was observed between the empty and encapsulated-BSA. Error bars represent standard deviation; N=3 biological replicates; ** $p \leq 0.01$.*

A micro-BCA assay was performed using BSA standards. The average encapsulated-BSA absorbance result (0.478 at 562 nm) was normalised against the empty PLGA nano-capsule control. This was then extrapolated using a standard curve formula to determine the concentration of protein present. It was determined that there was 0.882 mg/ml of BSA within the lysed nanoparticle solution, which therefore indicates an encapsulation efficiency of 88%.

After obtaining the results for the encapsulated BSA samples, the experiments were repeated with 0.2 mg of GFP (Figure 4.27). However, no significant difference was observed between the lysed nanoparticle solution containing GFP and the empty nanoparticles, as well as in the respective supernatants, indicating that the process of encapsulation of GFP was unsuccessful.

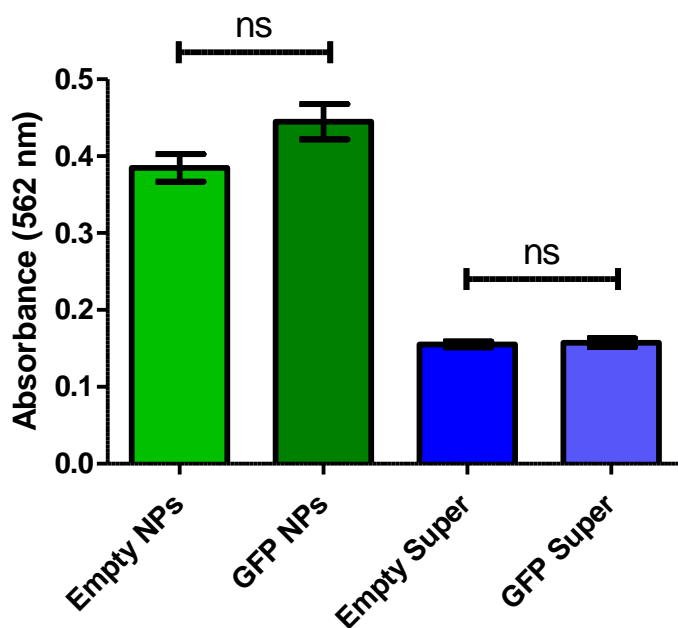


Figure 4.27: Micro-BCA assay results of encapsulated-GFP PLGA nano-capsules

PLGA was used to encapsulate GFP, and a micro-BCA assay was performed on both the empty nano-capsule control as well as the encapsulated-GFP nanoparticles. This was then analysed using a student's t-test at 95% confidence. No significant difference was observed between the empty and encapsulated-GFP. Error bars represent standard deviation; N=3 biological replicates; ns $p > 0.05$.

A micro-BCA assay was performed using BSA standards. The average encapsulated-GFP absorbance result (0.068 at 562 nm) was normalised against the empty PLGA nano-capsule control. This was then extrapolated using a standard curve formula to determine the concentration of protein present. It was determined that there was 0 mg/ml of GFP in the sample, as well as the supernatant, suggesting that the GFP was not detected. Since the amount of protein used in the encapsulation process for BSA was 1 mg, compared to 0.2 mg used in the GFP encapsulation, we therefore suggest that the minimum amount of protein required for encapsulation is 1 mg. This encapsulation could not be repeated at higher concentrations due to the cost of the GFP. In addition, the encapsulation of BSA showed 0.88 mg was encapsulated and present post-purification, therefore showing approximately 0.2 mg is lost in the encapsulation

and purification process. This further suggests that the 0.2 mg used in the encapsulation of GFP was too low an amount and was lost during encapsulation and purification.

4.1.4. LRP protein encapsulation

The results obtained from the optimisation of the BSA and GFP-encapsulation experiments showed that future protein encapsulations require at least 1 mg of protein. This would ensure successful and detectable protein encapsulations. Synthesis and purification of the LRP protein was performed with assistance from the Protein Structure Function Research Unit (PSFRU) at the University of the Witwatersrand (see supplementary section for further details; Figure 7.2 - Figure 7.10). The synthesized LRP protein (1 mg) was then encapsulated in PLGA nano-capsules using the double emulsification solvent evaporation method as detailed in section 3.3.1.1. Multiple encapsulations were performed, and protein was detected after the polymer shell was disrupted using RIPA buffer. Subsequently, a micro-BCA assay was performed to detect the proteins levels and there was a significant 2.5-fold increase in protein levels in the sample containing the LRP encapsulation, when compared to the empty nanoparticle control (Figure 4.30). Therefore, indicating that LRP was successfully encapsulated into the PLGA nanoparticles.

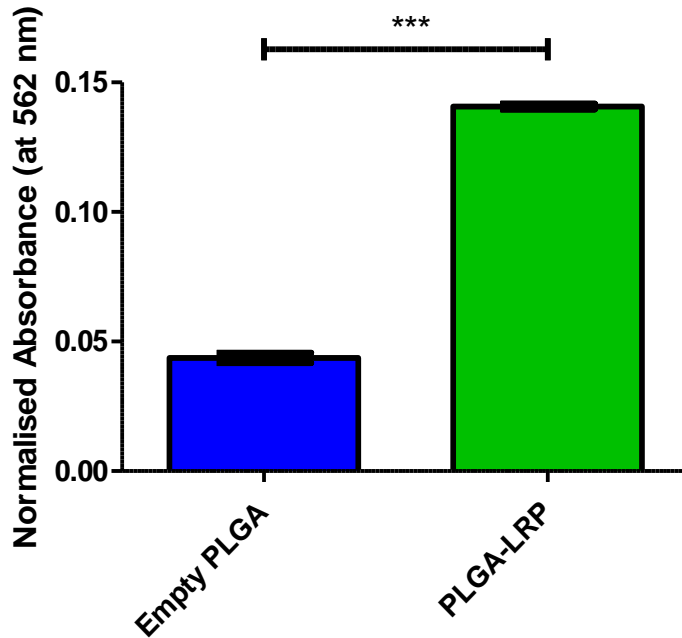


Figure 4.28: Micro-BCA assay results of empty and encapsulated-LRP PLGA nanoparticles

*Micro-BCA protein quantification assay was performed on both empty and encapsulated-LRP PLGA nano-capsules after polymer shell disruption via RIPA buffer. The LRP was detected at a wavelength of 562 nm and the absorbance was significantly higher ($p \leq 0.001$) than the empty PLGA control. This data was analysed using a student's t-test at 95% confidence interval. This served as confirmation of LRP encapsulation within PLGA nano-capsules. Error bars represent standard deviation; $N=3$ biological replicates; *** $p \leq 0.001$.*

A micro-BCA assay was consequently performed using BSA standards. The average encapsulated-LRP absorbance result (0.141 at 562 nm) was normalised against the empty PLGA nano-capsule control. This was then extrapolated using the standard curve formula ($y = 0.1763x$, $R^2 = 0.9717$) to determine the concentration of protein present in the nano-capsule solution. Here, it was observed that 0.798 mg/ml LRP protein was successfully encapsulated into the PLGA nano-capsules, therefore indicating an encapsulation efficiency of 80%.

4.1.5. Effect of encapsulated LRP treatments on total LRP levels, cell viability and telomerase activity

It has previously been shown that overexpression of LRP causes an increase in telomerase activity (Bignoux et al., 2019; Bodnar et al., 1998; Cuttler et al., 2020; Otgaar et al., 2017) and to confirm this trend, HEK-293 cells were treated with LRP encapsulated in the PLGA nano-capsules. Total LRP levels were assessed for cells treated with 1, and 5% empty and PLGA encapsulated LRP after a 48h treatment and compared to an untreated control. Subsequently, an MTT assay was performed to assess the effect of the treatment on cell viability.

Western blots were performed to determine whether the encapsulated-LRP nanoparticle treatments would increase the total endogenous LRP within the treated cells (Figure 4.29). A significant increase in LRP levels was detected in both the 1 % and 5 % encapsulated-LRP samples (22 % and 25 % increase respectively). Conversely, however, a decrease in LRP levels was detected for the empty 1 % sample (20 % decrease).

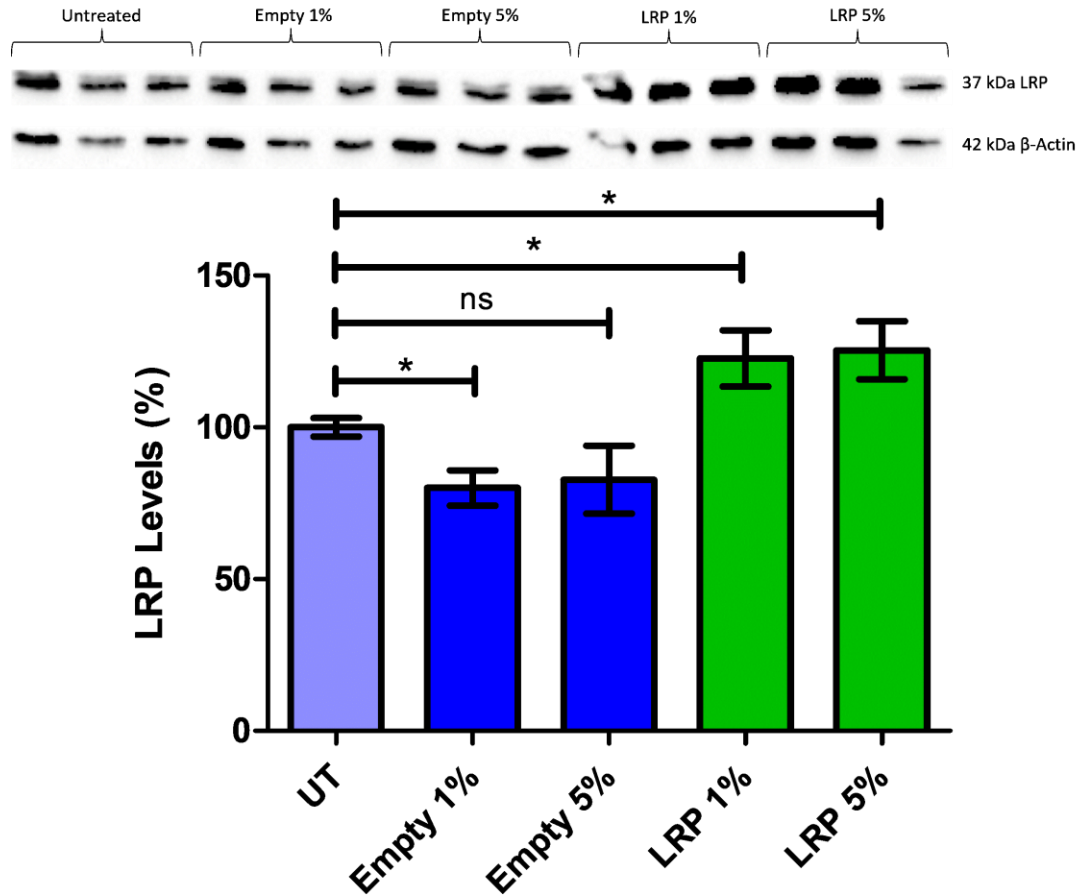


Figure 4.29: Western blot analysis of encapsulated-LRP PLGA nanoparticle treatments on HEK-293 cells

Western blots were performed to determine the total LRP protein levels in both untreated and PLGA nano-capsule treated HEK-293 cells. The band density of the 37 kDa LRP was compared to a 42 kDa β-actin control using Image Lab 4.0 - Bio-Rad. LRP levels of the treated samples were then compared to the untreated control (set to 100 %). Error bars represent standard deviation; N=3 biological replicates; ns $p > 0.05$.

To determine if the nano-capsule treatment did, however, have an effect on the cells, an MTT cell viability assay was performed. The encapsulated LRP treatment caused a significant increase in viability compared to the untreated control at all concentrations, whereby the 1, 5 and 10 % LRP-nanoparticle treatments increased cell viability by 49.64 %, 51.93 %, and 30.82 %

respectively. (Figure 4.30). Interestingly, the 10% treatment showed a significant increase, despite the empty nano-capsule treatment normally reducing viability at this concentration. Despite this, the 10 % nanoparticle treatment was removed from future experiments due to the slight toxicity of the empty nano-capsule treatment previously observed (Figure 4.24), as well as the cost of producing sufficient LRP protein for this treatment concentration. Furthermore, this treatment represents a concentration far in excess of what would be considered for therapeutic use *in vivo* (treatment/blood volume).

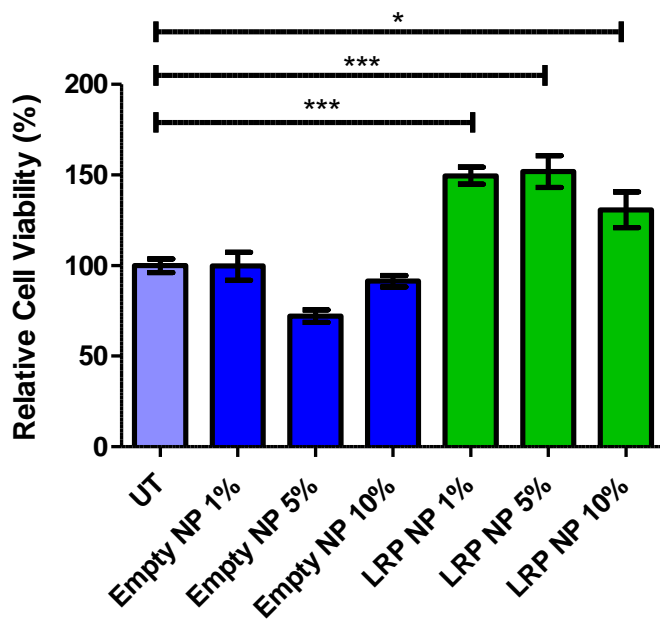


Figure 4.30: Improved cell viability after LRP-nanoparticle treatment *in vitro*

HEK-293 cells were treated with 1, 5, and 10 % of both empty and encapsulated-LRP PLGA nanoparticles and an MTT assays were performed. The 5 % empty nano-capsule treatment significantly decreased cell viability, while 1, 5 and 10 % LRP-nanoparticle treatments increased cell viability by 49.64 % ($p \leq 0.001$), 51.93 % ($p \leq 0.001$), and 30.82 % ($p \leq 0.05$) respectively. Error bars represent standard deviation; N=3 biological replicates; * $p \leq 0.05$, *** $p \leq 0.001$.

To further confirm that the encapsulated LRP treatment has a similar effect to LRP::FLAG overexpression described previously, the TRAPEze® RT Telomerase Detection Kit (Merck, Darmstadt, Germany) was used to measure relative telomerase activity of the untreated and treated samples. It was observed that the LRP treatment indeed increased telomerase activity by 24.85% and 46.56% in the HEK-293 cells treated with 1% and 5% LRP-PLGA nanoparticles, respectively (Figure 4.30). This corroborates previous findings in which LRP protein overexpression studies also found a significant increase in telomerase activity (Bignoux et al., 2019; Cuttler et al., 2020; Otgaar et al., 2017). This, furthermore, confirms the efficacy of using the LRP encapsulated in PLGA nanoparticles.

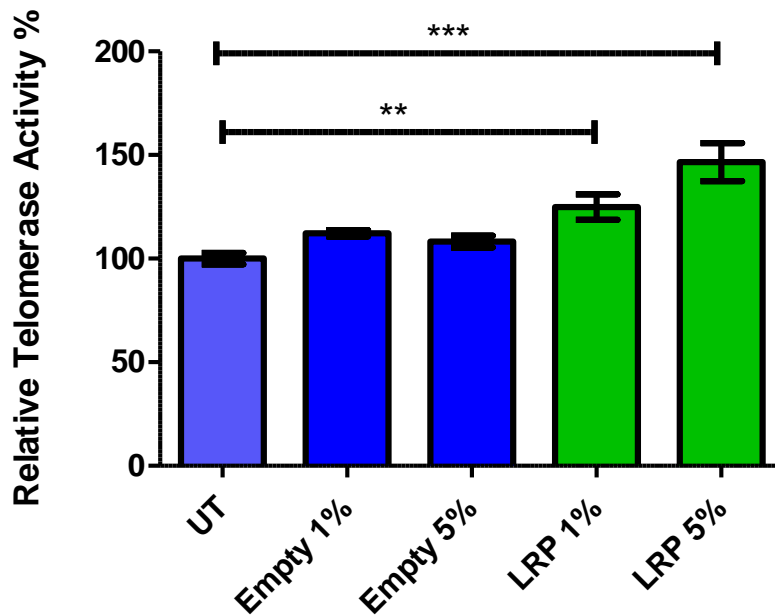


Figure 4.31: LRP-nanoparticle treatment elevates telomerase activity *in vitro*

HEK-293 cells were treated with 1 and 5 % (v/v) of both empty and encapsulated-LRP PLGA nanoparticles. qPCR was used in conjunction with the TRAPEze® RT Telomerase Detection Kit (Merck, Darmstadt, Germany) was used to determine the effects of the PLGA treatments on telomerase activity. The empty nanoparticle control treatments did not have any significant effect on telomerase activity whereas, the

*encapsulated-LRP treatments increased telomerase activity for both 1% and 5% treatments by 24.85 % (** $p \leq 0.01$) and 46.56 % ($p \leq 0.001$) respectively. Error bars represent standard deviation; N=3 biological replicates; ** $p \leq 0.01$, *** $p \leq 0.001$.*

The PLGA-encapsulated LRP treatment (Figure 4.34) showed that telomerase activity significantly increased for both the 1 and 5 % treatments (24.85 % and 46.56 % respectively), while both empty nanoparticle treatments did not. This indicates that using the PLGA nanoparticles to encapsulate LRP as a therapeutic, is effective and produces the desired results.

5. Discussion

5.1. Section 1: AuNP-based telomerase activity assay

AuNPs have very interesting optical properties, as the colour of the nanoparticle solution can change based on their size and proximity to one another (Yarbakht & Nikkhah, 2016). Exploiting this property of the nanoparticles, a colourimetric assay was designed to detect telomerase activity. The previous work of Wang et al. was used as a basis for this assay, and subsequent modifications were made in order to simplify and speed up the workflow. AuNP-based assays have utilised this property to detect the presence of proteases, as cleaved proteins do not induce nanoparticle aggregation whereas intact proteins do. This leads to a detectable colour change for samples containing proteases (Guarise et al., 2006). Additionally, this has also been used for the detection of cancer cells, by functionalising AuNPs to DNA aptamers specific to certain cancer cells. In the presence of the target cells, the functionalised AuNPs attach to the cell surface and the solution colour shifts from red to blue (Medley et al., 2008). For this study, we aimed to design a new, cost-effective colourimetric telomerase activity assay, utilising DNA-functionalised AuNPs. Telomerase activity has been implicated in a variety of disease pathologies such as cancer, where telomerase activity is elevated in 80-90 % of cancers to bypass replicative senescence (Shay & Wright, 2005). In age-related diseases, such as CVD shortened telomeres have been implicated in the degradation of blood vessels (Serrano & Andrés, 2004). Finally in neurodegenerative diseases, such as Alzheimer's disease, an increase in TERT levels is thought to decrease A β shedding and concomitantly intracellular A β levels (Bignoux et al., 2019). Due to these multiple associated diseases, telomerase activity is therefore an important subject of study.

5.1.1. Synthesis and characterisation

A AuNP-based telomerase activity assay was designed using functionalised gold nanoparticles to determine telomerase activity in cell extracts. For this purpose, gold nanoparticle synthesis had to be optimised to consistently form AuNPs within the desired size range of roughly 14 nm in diameter, as nanoparticles of this size would form a red-coloured solution. To do this, temperature and reducing agent concentration were tested using the chemical hydrothermal metal salt reduction method. Figure 4.1. From these initial reactions, it is evident that the colour of the AuNP colloid solution does indeed change due to the size of the AuNPs, as the first reactions produced blue-purple-coloured solutions (Figure 4.1, A-C), where the nanoparticles were in the size range of 50-300 nm in diameter. This was accompanied by variations in morphology, most notably in Figure 4.1-A where large gold rods and triangles were present as well as in Figure 4.1-B where the particles were notably oblong instead of spherical (Figure 4.1). Through multiple attempts at creating a crimson coloured AuNP solution, it was found that the gold chloride solution needed to be brought to a boil before rapidly adding 2 ml of 10 mg/ml sodium citrate (reducing agent). This produced the most consistently crimson-coloured solutions, containing small spherical nanoparticles, ideal for downstream applications (Figure 4.1, E). This may be due to the rapid reducing agent addition causing multiple simultaneous nucleation events, compared to more sporadic nucleation. This would ensure that the AuNPs would be unable to “grow” beyond the desired size range, as all atomic gold would have been consumed. Conversely, slower, more sporadic nucleation would likely result in larger nanoparticle formation with more varied morphology (Polte et al., 2010).

After the optimisation of AuNP synthesis, the AuNPs were characterised using spectrophotometry and TEM as described in section 3.2.4. Multiple batches of AuNPs were prepared and spectra were obtained from 400 to 700 nm (Figure 4.2). This range was chosen, as it would encompass the peak absorbance, which is known to be the surface plasmon resonance, of the AuNPs of approximately 520 nm (Polte et al., 2010). It was observed that the spectra of the three batches closely overlap, suggesting a consistent synthesis method resulting in solutions of similarly sized AuNPs. The resulting distinct peaks shown in all batches suggest that the

nanoparticles have a relatively low polydispersity, further confirming that optimisation of this synthesis method was successful. It is important to maintain low polydispersity to ensure subsequent uniform DNA functionalisation as well as nanoparticle stability. Furthermore, absorbance ratios of 610 nm/520 nm were obtained, where 610 nm represents the theoretical peak absorbance of the DNA-functionalised AuNPs. The ratio of each batch was compared (Figure 4.3) and the results were consistent.

Furthermore, TEM images were obtained of each batch and the nanoparticle diameter determined using the ImageJ software (Figure 4.4). TEM showed that the AuNPs were of similar size and shape (Figure 4.4, A-C). ImageJ analysis further confirmed that the AuNPs had an average diameter of 14 nm with a standard deviation of only 0.936 nm. This size is important as the nanoparticle solution produced a deep red colour. Therefore, this optimised protocol was used for all subsequent synthesis reactions.

5.1.2. DNA functionalisation

The initial AuNP-based telomerase activity assay was modified from that used by (Wang et al., (2012) who functionalised AuNPs by using a thiol-modified telomerase substrate (Table 3.2) as shown in the schematic diagram (Figure 4.5). The addition of an unprotected thiol group to the DNA was to aid in the attachment to the nanoparticles, as the thiol group is able to easily adsorb to gold (Cárdenas et al., 2006). DNA functionalisation was accomplished as described in section 3.2.2 in order to attach the synthetic telomerase substrate to the AuNPs. After functionalisation, a clear DNA halo was seen around the AuNPs (Figure 4.6, B) compared to the non-functionalised AuNP control (Figure 4.6, A). After the addition of the extracted telomerase (as described in section 3.2.3), there was a rapid change in the colour of the solution, similar to that seen when inducing AuNP aggregation. These AuNPs were subsequently viewed under TEM (Figure 4.6, C) and indeed the AuNPs were found to have aggregated. This aggregation was most likely caused when the functionalised AuNPs were exposed to the protein extract, as intact proteins can cause aggregation (Guarise et al., 2006). This suggests that the attached DNA did not confer enough

stability to the nanoparticles to prevent aggregation. Methods such as dilution, resuspension, and sonication were employed in an attempt to reverse it. This was done despite the possibility of DNA shearing, as it is believed that with non-excessive sonication, DNA will not shear if smaller than 300 bp (Sambrook & Russell, 2006). None of these methods proved able to adequately reverse this aggregation, therefore an improvement to the AuNP-based telomerase activity assay was conceptualised.

The improved AuNP-based telomerase activity assay (Figure 4.7) made use of two separate DNA strands compared to single strand of the original concept (Figure 4.5). The improved concept utilises a thiolated linker strand as well as a complimentary extension strand (Table 3.2). The longer DNA as well as the double stranded section were included to resist aggregation, as it has previously been shown to improve AuNP stability by preventing the close association of the AuNPs (Zhao et al., 2007).

The AuNPs were then functionalised using the pH-dependant method as described in section 3.2.2 and the resulting AuNPs characterised using spectrophotometry (section 3.2.4). A spectrum was taken for the functionalised and non-functionalised AuNPs (Figure 4.9), which showed a distinct shift in the peak wavelength from 520 nm to around 650 nm after functionalisation, from red to a bluer solution colour. This shift in absorbance peak may be due to the increased distance between the functionalised nanoparticles caused by the addition of DNA to the nanoparticle surface (Wang et al., 2012). The DNA-functionalised sample was also shown to have a shoulder at 520 nm, corresponding to the unmodified AuNP peak. This shoulder represents the fraction of unmodified AuNPs present in the solution, as it corresponds to the surface plasmon resonance of AuNPs (Polte et al., 2010). Additionally, comparing the $A_{610/520}$ ratio (Figure 4.10), showed a distinct difference between the modified and un-modified AuNP samples.

Additionally, TEM micrographs of DNA-functionalised and non-functionalised AuNPs were compared (Figure 4.11) to determine the effect of the functionalisation on the AuNPs. There was a clear DNA halo present (Figure 4.11, B) around multiple AuNPs which is not present in the unmodified AuNP sample (Figure 4.11, A). This further confirmed that DNA functionalisation was

successful. Therefore, the functionalising of the nanoparticles was optimised, and the assay was ready to be tested on *in vitro* samples.

In addition to these improvements, it was also noted that the functionalised AuNPs of the improved assay concept have the potential to be reused, as the extension strand could be decoupled from the linker strand by simple thermal denaturation. The elongated extension strand could then be removed (by centrifugation), amplified by PCR and resolved on a gel to generate a single telomere length analysis (STELA)-like pattern. In addition, a new extension strand could be annealed to the thiol-DNA modified AuNPs, making the nanoparticles potentially reusable. This would not only allow for a simple colorimetric telomerase activity assay, but also potentially allow for a quantitative STELA-like analysis to be performed. Testing and optimising this, however, was beyond the scope of this study.

5.1.3. AuNP-based telomerase activity assay

5.1.3.1. *Initial telomerase activity results*

The AuNP-based telomerase activity assay was performed and compared to the commercially available TRAPeze® RT Telomerase Detection Kit (Merck, Darmstadt, Germany). Initially, the AuNP-based telomerase activity assay was performed on HEK-293, and heat-treated HEK-293 (Figure 4.12). The heat treatment inactivated the majority of the telomerase present in the sample and therefore acted as a negative control. The $A_{610/520}$ ratio was recorded every 5 minutes for both samples and the results showed that the HEK-293 sample clearly had an elevated reading compared to the negative control. In fact, the results resembled an enzyme activity profile where the HEK-293 sample readings were consistently higher than that of the heat-treated control. The results were fitted to a non-linear regression, which resulted in a very good fit with an R^2 value of 0.9893. This initial result was very promising, as the assay was able to successfully distinguish between heat-inactivated and functioning telomerase in the samples. Further experimentation was carried out on WHCO-5 (oesophageal cancer) cells, as oesophageal cancer cell lines have previously been shown to have high telomerase activity (Figure 7.1).

5.1.3.2. *Comparing telomerase activity results to a commercially available kit*

HEK-293 and WHCO-5 cells were treated with 4 μ M of the MST-312 telomerase inhibitor as well as 10 mM metformin for a period of 48h as described in section 3.1.5. Metformin was chosen, as it had previously been shown to reduce telomerase activity in oesophageal cancer cells (Figure 7.1). Samples were analysed using both qPCR via the TRAPeZe[®] RT Telomerase Detection Kit (Merck, Darmstadt, Germany) (Figure 4.13), as described in section 3.1.8.1 and the AuNP-based telomerase activity assay (Figure 4.14) as described in section 3.2.3 and compared. The qPCR results showed that both the inhibitor and metformin treatment significantly decreased telomerase activity in both cell lines (80 % and 55 % reduction as well as a 62 % and 52 % reduction for HEK-293 and WHCO-5 cell lines respectively). These results were used as a baseline to evaluate the capabilities of the AuNP-based telomerase activity assay. The AuNP-based telomerase activity assay, however, was only able to detect a significant difference between the treatments and the heat-treated controls ($p \leq 0.001$), as well as an 18 % decrease between the untreated and 10 mM metformin treated HEK-293 samples. Interestingly, the assay showed greater differences between the treated and heat treated WHCO-5 cells. This may be due to the WHCO-5 cell line possessing a comparatively high telomerase activity to that of the HEK-293 cell line, as cancerous cells typically have elevated telomerase activity (Cesare & Reddel, 2010). However, the assay was unable to detect a significant difference between the majority of paired untreated and treated samples. This, in conjunction with the results seen in Figure 4.14, where the AuNP-based telomerase activity assay was only able to detect differences between samples and their telomerase heat-inactivated controls, suggests that the assay is indeed able to detect telomerase activity, but currently lacks the sensitivity necessary to distinguish between samples with similar telomerase activity. One explanation could be that this may be due to the limitations of the spectrophotometer being used. In an effort to improve the overall speed of the AuNP-based assay, simple plate readers were primarily considered due to the ability to multiplex readings as well as the low volumes (50 μ l) needed to acquire spectrophotometric readings. This could make it difficult to distinguish between more similar readings, as the absorbance of the AuNP solution may not shift enough to be easily detectable. Another possibility is the low

reaction volume, as the colour shift is more noticeable at higher volumes. An increase in the volume of functionalised AuNPs as well as an increased incubation time could allow for increased sensitivity, to better detect differences between samples with similar levels of telomerase activity, as it would allow for the extracted telomerase to further elongate the extension strand (Wang et al., 2012) and potentially reduce the effects of interfering cell lysate components. Furthermore, it is possible that the overall length of the linker-extension strand construct is preventing telomerase from binding or reducing the colourimetric effects of the elongation of the extension strand. It has also been suggested that the formation of a G-quadruplex structure, which occurs in both this AuNP-based assay and that of Wang et al. (2012), may hinder the sensitivity of the assay (Duan et al., 2014). Any of these scenarios could explain the lack of sensitivity but it is most likely that the lack of sensitivity is due to a combination of the above possibilities. Even though the assay lacked sensitivity, the addition of the linker strand did improve the assay by reducing the nanoparticle aggregation (Figure 4.6 vs Figure 4.11), which could allowed the telomerase to interact with the extension strand more easily. Therefore, future work could include testing linker strands with different lengths to improve sensitivity.

Besides this assay and that designed by Wang et al. (2012), other researchers have utilised AuNPs for the detection of telomerase activity. Most similar is a concept where a thiolated DNA telomerase extension strand as well as a thiolated DNA “reporter” probe are functionalised to the AuNPs. This additional reporter probe is complimentary to the telomeric repeats added by telomerase to the extension strand. This leads to the formation of DNA crosslinks between two or more functionalised AuNPs. After the addition of salt, low telomerase activity samples aggregate, whereas the crosslinks prevent aggregation. This causes the low telomerase activity samples to blue-shift and the high activity samples to red-shift, which is detected via UV-vis spectroscopy (Duan et al., 2014). This method is able to avoid the potential reduction in sensitivity due to the G-quadruplex formation, as the elongated extension strands should be captured by the reporter probe before formation. A potential flaw, however, is that since telomeric repeats are short, this could lead to the possibility for the extension strand to be prematurely captured by the reporter probe, resulting in a false reduction in reported telomerase activity or even false negative results. Another assay uses an opposite colour change strategy to

determine telomerase activity compared to that of the AuNP-based telomerase activity assay described by Wang et al, (2012) and Duan et al. (2014). This assay begins in a multi-DNA probe solution containing AuNPs. An extension strand is elongated by telomerase, which results in the disruption of a partial probe duplex as one half preferentially binds to the elongated strand. This causes the now free single stranded (displacement) probe to disrupt a hairpin probe. This allows the single stranded region of the disrupted hairpin probe to further disrupt a second hairpin probe and hybridise with it, forming a duplex structure with a sticky end. This once again releases the free (displacement) probe, which can initiate another displacement reaction. The sticky end of the duplex structure is then cleaved using exonuclease 1 and the assembly is confirmed by PAGE. The non-duplexed hairpin probes adsorb to the AuNPs, whereas the duplex structures do not, conferring a resistance against aggregation after the addition of salt. This means that the higher the telomerase activity, the more duplex structures form, the less resistance to aggregation the solution has, resulting in a blue-shift in UV-vis spec (Huang et al., 2021). This assay has some advantages over the previous assays, as it does not require the formation of secondary structures on the AuNPs, which could hinder the binding efficiency of telomerase. Conversely, however, a “runaway” displacement reaction could lead to false positive results, making the exact data acquisition time crucial, especially when comparing data from different runs.

5.1.4. AuNP section conclusion

In conclusion, although the sensitivity of the AuNP-based telomerase activity assay is currently lower than that of a conventional qPCR-based assay, however, telomerase activity was successfully detected in both HEK-293 and WHCO-5 cells. Furthermore, this work has secured a patent (South Africa patent No. WO/2019/116334) and has been evaluated by external experts through a technological feasibility study. Cancers utilise telomerase to prevent DNA damage responses such as senescence or apoptosis and hence drive cancer progression (Cesare & Reddel, 2010; Shay & Keith, 2008). Additionally, since telomerase is implicated in a variety of age-related

diseases (Bignoux et al., 2019; Cuttler et al., 2020; Otgaar et al., 2017), this confirms that telomerase activity is an important field of study. This, therefore, represents a promising focus for future development of the assay. Therefore, although more work needs to be completed to finalise and rigorously evaluate the AuNP-based telomerase activity assay, it is a very promising alternative to the currently available telomerase activity assays.

5.1.5. Future research for the AuNP-based telomerase activity assay

Future work will include improving the sensitivity of the assay, as there are some improvements that could be made to the AuNP-based telomerase activity assay. Firstly, the sensitivity of the assay will be improved. This could be achieved by increasing the reaction volume and incubation times for the assay. Furthermore, the assay could be performed using more sensitive spectrophotometric equipment to determine if any smaller changes can be detected. Although one of the initial aims of this work was to develop a cheaper alternative to the expensive qPCR-based telomerase activity assays, the reaction size could also be increased to improve detection, while remaining more cost effective than the alternatives. This is a feasible goal, as the cost per reaction of the TRAPeze® RT Telomerase Detection Kit (Merck, Darmstadt, Germany) was calculated to be 560 % higher than that of the current iteration of the AuNP-based assay. Additionally, this assay will be compared to other commercially available kits. Secondly, the assessment of the potential additional functions of the assay discussed in section 3.2.2, could lead to the addition of a quantitative STELA-like analysis as well as the reusability of the functionalised AuNPs. This would lead to more accurate results and decrease the overall cost of the assay.

5.2. Section 2: LRP-encapsulated PLGA nano-capsules

The elevation of LRP has been shown to have therapeutic effects in ageing and neurodegenerative disease models (Bignoux et al., 2019; Cuttler et al., 2020). However, transfection is not a viable treatment option *in vivo*, as this leads to immunogenic response and so PLGA nano-capsules were chosen to become the drug delivery system for the therapeutic protein due to the biocompatibility and biodegradability of PLGA. PLGA has been studied for the treatment of a multitude of diseases including cancer (targeted chemotherapeutic delivery system), diabetes (insulin carrier), bacterial infections (antibiotics) vaccines, dissolvable stitches and many others (Danhier et al., 2012; McCall & Sirianni, 2013). In this study, LRP was successfully encapsulated within hollow PLGA nano-capsules and the effect on cell viability, LRP levels and telomerase activity was determined in HEK-293 cells.

5.2.1. Optimisation of synthesis

Multiple optimisations were performed for both synthesis and purification of the PLGA nano-capsules, which resulted in a consistent production method. The double emulsion solvent evaporation technique was used to produce a high yield of uniform PLGA nano-capsules of the desired size (200-450 nm in diameter). The purpose of this study was to optimise a polymer nanoparticle synthesis method for the creation of an LRP-based drug delivery system. For this optimisation, several different PLGA synthesis methods were tested to determine the best method to produce consistently sized nano-capsules.

Both PVA and Vitamin-E (TPGS) were initially tested as emulsifiers. The use of PVA produced an inconsistent size distribution and therefore, after purification and removal of micro-particles, had far reduced yield compared to the reactions performed with vitamin-E (TPGS) (Figure 4.17). Additionally, multiple synthesis reactions using PVA resulted in the formation of long polymer filaments, resembling a fine web. This “spiderwebbing” resulted in a large decrease in nano-

capsule yield and even caused non-hardened nanoparticles to adhere to the filaments, further decreasing the recoverable yield. After purification of these samples, the recovered nano-capsules were too few in number to be used for downstream applications. This could be due to the concentration of the PVA, as it has been found that increasing PVA concentration increases the viscosity of the solution. This can lead to larger, more inconsistent nanoparticle formation (Shokoohinia et al., 2019). This would corroborate later observations where decreasing the viscosity of the dissolved PLGA solution improved the consistency of the synthesised nano-capsules Figure 4.17. This inconsistency coupled with the high cost and time investment needed to produce the LRP protein meant that any wastage of the protein due to inconsistent synthesis could have significantly disrupted the study. Therefore, vitamin-E (TPGS) was used as the emulsifier for future experiments.

The PLGA polymer can be solubilised in a variety of solvents, including DCM and EA (McCall & Sirianni, 2013). These compounds are water-immiscible and are able to dissolve the polymer in preparation for emulsion (Astete & Sabliov, 2006). However, each compound has its upsides and drawbacks. Initially, each solvent was tested under the same conditions (section 3.3.1.1, initial PLGA concentration of 100 mg/ml), to evaluate the resulting nano-capsules. Both EA and DCM were used to successfully synthesise PLGA nano-capsules, using an initial PLGA concentration of 100 mg/ml. However, DCM seemed to produce the desired nanoparticles more consistently than EA. This seems to contrast with (Sahana et al., 2008) who found that EA produced the most consistent and stable nanoparticles. This was thought to be due to the viscosity and interface tension of EA, as it has a comparable viscosity and a far lower interface tension than DCM (1.7 and 28.3 dyne/cm respectively) (Sahana et al., 2008). Despite this, DCM was initially used as the primary solvent due to the results obtained in the current study. Next, the effect of initial PLGA concentration (solvent:polymer ratio) on nano-particle synthesis was tested.

After the PLGA was dissolved in the primary solvent (DCM), the resulting solution was rapidly added to a vitamin-E (TPGS) solution. It was observed, however, that the dissolved polymer took more than 5 minutes to form an emulsion with the vitamin-E (TPGS). It was therefore theorised that doubling the solvent volume, while keeping the amount of PLGA polymer consistent, would lead to more rapid and consistent synthesis as well as nanoparticle size distribution. It was

inferred that a decrease in viscosity of the dissolved polymer would allow for more rapid formation of an emulsion due to more effective vortexing and sonication. Indeed, there seems to be a consensus that the viscosity of the initial polymer/solvent solution is vital for the formation of low-polydisperse PLGA nano-capsules (Sahana et al., 2008; Shokoohinia et al., 2019). Therefore, both a 50 and 100 mg/ml initial PLGA (in DCM) concentration were tested. As expected, the lower initial concentration led to a preferable and consistent nano-capsule size distribution (Figure 4.17).

5.2.2. Purification of PLGA nano-capsules

After the optimisation of the nano-capsule synthesis, various centrifugation parameters (8000 xg, 10000 xg, 12000 xg, 14000 xg, and 500 xg for 5 minutes) as well as syringe filtration (0.45 μm) were tested to isolate and purify nano-capsules of the desired size (under 450 nm) (section 3.3.1.1). These centrifugation parameters were chosen to remove larger particles found in the subsequent pellet and retain smaller nanoparticles within the supernatant. Due to the nanometer size range of the particles, it was postulated that the high centrifugation speeds would still retain the desired nano-capsules while removing the vast majority of larger particles. Two batches (50 and 100 mg/ml initial PLGA (in solvent) concentration) of PLGA nano-capsules were aliquoted into multiple vials, each of which were then used to test the centrifugation parameter. This was done to ensure that the results would not be influenced by any differences between syntheses. After centrifugation, the supernatant of each sample was viewed using SEM (section 3.2.4 with amendment in 3.3.1.1).

The PLGA nano-capsules isolated at 8000 xg (Figure 4.18) showed a significant decrease in particle polydispersity compared to the raw sample (Figure 4.17), however, this was accompanied by a substantial decrease in the overall numbers of nano-capsules observed. This could be due to the sample containing a higher proportion of larger nanoparticles compared to the lower initial PLGA (in solvent) concentration sample and those nanoparticles being removed via centrifugation. The nanoparticles produced using the 100 mg/ml initial PLGA solution

exhibited a greater size distribution (Figure 4.18. A-C) than that of the nanoparticles produced using the 50 mg/ml initial PLGA solution (Figure 4.18, D-E). This initially corroborates the hypothesis that a lower initial PLGA (in solvent) concentration would lead to a corresponding increase in particle size uniformity. This too was the case for the 10000 xg (Figure 4.19), 12000 xg (Figure 4.20) and 14000 xg (Figure 4.21) isolation attempts. It can therefore be seen that although the high centrifugation speed can isolate nano-capsules of the desired size, it comes at an overall considerable loss in nano-capsule yield. This can be seen both under the SEM and by the naked eye, through a reduction in opacity in the nano-capsule suspension. Furthermore, the lower initial PLGA (in solvent) concentration (50 mg/ml) consistently produced less polydisperse nano-capsules than the higher concentration (100 mg/ml) (Figure 4.18-Figure 4.21). This once again confirms that the viscosity of the initial (Sahana et al., 2008; Shokoohinia). It was thus decided to attempt low centrifugation isolation, where samples would be centrifuged at 500 xg for 5 minutes as well as syringe filtration (0.45 μm). Additionally, through further review of the literature, it was found that DCM could potentially cause protein aggregation (Olvera-Bello et al., 2010). Since the LRP protein would be in short supply and would have to be added to the PLGA/DCM solution during the first step of the double emulsion reaction, there could be a risk of inactivating the added LRP protein. To avoid this potential pitfall, EA was revisited as a candidate for the synthesis of the PLGA nano-capsules. It was determined that, at the 50 mg/ml initial PLGA (in solvent) concentration, previous inconsistencies in synthesis using EA (at 100 mg/ml initial PLGA concentration) were no longer apparent and the nano-capsules produced were of a more consistent size and morphology (Figure 4.17), which as mentioned before. Furthermore, since isolation via centrifugation will only separate the particles by size and weight alone, the solvent used in the synthesis reaction should not have any effect on the isolation of the nano-capsules. Therefore, it was assumed that the previous isolation results would be analogous for all syntheses using EA instead of DCM.

After the isolation by high centrifugation resulted in significant loss of yield, both centrifugation at 500 xg and 0.45 μm filtration was attempted. Both methods successfully removed large nano-capsules and isolated the desired smaller nano-capsules from the solution Figure 4.22. It was evident that both techniques showed significantly more uniform nano-capsule size distribution

than was seen with the high centrifugation particle isolation techniques. The overall yield for both techniques was also substantially improved over the previous isolation attempts. The filtered sample (Figure 4.22, panels A-C), however, showed a reduced yield compared to the 500 xg isolated sample (Figure 4.22, D-E). This was due to the filters rapidly becoming clogged, which prevented smaller nanoparticles from passing through. This was confirmed by the number of particles seen in the electron micrographs as well as the opacity of the resultant nanoparticle solution. Additionally, despite having very uniform nanoparticle size distribution, the filtered sample contained far smaller nano-capsules than that of the 500 xg isolated sample. These nanoparticles (± 200 nm in diameter) were in the lower end of the desired size range of around 450 nm in diameter. Interestingly, the size of the PLGA nano-capsules has been found to be a significant contributor to the bioavailability and distribution of the therapeutic construct. It has been found that smaller nanoparticles (>10 nm in diameter) are more likely to be rapidly removed by the body through the kidneys (Owens & Peppas, 2006), whereas larger particles (>200 nm in diameter) can become more concentrated in the spleen, liver, bone marrow and lungs (Moghimi et al., 2012). Medium sized nanoparticles (± 100 nm in diameter) on the other hand have been found to circulate in the blood for longer periods than larger nanoparticles, as they do not get trapped in these organs as easily, however, can have a larger initial release of the therapeutic compound (Huynh et al., 2010; Moghimi et al., 2012; Owens & Peppas, 2006). This means that without targeting molecules or surface modifications, PLGA nanoparticles can be made to target relatively specific sets of organs or be designed for a prolonged release through size alone. For this reason, the size and consistency of the nano-capsules would need to be strictly controlled. Due to these factors, the 500 xg isolation technique was used for future experiments.

5.2.2.1. *DLS and Size Distribution*

Samples of PLGA nano-capsules, isolated by centrifugation at 500 xg, were analysed by DLS (Table 4.1). DLS obtains both the average diameter of the nanoparticles, as well as their PDI. Isolated, purified (resuspended in RNase-free water) nanoparticles were compared to isolated, non-purified and raw nanoparticle samples. The raw nanoparticle sample had an average diameter of 324.87 nm and a PDI of 0.71, whereas the 500 xg isolated sample had an average diameter of

200.27 nm and a PDI of 0.79. This suggests that the isolation procedure does indeed remove many of the larger nanoparticles present in the solution, however, with a PDI of over 0.7, these solutions were considered polydisperse. After a purification step, however, the average diameter increased to 502.8 nm and the PDI decreased to 0.38. This improvement in the PDI suggests that the purification step further reduces the size distribution of the sample. The increase in average diameter is most likely due to the loss of small nanoparticles in the supernatant during the removal of the vitamin-E (TPGS). This is supported by the presence of nanoparticles in the supernatant of the 14000 xg centrifugation experiment (Figure 4.21). Furthermore, a PDI of 0.38 is considered to be relatively low for polymer nanoparticles such as PLGA. This means that the initial synthesis (raw sample) was successful and a subsequent 500 xg isolation, followed by a purification step, significantly improved the polydispersity of the nanoparticle solution. Additionally, a size distribution of the diameter of the purified PLGA nano-capsule sample was performed by analysing SEM images using the ImageJ software (National Institutes of Health and LOCI, University of Wisconsin) (Figure 4.23). The average diameter was found to be 390 nm with a standard deviation of 88.5 nm. This size disparity between the average diameter obtained by DLS (502.8 nm) and that obtained by SEM could be partially explained by the fact that DLS measures hydrodynamic size whereas SEM closely represents the actual size of the nano-capsules. Hydrodynamic size is considered to be the actual size of the particle in addition to an associated aqueous layer which surrounds the particle. This would mean that the reported size of the nanoparticles, via DLS, would be slightly larger than the actual size of the nanoparticles.

5.2.3. Protein encapsulation trials

Due to the cost and time required to produce the LRP protein, the optimisation of protein encapsulation was first performed on more readily available proteins: GFP and BSA. These trials were performed in order to determine if the addition of the protein would affect the size and morphology of the synthesised nano-capsules. Furthermore, these proteins were chosen because of their similar size to LRP (37 kDa), to approximate the effect of encapsulating LRP more

accurately. The encapsulation of GFP (28 kDa - Merck, Darmstadt, Germany) and BSA (68 kDa - Merck, Darmstadt, Germany) would therefore additionally show the effect of the size of the encapsulated protein on the morphology of the PLGA nano-capsules. A protein in water suspension was prepared with 0.2 mg of GFP and 1 mg of BSA respectively, and these were used to perform a successful encapsulation, using the double emulsion solvent evaporation method described in section 3.3.1.1. It was seen that, compared to the empty nano-capsule control (Figure 4.25, A), the encapsulation of GFP (Figure 4.25, B) and BSA (Figure 4.25, C) did not seem to significantly affect the size and morphology of the resultant nano-capsules. This was assumed to be the case, as the size of the encapsulated proteins are far smaller than that of the nano-capsules, with the largest (BSA) being less than 20 nm in height (A. K. Wright & Thompson, 1975), compared to the average diameter of the nano-capsules being approximately 400 nm.

To confirm successful encapsulation of BSA and GFP, a micro-BCA assay was performed on the extract from these nanoparticles, which were concentrated down to 1 ml and disrupted using DMSO as described in section 3.3.2. BCA assay results of the encapsulated BSA PLGA nanoparticles (Figure 4.26) clearly showed the presence of protein compared to the empty nanoparticle control. Additionally, BSA standards were created, and the sample readings compared to the resultant linear regression. Through this comparison, it was determined that the BSA protein concentration was 0.882 mg compared to the 1 mg of added BSA (88.2 % encapsulation efficiency). This encapsulation efficiency is relatively high, as there is an inevitable loss of protein through the removal of larger particles by centrifugation as well as subsequent purification steps. In fact, it is comparable to that of (Amini et al., (2017) who encapsulated BSA and obtained an encapsulation efficiency of 81-89 %. This encapsulation efficiency could also partially be the result of the larger nano-capsule size range of about 450 nm in diameter, as BSA is far smaller (< 20 nm in height (A. K. Wright & Thompson, 1975)) than the nanoparticles and therefore, more protein can be encapsulated. These tests were repeated on the 0.2 mg of encapsulated GFP (Figure 4.27), however, no difference was detected between the empty nanoparticles and the encapsulated GFP samples. This is suggested to have been due to the low amount of protein added to the initial encapsulation reaction in addition to the expected losses through isolation and purification steps, which may have resulted in values below the detectable

threshold of the assay. Based on these results, it was decided to use 1 mg LRP protein during subsequent encapsulation of LRP.

Subsequent to the completion of the initial protein encapsulation trials, 1 mg of newly purified LRP was encapsulated in PLGA nano-capsules using the double emulsion solvent evaporation method, and micro-BCA assays were performed as described above. The results showed a significant difference between the empty nano-capsule control and the encapsulated LRP sample (Figure 4.28), which confirmed the presence of protein in the sample. Additionally, as with the encapsulated BSA nanoparticles, the encapsulated LRP sample was compared to a set of known BSA standards and compared to the resultant linear regression. The micro-BCA assay confirmed that there was approximately 0.798 mg LRP present in the concentrated sample out of the initial 1 mg added (79.8 % encapsulation efficiency). This would once again suggest a high encapsulation efficiency, comparable to that of the encapsulated BSA trial and that seen in previous studies (Amini et al., 2017).

5.2.4. LRP-PLGA nano-capsule treatments

5.2.4.1. *The effects of PLGA nano-capsule treatments on cell viability*

Once the optimisation of the synthesis, isolation, and purification of the PLGA nano-capsules was completed, the cytotoxicity of the empty nano-capsules was evaluated in HEK-293 cells by MTT assay. HEK-293 cells were treated with PCA (positive cell death control) as well as 1, 5 and 10 % (v/v) empty PLGA nano-capsules to the cell culture media. This treatment represents percentage blood volume of an organism, as a comparison to intravenous treatment, and were chosen to assess the minimum concentration at which the treatments become cytotoxic. The 10 % treatment was intentionally made to be far in excess of what would normally be considered for treatment, in order to determine a maximum dosage. Treatments were then compared to an untreated control. All treatments were performed in (biological) triplicate, and three technical replicates were performed per treatment to ensure accuracy. Here treatment with 1 and 5 % (v/v) empty PLGA nano-capsules did not significantly decrease cell viability compared to the non-treated control (Figure 4.24). The 10 % (v/v) treatment, however, did significantly decrease cell

viability with a relative decrease of 30.41 % ($p = 0.0211$) compared to the control. At this treatment concentration, however, the number of nanoparticles present visibly clouded the media and settled on the adherent cells. This could have led to a decreased area in which the cells could migrate to or even caused contact inhibition, preventing cell proliferation rather than decreasing cell viability. Interestingly, (Derman et al., (2017) showed that treating L929 cells (mouse fibroblast) with empty nanoparticles at very high concentrations (0.5 mg/ml) resulted in a decrease of 30 % cell viability. The 10 % empty PLGA treatment mirrors this outcome almost exactly. Nevertheless, the 1 and 5 % treatments confirm that the empty PLGA nano-capsules have no significant effect on cell viability and the 10 % treatment only minimally affected it. Altogether, this confirms that the PLGA nanoparticles are non-toxic, at concentrations lower than 5 %, and can be used as a delivery vehicle for the LRP protein *in vivo*.

Following the confirmation of LRP encapsulation HEK-293 cells were then treated with both empty and encapsulated LRP nanoparticles at 1, 5 and 10 % (v/v) as previously described. The 1 and 10 % empty nano-capsule treatments did not significantly affect the cell viability, however, the 5 % empty nano-capsule treatment significantly decreased cell viability (Figure 4.30). This was not seen in any previous experiments and could have been due to experimental error and will therefore need to be repeated in future work to confirm the results. On the other hand, the 1, 5 and 10 % encapsulated LRP treatments significantly improved cell viability for the HEK-293 cells by 49.64 % ($p < 0.0001$), 51.93 % ($p < 0.0001$), and 30.82 % ($p = 0.0105$) respectively. This was a very interesting result, as it corroborates previous observations, where an increase in LRP::FLAG was observed to increase cell viability (Bignoux et al., 2019; Otgaar et al., 2017). Additionally, despite the empty 10 % PLGA treatment decreasing cell viability, the 10 % encapsulated LRP treatment caused an increase in cell viability. Despite the increase being lower than that of the 1 and 5 % encapsulated LRP treatments, this may be due to a variety of factors, such as the recently discovered link between LRP and telomerase activity, where an increase in LRP::FLAG expression resulted in a concomitant increase in telomerase activity (Otgaar et al., 2017). This increase in telomerase activity may lead to a rescuing effect from cellular senescence (Otgaar et al., 2017) and therefore resist the decrease in cell viability seen in the 10 % empty nano-capsule treatment.

5.2.4.2. *The effects of encapsulated LRP treatments on total endogenous LRP levels*

Western blots were performed on the empty PLGA nano-capsule and encapsulated LRP treated HEK-293 cells (Figure 4.29). Due to the toxicity observed with the 10 % empty PLGA nano-capsule treatment, and since this treatment is far in excess of what would be considered for a treatment in a physiological setting, it was not included in subsequent experiments. It was expected that the encapsulated LRP treatments would increase the overall LRP levels within the cells. A band density analysis showed a significant increase for both the 1 and 5 % encapsulated LRP treatments (22 % and 25 % increase respectively). This result shows that the treatment increases overall LRP levels. Strangely, a 20 % decrease in LRP levels was also detected in the 1 % empty nano-capsule treatment. This could be due to surface interactions with the nano-capsules or degradation of the surface LRP after cellular inclusion of the nano-capsules. It is also important to note that it has previously been shown that the PLGA nanoparticles undergo a random degradation due to hydrolysis in an aqueous environment, such as cell culture media, which creates a slow-release profile (Makadia & Siegel, 2011). This could therefore cause the LRP-PLGA treatments to release the encapsulated LRP slowly over time. The overall LRP levels may, therefore, not be drastically elevated at any given time, but rather slightly elevated for longer periods. Future experiments would therefore include a drug release profile and a long-term leakage study to provide further information.

5.2.4.3. *The effects of encapsulated LRP treatments on Telomerase activity*

Since we have previously observed an increase in telomerase activity in cells overexpressing LRP::FLAG, telomerase activity was subsequently evaluated in the HEK-293 cells after encapsulated LRP treatments. This was done using the TRAPeze® RT Telomerase Detection Kit (Merck, Darmstadt, Germany) and was performed as described in section 3.1.8.1. The results of the RT qPCR (Figure 4.31) revealed that telomerase activity significantly increased for both the 1 and 5 % encapsulated LRP treatments, with a respective increase of 24.85 % ($p=0.002$) and 46.56 % ($p<0.0001$), while both the 1 and 5 % empty nano-capsule treatments did not significantly affect telomerase activity. This corroborates our previous findings in which LRP protein overexpression studies also found an increase in telomerase activity (Otgaar et al., 2017)

and mirrors the increase seen in overall LRP levels. Altogether, this indicates that using the PLGA nanoparticles as a delivery vehicle by encapsulating the LRP therapeutic, is effective, and produces results following the same trend as previously observed. This will therefore allow for further research into using LRP as a therapeutic *in vivo*.

5.2.5. PLGA section conclusion

In conclusion, the creation of a PLGA-based drug delivery system for the purposes of delivering a therapeutic protein was successful. Both synthesis of the nanoparticles and encapsulation of the LRP protein were successfully optimised and the completed drug was tested in a cell culture model. It was shown that the LRP drug treatment significantly increased LRP levels and subsequently increased cell viability, as well as telomerase activity, as previously observed using the LRP::FLAG construct (Bignoux et al., 2019; Otgaar et al., 2017). Therefore, this LRP drug delivery system has great potential to assist in the translation of our *in vitro* studies into an *in vivo* context, which will ultimately aid in the treatment of age-related diseases including neurodegenerative diseases and cardiovascular disease. This work is also covered in the South Africa patent: WO2020008442A3.

5.2.6. Future research for the LRP-encapsulated PLGA nano-capsules

Although much of the optimisation has already been completed, efforts will be made to improve the drug delivery system. Firstly, additional encapsulation efficiency assays will be performed to corroborate existing data. This would include multiple additional protein encapsulations and the testing of different compounds for the disruption of the PLGA polymer shell. Additionally, experiments will be carried out to determine if the protein is attaching to the outside of the PLGA nano-capsules as well as whether the proteins are being incorporated into the polymer shell. This could be partially accomplished by salting out, as the salt concentration increases, any proteins

on the outside of the nano-capsules should become detached. A long-term protein leakage test, as well as a release profile, will also be performed, whereby encapsulated protein nanoparticles will be incubated over a period of multiple weeks and periodically samples will be removed and tested using a micro-BCA assay. This will allow to determine the amount of protein that has naturally leaked out of the nano-capsules over time. Optimisation of the upscaling of both LRP protein production and PLGA nano-capsules will need to be done, as well as the evaluation of this drug delivery system for other therapeutic compounds, such as siRNA. Additionally, by using confocal microscopy it would be possible to view the exact method of nano-capsule internalisation by a cell through live cell imaging. This in conjunction with flow cytometry could add valuable insights to the absorption efficiency of the of the LRP-based drug. Lastly, this work has been successful in cell culture models and could potentially be used in animal studies. If the treatment is required to target specific tissues or organs, the nano-capsules could be modified for this purpose. This could include controlling the size of the nanoparticles, as this can influence where the nano-capsules concentrate in the body. Or this could include surface modification, in the form of PEGylation and target molecule functionalisation, which would specifically target the desired tissue type.

5.3. Conclusion

Telomere dynamics, specifically telomerase activity, have been implicated in a variety of age-related diseases, such as CVD, Alzheimer's disease, and cancer. This makes the accurate detection of telomerase activity within cell cultures and tissue samples a necessity. In this novel assay the extracted telomerase leads to a colour change in the solution through the action of telomerase. This colour change, and therefore telomerase activity, is then detected by spectrophotometry. The AuNP-based telomerase activity assay developed during this research, was able to successfully detect telomerase activity in HEK-293 and WHCO-5 cells. However, there is still room for improvement, as the assay does not yet possess the sensitivity found in qPCR-based telomerase activity assays. This could be due to a variety of reasons, including the sensitivity of the equipment used as well as the assay requiring additional optimisation in sample volume and

extracted telomerase concentration. Further validity tests on the effects of the longer linker-extension strand construct must be performed to ensure that it is not interfering with the colour shift of the AuNP solution or telomerase binding efficiency. The goal of improving the sensitivity of this assay is therefore achievable and would provide a very promising, cost-effective alternative telomerase activity assay for use in age-related disease research. This assay, however, is not limited to age related diseases, but can easily be used for any telomerase-related research field as a general telomerase activity assay. A secured patent as well as external evaluation of the technology, through a technical feasibility report, further supports that the AuNP-based telomerase activity assay has the potential of becoming a valuable tool for research.

Previous research has shown that telomerase activity is directly affected by the LRP protein, which has been shown to have therapeutic effects in Alzheimer's disease models. This is theorised to be partially due to a protective role conveyed by telomerase after being elevated by increased LRP levels. Previously this increase in LRP levels has been achieved by plasmid transfection, which is not an ideal treatment option, therefore, a protein-based therapeutic option was developed. However, to deliver a protein-based drug, a delivery system had to be designed. Utilising PLGA nano-capsules as a delivery method was ideal since the nano-capsules would protect the therapeutic agent from degradation and would facilitate the safe uptake into cells without the LRP being degraded early via natural immune responses. The creation of this PLGA-based drug delivery system for the purposes of delivering LRP as a therapeutic compound was successful as both synthesis of the nano-capsules and encapsulation of the LRP protein were successfully optimised. The encapsulated LRP drug was tested in a cell culture model, and it was shown that the treatment significantly increased LRP levels, cell viability, as well as telomerase activity in HEK-293 cells. This corroborates similar findings with LRP::FLAG-plasmid transfection experiments. Due to the wide range of applications elevating LRP levels has in the treatment of different disorders, this LRP-based drug delivery system could ultimately aid in the treatment of age-related diseases including neurodegenerative diseases and cardiovascular disease, through its ability to increase telomerase activity.

6. References

- Alaouna, M., Hull, R., Penny, C., & Dlamini, Z. (2019). Esophageal cancer genetics in South Africa. *Clinical and Experimental Gastroenterology*, *12*, 157. <https://doi.org/10.2147/CEG.S182000>
- Amini, Y., Amel Jamehdar, S., Sadri, K., Zare, S., Musavi, D., & Tafaghodi, M. (2017). Different methods to determine the encapsulation efficiency of protein in PLGA nanoparticles. *Bio-Medical Materials and Engineering*, *28*(6), 613–620. <https://doi.org/10.3233/BME-171705>
- Arnal, M. J. D., Arenas, Á. F., & Arbeloa, Á. L. (2015). Esophageal cancer: Risk factors, screening and endoscopic treatment in Western and Eastern countries. *World Journal of Gastroenterology : WJG*, *21*(26), 7933. <https://doi.org/10.3748/WJG.V21.I26.7933>
- Arnold, M., Soerjomataram, I., Ferlay, J., & Forman, D. (2015). Global incidence of oesophageal cancer by histological subtype in 2012. *Gut*, *64*(3), 381–387. <https://doi.org/10.1136/gutjnl-2014-308124>
- Astete, C. E., & Sabliov, C. M. (2006). Synthesis and characterization of PLGA nanoparticles. In *Journal of Biomaterials Science, Polymer Edition* (Vol. 17, Issue 3, pp. 247–289). VSP BV. <https://doi.org/10.1163/156856206775997322>
- Bailey, S. M., & Murnane, J. P. (2006). Telomeres, chromosome instability and cancer. *Nucleic Acids Research*, *34*(8), 2408–2417. <https://doi.org/10.1093/nar/gkl303>
- Bentzon, J. F., Otsuka, F., Virmani, R., & Falk, E. (2014). Mechanisms of plaque formation and rupture. *Circulation Research*, *114*(12), 1852–1866. <https://doi.org/10.1161/CIRCRESAHA.114.302721>
- Berno, V., Porrini, D., Castiglioni, F., Campiglio, M., Casalini, P., Pupa, S. M., Balsari, A., Mé Nard, S., & Tagliabue, E. (2005). The 67 kDa laminin receptor increases tumor

- aggressiveness by remodeling laminin-1. *Endocrine-Related Cancer*, 12, 393–406.
<https://doi.org/10.1677/erc.1.00870>
- Bignoux, M. J., Cuttler, K., Otgaar, T. C., Ferreira, E., Letsolo, B. T., & Weiss, S. F. T. (2019). LRP::FLAG Rescues Cells from Amyloid- β -Mediated Cytotoxicity Through Increased TERT Levels and Telomerase Activity. *Journal of Alzheimer's Disease*, 69(3), 729–741.
<https://doi.org/10.3233/JAD-190075>
- Bignoux, M. J., Otgaar, T. C., Bernert, M., Weiss, S. F. T., & Ferreira, E. (2023). Downregulation of LRP/LR with siRNA inhibits several cancer hallmarks in lung cancer cells. *FEBS Open Bio*, 13(2), 323–340. <https://doi.org/10.1002/2211-5463.13544>
- Blackburn, E. H. (1991). Structure and function of telomeres. *Nature*, 350, 569–573.
<https://doi.org/10.1146/annurev.genet.23.1.579>
- Bodnar, A. G., Ouellette, M., Frolkis, M., Holt, S. E., Chiu, C. P., Morin, G. B., Harley, C. B., Shay, J. W., Lichtsteiner, S., & Wright, W. E. (1998). Extension of Life-Span by Introduction of Telomerase into Normal Human Cells. *Science*, 279(5349), 349–352.
<https://doi.org/10.1126/SCIENCE.279.5349.349>
- Brown, L. M., Hoover, R., Silverman, D., Baris, D., Hayes, R., Swanson, G. M., Schoenberg, J., Greenberg, R., Liff, J., Schwartz, A., Dosemeci, M., Pottern, L., & Fraumeni, J. F. (2001). Excess Incidence of Squamous Cell Esophageal Cancer among US Black Men: Role of Social Class and Other Risk Factors. *American Journal of Epidemiology*, 153(2), 114–122.
- Buzzai, M., Jones, R. G., Amaravadi, R. K., Lum, J. J., DeBerardinis, R. J., Zhao, F., Viollet, B., & Thompson, C. B. (2007). Systemic treatment with the antidiabetic drug metformin selectively impairs p53-deficient tumor cell growth. *Cancer Research*, 67(14), 6745–6752. <https://doi.org/10.1158/0008-5472.CAN-06-4447>
- Calado, R. T., & Young, N. S. (2009). *Telomere Diseases*.
<https://doi.org/10.1056/NEJMra0903373>

- Capper, R., Britt-compton, B., Tankimanova, M., Rowson, J., Letsolo, B., Man, S., Haughton, M., & Baird, D. M. (2007). The nature of telomere fusion and a definition of the critical telomere length in human cells. *Genes and Development*, 21(19), 2495–2508. <https://doi.org/10.1101/gad.439107.somatic>
- Cárdenas, M., Barauskas, J., Schullén, K., Brennan, J. L., Brust, M., & Nylander, T. (2006). Thiol-specific and nonspecific interactions between DNA and gold nanoparticles. *Langmuir*, 22(7), 3294–3299. <https://doi.org/10.1021/la0530438>
- Carlin, A. S., Grant, I., Adams, K. M., Reed, R., Am, J., Nakamura, T. M., Morin, G. B., Chapman, K. B., Weinrich, S. L., Andrews, W. H., Lingner, J., Harley, C. B., & Cech, T. R. (1997). Telomerase Catalytic Subunit Homologs from Fission Yeast and Human. *Science*, 277(5328), 955–960.
- Carneiro, M. C., de Castro, I. P., & Ferreira, M. G. (2016). Telomeres in aging and disease: lessons from zebrafish. *Disease Models & Mechanisms*, 9(7), 737–748. <https://doi.org/10.1242/DMM.025130>
- Cesare, A. J., & Reddel, R. R. (2010). Alternative lengthening of telomeres: Models, mechanisms and implications. In *Nature Reviews Genetics* (Vol. 11, Issue 5, pp. 319–330). <https://doi.org/10.1038/nrg2763>
- Chetty, C., Khumalo, T., da Costa Dias, B., Reusch, U., Knackmuss, S., Little, M., & Weiss, S. F. T. (2013). *In Vitro Inhibition of Angiogenesis by Antibodies Directed against the 37kDa/67kDa Laminin Receptor*. <https://doi.org/10.1371/journal.pone.0058888>
- Chetty, C., Khumalo, T., da Costa Dias, B., Reusch, U., Knackmuss, S., Little, M., & Weiss, S. F. T. (2014). Anti-LRP/LR specific antibody IgG1-iS18 impedes adhesion and invasion of liver cancer cells. *PLoS ONE*, 9(5). <https://doi.org/10.1371/JOURNAL.PONE.0096268>
- Chetty, C., Khumalo, T., da Costa Dias, B., Reusch, U., Knackmuss, S., Little, M., & Weiss, S. F. T. (2015). Knockdown of LRP/LR Induces Apoptosis in Breast and Oesophageal Cancer Cells. *PloS One*, 10(10). <https://doi.org/10.1371/JOURNAL.PONE.0139584>

- Corrie, P. G. (2007). *SyStemic therapy meDiciNe* 36:1 24 Cytotoxic chemotherapy: clinical aspects *Clinical applications of cytotoxic chemotherapy*.
- Cuttler, K., Bignoux, M. J., Otgaar, T. C., Chigumba, S., Ferreira, E., & Weiss, S. F. T. (2020). LRP::FLAG Reduces Phosphorylated Tau Levels in Alzheimer's Disease Cell Culture Models. *Journal of Alzheimer's Disease*, 76(2), 753–768. <https://doi.org/10.3233/JAD-200244>
- da Costa Dias, B., Jovanovic, K., Gonsalves, D., Moodley, K., Reusch, U., Knackmuss, S., Penny, C., Weinberg, M. S., Little, M., & Weiss, S. F. T. (2013). Anti-LRP/LR specific antibody IgG1-iS18 and knock-down of LRP/LR by shRNAs rescue cells from A β 42 induced cytotoxicity. *Scientific Reports*, 3. <https://doi.org/10.1038/SREP02702>
- da Costa Dias, B., Jovanovic, K., Gonsalves, D., Moodley, K., Reusch, U., Knackmuss, S., Weinberg, M. S., Little, M., & Weiss, S. F. T. (2014). The 37kDa/67kDa Laminin Receptor acts as a receptor for A β 42 internalization. *Scientific Reports*, 4. <https://doi.org/10.1038/SREP05556>
- Damelin, L. H., Jivan, R., Veale, R. B., Rousseau, A. L., & Mavri-Damelin, D. (2014). Metformin induces an intracellular reductive state that protects oesophageal squamous cell carcinoma cells against cisplatin but not copper-bis(thiosemicarbazones). *BMC Cancer*, 14(1), 314–325. <https://doi.org/10.1186/1471-2407-14-314>
- Danhier, F., Ansorena, E., Silva, J. M., Coco, R., le Breton, A., & Pr at, V. (2012). PLGA-based nanoparticles: an overview of biomedical applications. *Journal of Controlled Release : Official Journal of the Controlled Release Society*, 161(2), 505–522. <https://doi.org/10.1016/J.JCONREL.2012.01.043>
- de Jesus, B. B., Schneeberger, K., Vera, E., Tejera, A., Harley, C. B., & Blasco, M. A. (2011). The telomerase activator TA-65 elongates short telomeres and increases health span of adult/old mice without increasing cancer incidence. *Aging Cell*, 10(4), 604–621. <https://doi.org/10.1111/j.1474-9726.2011.00700.x>

- Denchi, E. L. (2009). Give me a break: how telomeres suppress the DNA damage response. *DNA Repair*, 8(9), 1118–1126. <https://doi.org/10.1016/j.dnarep.2009.04.013>
- Derman, S., Akdeste, Z. M., Canim Ates, S., Mansuroglu, B., Kizilbey, K., Bagirova, M., & Allahverdiyev, A. (2017). *The Study Of Synthetic Peptide Loaded PLGA Nanoparticles Cytotoxicity In Vitro*.
- Duan, R., Wang, B., Zhang, T., Zhang, Z., Xu, S., Chen, Z., Lou, X., & Xia, F. (2014). Sensitive and bidirectional detection of urine telomerase based on the four detection-color states of difunctional gold nanoparticle probe. *Analytical Chemistry*, 86(19), 9781–9785. <https://doi.org/10.1021/ac5024364>
- Evans, J. M. M., Donnelly, L. A., Emslie-Smith, A. M., Alessi, D. R., & Morris, A. D. (2005). Metformin and reduced risk of cancer in diabetic patients. *BMJ (Clinical Research Ed.)*, 330(7503), 1304–1305. <https://doi.org/10.1136/bmj.38393.572188.EB>
- Fleming, A. M., & Burrows, C. J. (2013). G-Quadruplex Folds of the Human Telomere Sequence Alter the Site Reactivity and Reaction Pathway of Guanine Oxidation Compared to Duplex DNA. *Chemical Research in Toxicology*, 26(4), 593–607. <https://doi.org/10.1021/tx400028y.G-Quadruplex>
- Fragkos, M., Jurvansuu, J., & Beard, P. (2009). H2AX Is Required for Cell Cycle Arrest via the p53/p21 Pathway. *Molecular and Cellular Biology*, 29(10), 2828–2840. <https://doi.org/10.1128/mcb.01830-08>
- Franco, S., Blasco, M. A., Siedlak, S. L., Harris, P. L. R., Moreira, P. I., Perry, G., & Smith, M. A. (2006). Telomeres and telomerase in Alzheimer's disease: Epiphenomena or a new focus for therapeutic strategy? *Alzheimer's and Dementia*, 2(3), 164–168. <https://doi.org/10.1016/j.jalz.2006.03.001>
- Gauczynski, S., Nikles, D., El-Gogo, S., Papy-Garcia, D., Rey, C., Alban, S., Barritault, D., Lasmézas, C. I., & Weiss, S. (2006). The 37-kDa/67-kDa laminin receptor acts as a receptor for infectious prions and is inhibited by polysulfated glycanes. *Journal of Infectious Diseases*, 194(5), 702–709. <https://doi.org/10.1086/505914>

- Gauczynski, S., Peyrin, J. M., Haïk, S., Leucht, C., Hundt, C., Rieger, R., Krasemann, S., Deslys, J. P., Dormont, D., Lasmézas, C. I., & Weiss, S. (2001). The 37-kDa/67-kDa laminin receptor acts as the cell-surface receptor for the cellular prion protein. *EMBO Journal*, *20*(21), 5863–5875. <https://doi.org/10.1093/EMBOJ/20.21.5863>
- Geiger, T. R., & Peeper, D. S. (2009). Metastasis mechanisms. In *Biochimica et Biophysica Acta - Reviews on Cancer* (Vol. 1796, Issue 2, pp. 293–308). <https://doi.org/10.1016/j.bbcan.2009.07.006>
- Gholizadeh, A., Shapoury, R., Pakzad, P., Mahdavi, M., & Danafar, H. (2022). Evaluation of PLGA nanoparticles containing outer membrane proteins of *Acinetobacter baumannii* bacterium in stimulating the immune system in mice. *Research in Pharmaceutical Sciences*, *17*(4), 360–371. <https://doi.org/10.4103/1735-5362.350237>
- GLOBOCAN 2020: New Global Cancer Data | UICC*. (n.d.). Retrieved July 21, 2022, from <https://www.uicc.org/news/globocan-2020-new-global-cancer-data>
- Graham, F. L., Smiley, J., Russell, W. C., & Nairn, R. (1977). Characteristics of a human cell line transformed by DNA from human adenovirus type 5. *The Journal of General Virology*, *36*(1), 59–74. <https://doi.org/10.1099/0022-1317-36-1-59>
- Greenberg, R. a, O'Hagan, R. C., Deng, H., Xiao, Q., Hann, S. R., Adams, R. R., Lichtsteiner, S., Chin, L., Morin, G. B., & DePinho, R. a. (1999). Telomerase reverse transcriptase gene is a direct target of c-Myc but is not functionally equivalent in cellular transformation. *Oncogene*, *18*(5), 1219–1226. <https://doi.org/10.1038/sj.onc.1202669>
- Greider, C. W. (1999). Telomeres Do D-Loop-T-Loop. *Cell*, *97*, 419–422. [https://doi.org/https://doi.org/10.1016/S0092-8674\(00\)80750-3](https://doi.org/https://doi.org/10.1016/S0092-8674(00)80750-3)
- Guarise, C., Pasquato, L., de Filippis, V., & Scrimin, P. (2006). Gold nanoparticles-based protease assay. In *PNAS March* (Vol. 14, Issue 11). www.pnas.org/cgidoi10.1073pnas.0509372103

- Haass, C., & Mandelkow, E. (2010). Fyn-tau-amyloid: A toxic triad. In *Cell* (Vol. 142, Issue 3, pp. 356–358). Elsevier B.V. <https://doi.org/10.1016/j.cell.2010.07.032>
- Haendeler, J., Dröse, S., Büchner, N., Jakob, S., Altschmied, J., Goy, C., Spyridopoulos, I., Zeiher, A. M., Brandt, U., & Dimmeler, S. (2009). Mitochondrial telomerase reverse transcriptase binds to and protects mitochondrial DNA and function from damage. *Arteriosclerosis, Thrombosis, and Vascular Biology*, 29(6), 929–935. <https://doi.org/10.1161/ATVBAHA.109.185546>
- Hanna, R. K., Zhou, C., Malloy, K. M., Sun, L., Zhong, Y., Gehrig, P. a, & Bae-Jump, V. L. (2012). Metformin potentiates the effects of paclitaxel in endometrial cancer cells through inhibition of cell proliferation and modulation of the mTOR pathway. *Gynecologic Oncology*, 125(2), 458–469. <https://doi.org/10.1016/j.ygyno.2012.01.009>
- Harley, C. B., Liu, W., Blasco, M., Vera, E., Andrews, W. H., Briggs, L. A., & Raffaele, J. M. (2011). A natural product telomerase activator as part of a health maintenance program. *Rejuvenation Research*, 14(1), 45–56. <https://doi.org/10.1089/rej.2010.1085>
- Hayflick, L., & Moorhead, P. S. (1961). The Serial Cultivation of Human Diploid Cell Strains. *Experimental Cell Research*, 25, 585–621.
- Hirsch, H. A., Iliopoulos, D., Tschlis, P. N., & Struhl, K. (2009). Metformin selectively targets cancer stem cells, and acts together with chemotherapy to block tumor growth and prolong remission. *Cancer Research*, 69(19), 7507–7511. <https://doi.org/10.1158/0008-5472.CAN-09-2994>
- Hofer, P., Zerelles, J., Baierl, A., Madersbacher, S., Schatzl, G., Maj-Hes, A., Sutterlüty-fall, H., & Gsur, A. (2013). MNS16A tandem repeat minisatellite of human telomerase gene and prostate cancer susceptibility. *Mutagenesis*, 28(3), 301–306. <https://doi.org/10.1093/mutage/get003>
- Hoyos-Ceballos, G. P., Ruozi, B., Ottonelli, I., Da Ros, F., Vandelli, M. A., Forni, F., Daini, E., Vilella, A., Zoli, M., Tosi, G., Duskey, J. T., & López-Osorio, B. L. (2020). PLGA-PEG-Ang–

- 2 nanoparticles for blood–brain barrier crossing: Proof-of-concept study. *Pharmaceutics*, 12(1). <https://doi.org/10.3390/pharmaceutics12010072>
- Huang, R., Wang, M., Chen, X., Yu, N., & Jiang, C. (2021). Gold nanoparticle based colorimetric assay of telomerase activity using the cyclic strand displacement reaction. *New Journal of Chemistry*, 45(12), 5322–5326. <https://doi.org/10.1039/d1nj00036e>
- Huynh, N. T., Roger, E., Lautram, N., Benoît, J. P., & Passirani, C. (2010). The rise and rise of stealth nanocarriers for cancer therapy: Passive versus active targeting. In *Nanomedicine* (Vol. 5, Issue 9, pp. 1415–1433). <https://doi.org/10.2217/nnm.10.113>
- Jemal, A., Bray, F., Center, M. M., Ferlay, J., Ward, E., & Forman, D. (2011). Global cancer statistics. *CA: A Cancer Journal for Clinicians*, 61(2), 69–90. <https://doi.org/10.3322/caac.20107>
- Jovanovic, K., Chetty, C. J., Khumalo, T., da Costa Dias, B., Ferreira, E., Malindisa, S. T., Caveney, R., Letsolo, B. T., & Weiss, S. F. T. (2015). Novel patented therapeutic approaches targeting the 37/67 kDa laminin receptor for treatment of cancer and Alzheimer’s disease. *Expert Opinion on Therapeutic Patents*, 25(5), 567–582. <https://doi.org/10.1517/13543776.2015.1014802>
- Kanaya, T., Kyo, S., & Hamada, K. (2000). Adenoviral Expression of p53 Represses Telomerase Activity through Down-Regulation of Human Telomerase Reverse Transcriptase Transcription. *Clinical Cancer Research*, 6, 1239–1247.
- Kim, H. S., Heo, J. I., Park, S. H., Shin, J. Y., Kang, H. J., Kim, M. J., Kim, S. C., Kim, J., Park, J. B., & Lee, J. Y. (2014). Transcriptional activation of p21WAF1/CIP1 is mediated by increased DNA binding activity and increased interaction between p53 and Sp1 via phosphorylation during replicative senescence of human embryonic fibroblasts. *Molecular Biology Reports*, 41(4), 2397–2408. <https://doi.org/10.1007/s11033-014-3094-9>
- Kim, N. W., Piatyszek, M. A., Prowse, K. R., Harley, C. B., West, D., Ho, P. L. C., Coviello, G. M., Wright, W. E., Weinrich, S. L., Shay, W., West, M. D., & Shay, J. W. (1994). *Specific*

- Association of Human Telomerase Activity with Immortal Cells and Cancer*. 266(5193), 2011–2015.
- Kimling, J., Maier, M., Okenve, V., Kotaidis, V., Ballot, H., Plech, a, & Okenve, B. (2006). Turkevitch method for gold nanoparticle synthesis revisited. *J. Phys. Chem. B*, 110(95 mL), 15700–15707.
- Kirkpatrick, K. L., Clark, G., Ghilchick, M., Newbold, R. F., & Mokbel, K. (2003). hTERT mRNA expression correlates with telomerase activity in human breast cancer. *European Journal of Surgical Oncology*, 29(4), 321–326. <https://doi.org/10.1053/ejso.2002.1374>
- Klapper, W., Parwaresch, R., & Krupp, G. (2001). Telomere biology in human aging and aging syndromes. *Mechanisms of Ageing and Development*, 122(7), 695–712. <http://www.ncbi.nlm.nih.gov/pubmed/11322993>
- Kovacic, J. C., Moreno, P., Hachinski, V., Nabel, E. G., & Fuster, V. (2011). Cellular senescence, vascular disease, and aging: Part 1 of a 2-part review. *Circulation*, 123(15), 1650–1660. <https://doi.org/10.1161/CIRCULATIONAHA.110.007021>
- Lawenda, B. D., Kelly, K. M., Ladas, E. J., Sagar, S. M., Vickers, A., & Blumberg, J. B. (2008). Should supplemental antioxidant administration be avoided during chemotherapy and radiation therapy? *Journal of the National Cancer Institute*, 100(11), 773–783. <https://doi.org/10.1093/jnci/djn148>
- Lee, C., Jung, M., Jung, I., Heo, S. J., & Jeong, Y. H. (2015). *Cumulative Metformin Use and Its Impact on Survival in Gastric Cancer Patients After Gastrectomy*. 00(00). <https://doi.org/10.1097/SLA.0000000000001086>
- Leucht, C., Simoneau, S., Rey, C., Vana, K., Rieger, R., Lasmézas, C. I., & Weiss, S. (2003). The 37 kDa/67 kDa laminin receptor is required for PrPSc propagation in scrapie-infected neuronal cells. *EMBO Reports*, 4(3), 290. <https://doi.org/10.1038/SJ.EMBOR.EMBOR768>

- Levy, M. Z., Allsopp, R. C., Futcher, a B., Greider, C. W., & Harley, C. B. (1992). Telomere end-replication problem and cell aging. *Journal of Molecular Biology*, 225(4), 951–960. [https://doi.org/10.1016/0022-2836\(92\)90096-3](https://doi.org/10.1016/0022-2836(92)90096-3)
- Li, L., Roumeliotis, N., Sawamura, T., & Renier, G. (2004). C-reactive protein enhances LOX-1 expression in human aortic endothelial cells: Relevance of LOX-1 to C-reactive protein-induced endothelial dysfunction. *Circulation Research*, 95(9), 877–883. <https://doi.org/10.1161/01.RES.0000147309.54227.42>
- Makadia, H. K., & Siegel, S. J. (2011). Poly Lactic-co-Glycolic Acid (PLGA) as biodegradable controlled drug delivery carrier. *Polymers*, 3(3), 1377–1397. <https://doi.org/10.3390/polym3031377>
- Malhotra, V., & Perry, M. C. (2003). *Classical Chemotherapy: Mechanisms, Toxicities and the Therapeutic Window*. <https://doi.org/10.4161/cbt.199>
- Mallat, Z., & Tedgui, A. (2000). Apoptosis in the vasculature: Mechanisms and functional importance. In *British Journal of Pharmacology* (Vol. 130, Issue 5, pp. 947–962). John Wiley and Sons Inc. <https://doi.org/10.1038/sj.bjp.0703407>
- McCall, R. L., & Sirianni, R. W. (2013). PLGA nanoparticles formed by single- or double-emulsion with vitamin E-TPGS. *Journal of Visualized Experiments : JoVE*, 82, 51015. <https://doi.org/10.3791/51015>
- Mccall, R. L., & Sirianni, R. W. (2013). PLGA Nanoparticles Formed by Single-or Double-emulsion with Vitamin E-TPGS. *J. Vis. Exp*, 82, 51015. <https://doi.org/10.3791/51015>
- Medley, C. D., Smith, J. E., Tang, Z., Wu, Y., Bamrungsap, S., & Tan, W. (2008). Gold nanoparticle-based colorimetric assay for the direct detection of cancerous cells. *Analytical Chemistry*, 80(4), 1067–1072. <https://doi.org/10.1021/ac702037y>
- Mercurio, A. M. (1995). Laminin receptors: achieving specificity through cooperation. *Trends in Cell Biology*, 5(11), 419–423. [https://doi.org/10.1016/S0962-8924\(00\)89100-X](https://doi.org/10.1016/S0962-8924(00)89100-X)

- Moghimi, S. M., Hunter, A. C., & Andresen, T. L. (2012). Factors controlling nanoparticle pharmacokinetics: An integrated analysis and perspective. *Annual Review of Pharmacology and Toxicology*, *52*, 481–503. <https://doi.org/10.1146/annurev-pharmtox-010611-134623>
- Naidoo, K., Malindisa, S. T., Otgaar, T. C., Bernert, M., da Costa Dias, B., Ferreira, E., Reusch, U., Knackmuss, S., Little, M., Weiss, S. F. T., & Letsolo, B. T. (2015). Knock-Down of the 37kDa/67kDa Laminin Receptor LRP/LR Impedes Telomerase Activity. *PLoS One*, *10*(11). <https://doi.org/10.1371/JOURNAL.PONE.0141618>
- Ohno, Y., Ogiyama, Y., Kubota, Y., Kubo, T., & Ishii, K. (2016). Acentric chromosome ends are prone to fusion with functional chromosome ends through a homology-directed rearrangement. *Nucleic Acids Research*, *44*(1), 232–244. <https://doi.org/10.1093/nar/gkv997>
- Olvera-Bello, A. E., Estrada-Muñiz, E., Elizondo, G., & Vega, L. (2010). Susceptibility to the cytogenetic effects of dichloromethane is related to the glutathione S-transferase theta phenotype. *Toxicology Letters*, *199*(3), 218–224. <https://doi.org/10.1016/j.toxlet.2010.09.002>
- Otgaar, T. C., Ferreira, E., Malindisa, S., Bernert, M., Letsolo, B. T., & Weiss, S. F. T. (2017). 37 kDa LRP::FLAG enhances telomerase activity and reduces senescent markers in vitro. *Oncotarget*, *8*(49), 86646–86656. <https://doi.org/10.18632/oncotarget.21278>
- Owens, D. E., & Peppas, N. A. (2006). Opsonization, biodistribution, and pharmacokinetics of polymeric nanoparticles. In *International Journal of Pharmaceutics* (Vol. 307, Issue 1, pp. 93–102). <https://doi.org/10.1016/j.ijpharm.2005.10.010>
- Pirillo, A., Norata, G. D., & Catapano, A. L. (2013). LOX-1, OxLDL, and atherosclerosis. In *Mediators of Inflammation* (Vol. 2013). <https://doi.org/10.1155/2013/152786>
- Polte, J., Ahner, T. T., Delissen, F., Sokolov, S., Emmerling, F., Thünemann, A. F., & Kraehnert, R. (2010). Mechanism of gold nanoparticle formation in the classical citrate synthesis

- method derived from coupled in situ XANES and SAXS evaluation. *Journal of the American Chemical Society*, 132(9), 1296–1301. <https://doi.org/10.1021/ja906506j>
- Raffa, G. D., Cenci, G., Ciapponi, L., & Gatti, M. (2013). Organization and Evolution of Drosophila Terminin: Similarities and Differences between Drosophila and Human Telomeres. *Frontiers in Oncology*, 3, 112. <https://doi.org/10.3389/fonc.2013.00112>
- Roth, G. A., Mensah, G. A., Johnson, C. O., Addolorato, G., Ammirati, E., Baddour, L. M., Barengo, N. C., Beaton, A., Benjamin, E. J., Benziger, C. P., Bonny, A., Brauer, M., Brodmann, M., Cahill, T. J., Carapetis, J. R., Catapano, A. L., Chugh, S., Cooper, L. T., Coresh, J., ... Fuster, V. (2020). Global Burden of Cardiovascular Diseases and Risk Factors, 1990-2019: Update From the GBD 2019 Study. In *Journal of the American College of Cardiology* (Vol. 76, Issue 25, pp. 2982–3021). Elsevier Inc. <https://doi.org/10.1016/j.jacc.2020.11.010>
- Sahana, D. K., Mittal, G., Bhardwaj, V., & Kumar, M. N. V. R. (2008). PLGA nanoparticles for oral delivery of hydrophobic drugs: Influence of organic solvent on nanoparticle formation and release behavior in vitro and in vivo using estradiol as a model drug. *Journal of Pharmaceutical Sciences*, 97(4), 1530–1542. <https://doi.org/10.1002/jps.21158>
- Sahin, E., & Depinho, R. A. (2010). Linking functional decline of telomeres, mitochondria and stem cells during ageing. *Nature*, 464(7288), 520–528. <https://doi.org/10.1038/nature08982>
- Sambrook, J., & Russell, D. W. (2006). Fragmentation of DNA by sonication. *CSH Protocols*, 2006(4), pdb.prot4538-pdb.prot4538. <https://doi.org/10.1101/PDB.PROT4538>
- Saretzki, G. (2009). Telomerase, mitochondria and oxidative stress. *Experimental Gerontology*, 44(8), 485–492. <https://doi.org/10.1016/j.exger.2009.05.004>
- Saretzki, G. (2014). Extra-telomeric Functions of Human Telomerase: Cancer, Mitochondria and Oxidative Stress. *Current Pharmaceutical Design*, 20(41), 6386–6403. <https://doi.org/10.2174/1381612820666140630095606>

- Seimiya, H., Oh-Hara, T., Suzuki, T., Naasani, I., Shimazaki, T., Tsuchiya, K., & Tsuruo, T. (2002). *Telomere Shortening and Growth Inhibition of Human Cancer Cells by Novel Synthetic Telomerase Inhibitors MST-312, MST-295, and MST-199*. <http://aacrjournals.org/mct/article-pdf/1/9/657/2222090/gd0902000657.pdf>
- Serrano, A. L., & Andrés, V. (2004). Telomeres and Cardiovascular Disease: Does Size Matter? In *Circulation Research* (Vol. 94, Issue 5, pp. 575–584). <https://doi.org/10.1161/01.RES.0000122141.18795.9C>
- Sharma, S., Parmar, A., Kori, S., & Sandhir, R. (2016). PLGA-based nanoparticles: A new paradigm in biomedical applications. *TrAC Trends in Analytical Chemistry*, 80, 30–40. <https://doi.org/10.1016/J.TRAC.2015.06.014>
- Shay, J. W., & Keith, W. N. (2008). Targeting telomerase for cancer therapeutics. *British Journal of Cancer*, 98(4), 677–683. <https://doi.org/10.1038/sj.bjc.6604209>
- Shay, J. W., & Wright, W. E. (2005). Senescence and immortalization: Role of telomeres and telomerase. *Carcinogenesis*, 26(5), 867–874. <https://doi.org/10.1093/carcin/bgh296>
- Sheng, X., Tong, N., Tao, G., Luo, D., Wang, M., Fang, Y., Li, J., Xu, M., Zhang, Z., & Wu, D. (2013). TERT polymorphisms modify the risk of acute lymphoblastic leukemia in Chinese children. *Carcinogenesis*, 34(1), 228–235. <https://doi.org/10.1093/carcin/bgs325>
- Shokoohinia, P., Hajialyani, M., Sadrjavadi, K., Akbari, M., Rahimi, M., Khaledian, S., & Fattahi, A. (2019). Microfluidic-assisted preparation of PLGA nanoparticles for drug delivery purposes: experimental study and computational fluid dynamic simulation. *Research in Pharmaceutical Sciences*, 14(5), 459–470. <https://doi.org/10.4103/1735-5362.268207>
- Tang, B., Xie, R., Qin, Y., Xiao, Y. F., Yong, X., Zheng, L., Dong, H., & Yang, S. M. (2016). Human telomerase reverse transcriptase (hTERT) promotes gastric cancer invasion through cooperating with c-Myc to upregulate heparanase expression. *Oncotarget*, 7(10), 11364–11379. <https://doi.org/10.18632/ONCOTARGET.6575>

- Tran, S.-L., Puhar, A., Ngo-Camus, M., & Ramarao, N. (2011). Trypan Blue Dye Enters Viable Cells Incubated with the Pore-Forming Toxin HlyII of *Bacillus cereus*. *PLoS One*, *6*(9), e22876. <https://doi.org/10.1371/journal.pone.0022876>
- Tseng, C.-H. (2019). Metformin use is associated with a lower risk of uterine leiomyoma in female type 2 diabetes patients. *Therapeutic Advances in Endocrinology and Metabolism*, *10*, 2042018819895159. <https://doi.org/10.1177/2042018819895159>
- Vallianou, N. G., Evangelopoulos, A., & Kazazis, C. (2013). Metformin and Cancer. *The Review of Diabetic Studies*, *10*, 228–235. <https://doi.org/10.1900/RDS.2013.10.228>
- Vasir, J. K., & Labhasetwar, V. (2007). Biodegradable nanoparticles for cytosolic delivery of therapeutics. *Advanced Drug Delivery Reviews*, *59*(8), 718–728. <https://doi.org/10.1016/J.ADDR.2007.06.003>
- Veale, R. B., & Thornley, A. L. (1989). Increased Single Class Low-Affinity EGF Receptors Expressed by Human Oesophageal Squamous Carcinoma Cell Lines. *South African Journal of Science*, *85*, 375–379.
- Wang, J., Wu, L., Ren, J., & Qu, X. (2012). Visualizing human telomerase activity with primer-modified Au nanoparticles. *Small*, *8*, 259–264. <https://doi.org/10.1002/smll.201101938>
- Wang, J., Zhao, C., Zhao, A., Li, M., Ren, J., & Qu, X. (2015). New insights in amyloid beta interactions with human telomerase. *Journal of the American Chemical Society*, *137*(3), 1213–1219. <https://doi.org/10.1021/ja511030s>
- Wang, L., Soria, J.-C., Chang, Y.-S., Lee, H.-Y., Wei, Q., & Mao, L. (2003). Association of a functional tandem repeats in the downstream of human telomerase gene and lung cancer. *Oncogene*, *22*(46), 7123–7129. <https://doi.org/10.1038/sj.onc.1206852>
- Wick, M., Zubov, D., & Hagen, G. (1999). Genomic organization and promoter characterization of the gene encoding the human telomerase reverse transcriptase (hTERT). *Gene*, *232*(1), 97–106. [https://doi.org/10.1016/S0378-1119\(99\)00108-0](https://doi.org/10.1016/S0378-1119(99)00108-0)

- Wright, A. K., & Thompson, R. (1975). Hydrodynamic Structure Of Bovine Serum Albumin Determined By Transient Electric Birefringence. *Biophysical Journal*, *15*, 137–141.
- Wright, W. E., Piatyszek, M. A., Rainey, W. E., Byrd, W., & Shay, J. W. (1996). Telomerase Activity in Human Germline and Embryonic Tissues and Cells. *Developmental Genetics*, *18*, 173–179.
- Yarbakht, M., & Nikkhah, M. (2016). Unmodified gold nanoparticles as a colorimetric probe for visual methamphetamine detection. *Journal of Experimental Nanoscience*, *11*(7), 593–601. <https://doi.org/10.1080/17458080.2015.1100333>
- Zakikhani, M., Dowling, R., Fantus, I. G., Sonenberg, N., & Pollak, M. (2006). Metformin Is an AMP Kinase–Dependent Growth Inhibitor for Breast Cancer Cells. *Cancer Research*, *66*(21), 10269–10273. https://secureweb.mcgill.ca/pollak-lab/sites/mcgill.ca.pollak-lab/files/Zakikhani_et_al_2006.pdf
- Zhao, W., Chiuman, W., Brook, M. a, & Li, Y. (2007). Simple and rapid colorimetric biosensors based on DNA aptamer and noncrosslinking gold nanoparticle aggregation. *Chembiochem: A European Journal of Chemical Biology*, *8*(7), 727–731. <https://doi.org/10.1002/cbic.200700014>
- Zhou, X., & Xing, D. (2012). Assays for human telomerase activity: progress and prospects. *Chemical Society Reviews*, *41*, 4643–4656. <https://doi.org/10.1039/c2cs35045a>

7. Supplementary results

7.1. Metformin treatment reduces telomerase activity on oesophageal cancer cells:

Previous unpublished results: qPCR was performed on the WHCO-1 oesophageal cancer cell line using the TRAPeZe® RT Telomerase Detection Kit (Merck, Darmstadt, Germany). Telomerase activity in 10 mM metformin treated and untreated 24 and 48h samples were compared.

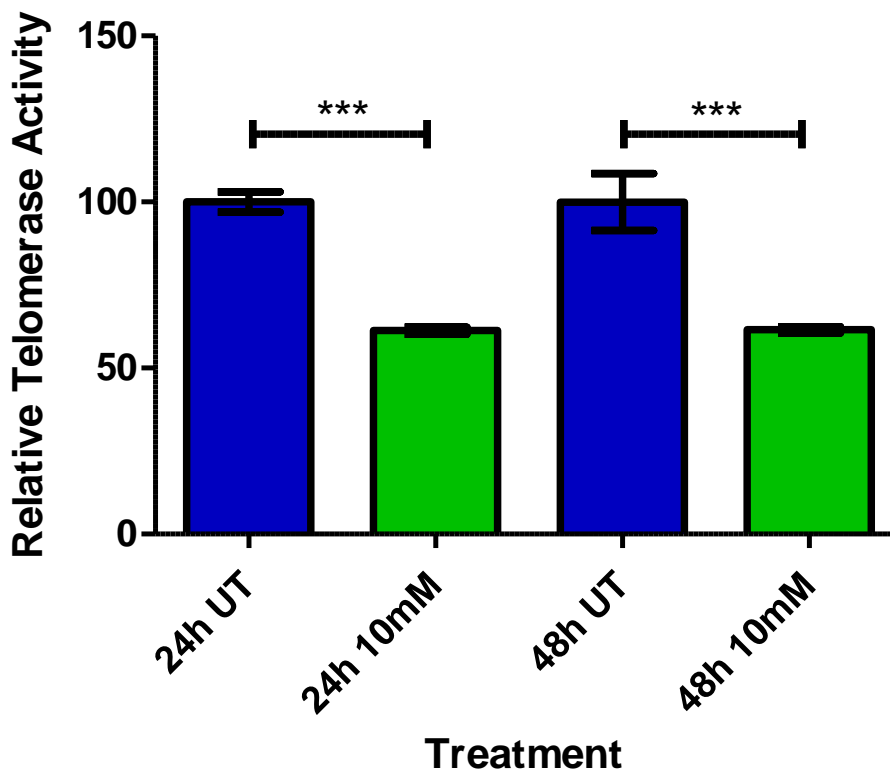


Figure 7.1: Metformin reduces telomerase activity in WHCO-1 cells

Assessment of telomerase activity by qPCR, using the TRAPeZe® RT Telomerase Detection Kit (Merck, Darmstadt, Germany), showed a significant decrease in WHCO-1 cells after metformin treatment. In fact,

*both 24 and 48h samples had a decrease in relative telomerase activity of 38.7 and 38.5 % respectively ($p=0.0005$). Error bars represent standard deviation; $N=3$ biological replicates; *** $p \leq 0.001$.*

7.2. LRP protein synthesis

Synthesis and purification of the LRP protein was performed with assistance of Monare Thulo and Riyaadh Mayet (Protein Structure Function Research Unit - University of the Witwatersrand) as well as Chandni Madhav and Sichumiso Gqeba (Cell Biology and Signalling Research Lab - University of the Witwatersrand). *E-coli* was first transformed using the LRP_pET-11a plasmid (GenScript) containing the LRP sequence as well as an ampicillin resistance gene for selection.

Sequence ID: BAC38701.1 Length: 295				
Range 1: 1 to 295				
Score:569 bits(1467), Expect:0.0,				
Method:Compositional matrix adjust.,				
Identities:295/295(100%), Positives:295/295(100%), Gaps:0/295(0%)				
Query	926	MSGALDVLQMKEEDVLKFLAAGTHLGGTNLDFQMEQYIYKRKSDGIYIINLKRTWEKLLL	747	
		MSGALDVLQMKEEDVLKFLAAGTHLGGTNLDFQMEQYIYKRKSDGIYIINLKRTWEKLLL		
Sbjct	1	MSGALDVLQMKEEDVLKFLAAGTHLGGTNLDFQMEQYIYKRKSDGIYIINLKRTWEKLLL	60	
Query	746	AARAIVAIENPADVSVISSRNTGQRAVLKFAAATGATPIAGRFTPGFTFNQIQAAFREPR	567	
		AARAIVAIENPADVSVISSRNTGQRAVLKFAAATGATPIAGRFTPGFTFNQIQAAFREPR		
Sbjct	61	AARAIVAIENPADVSVISSRNTGQRAVLKFAAATGATPIAGRFTPGFTFNQIQAAFREPR	120	
Query	566	LLVVDPRADHQPLTEASYVNLPTIALCNTDSPLRYVDIAIPCNKGAHSVGLMWWMLAR	387	
		LLVVDPRADHQPLTEASYVNLPTIALCNTDSPLRYVDIAIPCNKGAHSVGLMWWMLAR		
Sbjct	121	LLVVDPRADHQPLTEASYVNLPTIALCNTDSPLRYVDIAIPCNKGAHSVGLMWWMLAR	180	
Query	386	EVLRRMGTISREHPWEVMPDLYFYRDPeeiekeeqaaaekavtkeEFQGEWTAPAPEFTA	207	
		EVLRRMGTISREHPWEVMPDLYFYRDPeeiekeeqaaaekavtkeEFQGEWTAPAPEFTA		
Sbjct	181	EVLRRMGTISREHPWEVMPDLYFYRDPeeiekeeqaaaekavtkeEFQGEWTAPAPEFTA	240	
Query	206	AQPEVADWYEGVQVPSVPIQQFPTEDWSAQPATEDWSAAPTAQATEWVGATTEWS	42	
		AQPEVADWYEGVQVPSVPIQQFPTEDWSAQPATEDWSAAPTAQATEWVGATTEWS		
Sbjct	241	AQPEVADWYEGVQVPSVPIQQFPTEDWSAQPATEDWSAAPTAQATEWVGATTEWS	295	

Figure 7.2: LRP protein sequence homology

The LRP protein was expressed in bacteria and sequenced to confirm homology between the expected and expressed protein. The blasted sequence of LRP after Sanger Sequencing shows that there is a 100% sequence similarity. This confirms that there was no adverse change to the protein after being expressed.

After sequence homology was confirmed, initial LRP expression trial commenced at varying Isopropyl β -D-1-thiogalactopyranoside (IPTG) concentrations at a constant temperature of 37 °C. This would indicate the IPTG concentration for optimum LRP expression, as IPTG initiates LRP gene transcription through the lac operon in the modified plasmid.

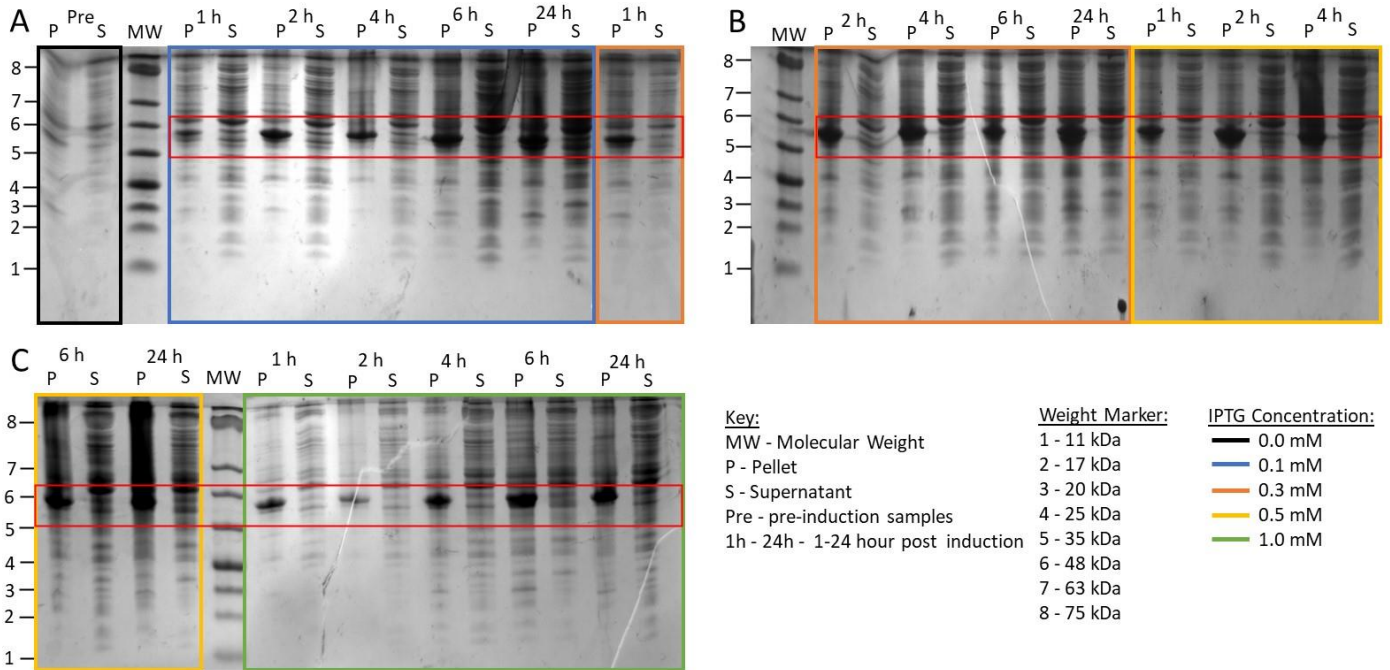


Figure 7.3: Initial expression of LRP at 37 °C using varying IPTG concentrations

These SDS-PAGE gels show that LRP was expressed over a period of 24h at varying IPTG concentrations. At all time-points and all IPTG concentrations (A- 0 mM, 0.1mM, 0.3 mM; B- 0.3mM, 0.5 mM; C- 0.5 mM, 1 mM) LRP was expressed in the protein pellet as inclusion bodies (red). Further optimisation and purification steps were later performed to increase the separation and purity of the LRP.

After the initial expression trials were completed, the LRP protein sample was purified using Ni²⁺ charged immobilized metal chelate affinity chromatography (IMAC). This purified the sample by binding the His-tag, attached to the LRP protein, and removing non-tagged contaminants in the flow through. A gradient elution profile was performed to determine the overall yield of the LRP protein. The higher the elution peak, the greater the amount of purified LRP.

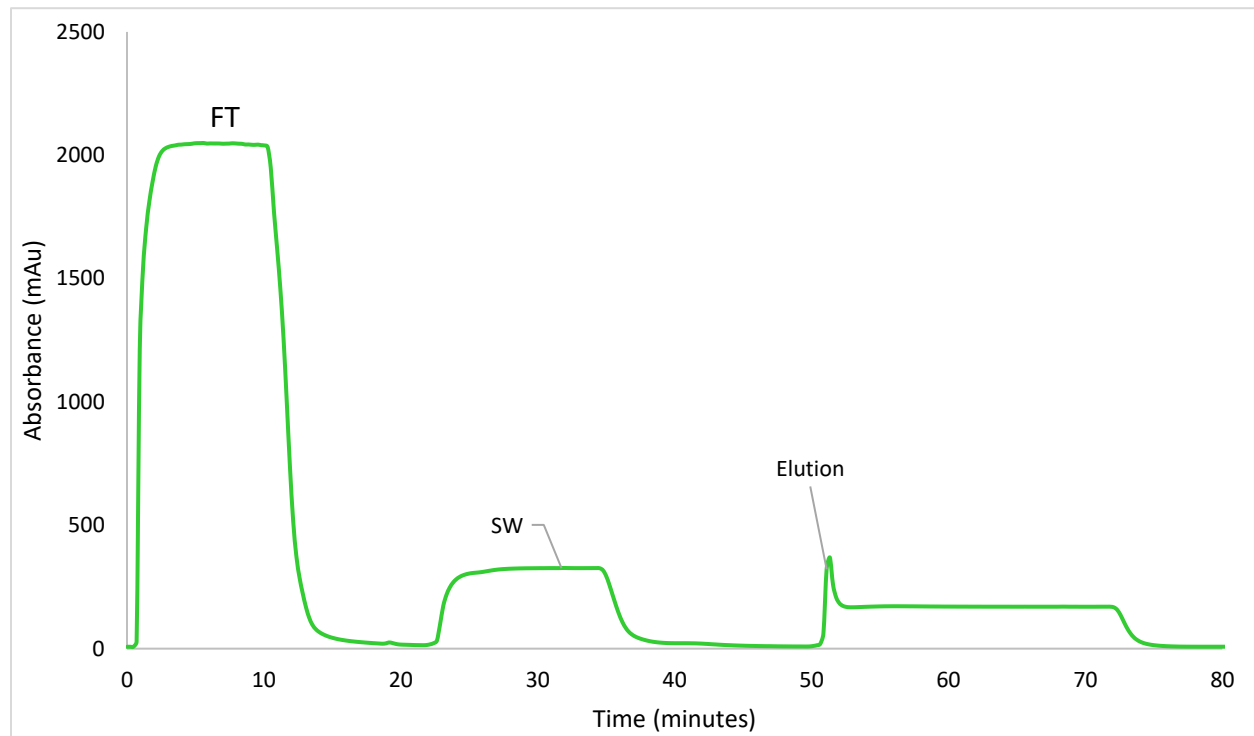


Figure 7.4: Initial IMAC purification of LRP

Immobilized metal affinity chromatography (IMAC) purification results of the initial synthesis. The flow through (FT) contains most unwanted proteins. This was followed by the salt wash (SW) and LRP was eluted off the column in the elution step. The yield was shown to be low (as seen by the low elution peak), however, pure LRP was confirmed.

For further confirmation of the LRP protein yield, the purified LRP was resolved on a coomassie blue stained SDS-PAGE gel.

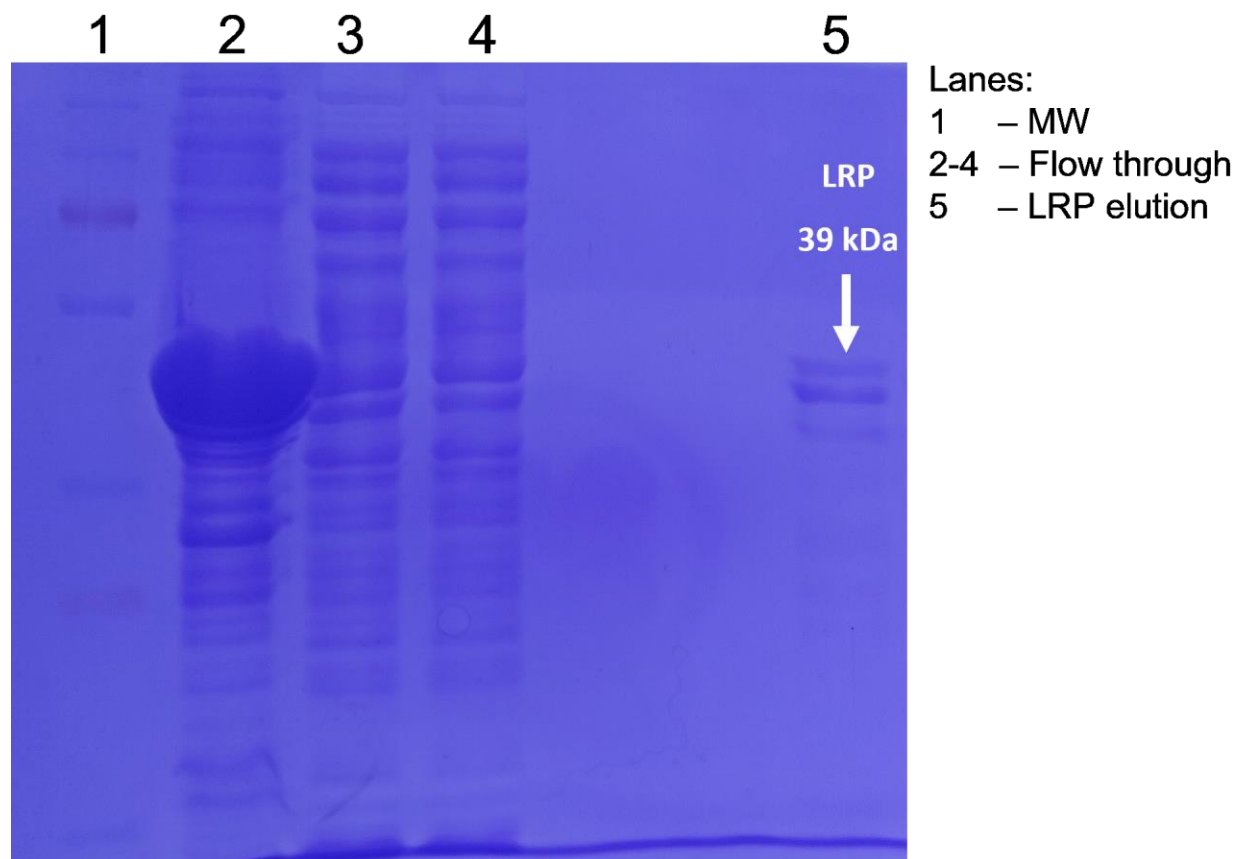


Figure 7.5: Coomassie blue stained SDS-PAGE gel of the purified LRP

An SDS-PAGE gel was stained with coomassie blue to visualise the purified LRP after the initial IMAC purification. Lanes 2-4 show the flow through, where the light bands (lane 5) show a relatively low yield of LRP, however, there are very few contaminants. This confirms the previous IMAC results (Figure 7.4).

The previous expression trial was repeated at 20 °C with varying IPTG concentrations to improve overall LRP expression, as previous yields were relatively low.

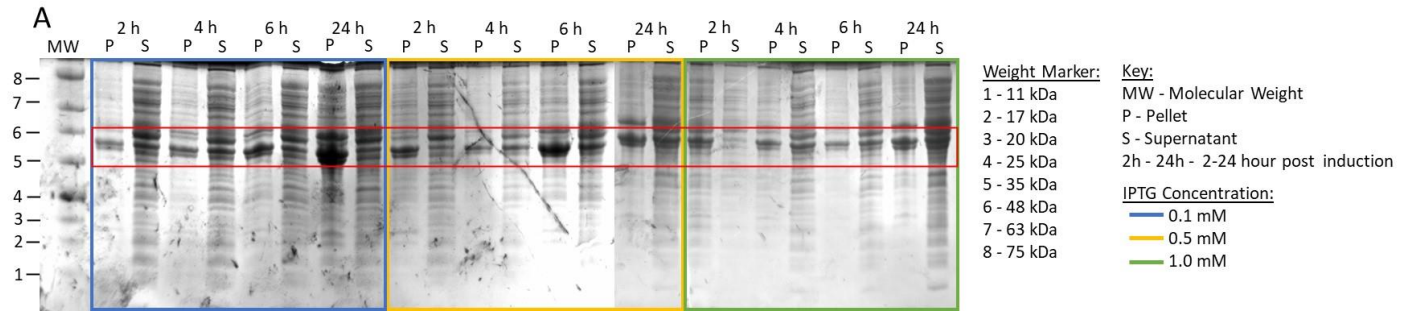


Figure 7.6: Expression of LRP at 20 °C using varying IPTG concentrations

This SDS-PAGE gel shows that LRP was expressed over a period of 24h at varying IPTG concentrations. In all cases, LRP was mostly expressed in the pellet as inclusion bodies (red). However, expression at 20 °C for 24 hours seem to have similar amounts of protein in both the pellet and supernatant. This would aid in future purification steps.

After the new expression trials were completed, the LRP protein sample was purified using IMAC as stated above. The yield of the LRP protein significantly increased from the previous trial Figure 7.3.

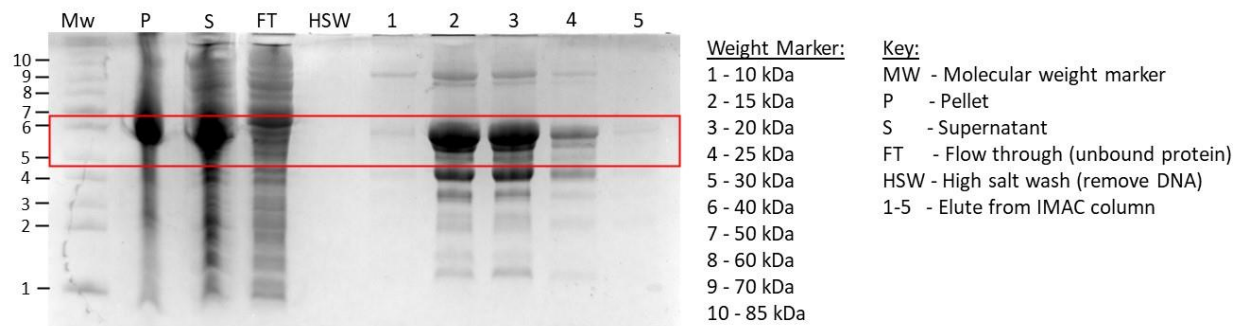


Figure 7.7: Purification of LRP using IMAC

A Tris-HCl buffer at pH 7.6 was used to elute LRP from the Ni²⁺ charged IMAC column, along with any other proteins which were also bound to the column. This significantly increased the purity of the LRP and produced a sufficient yield for the first LRP encapsulation trials. There was, however, a small amount of

potential contaminating proteins present; if they are determined to be unwanted proteins, a final purification step will be performed to yield pure LRP.

A gradient elution profile was performed as above, to determine the overall yield of the LRP protein. The elution peak was higher than the previous gradient profile (Figure 7.4), suggesting that LRP was purified in a higher concentration.

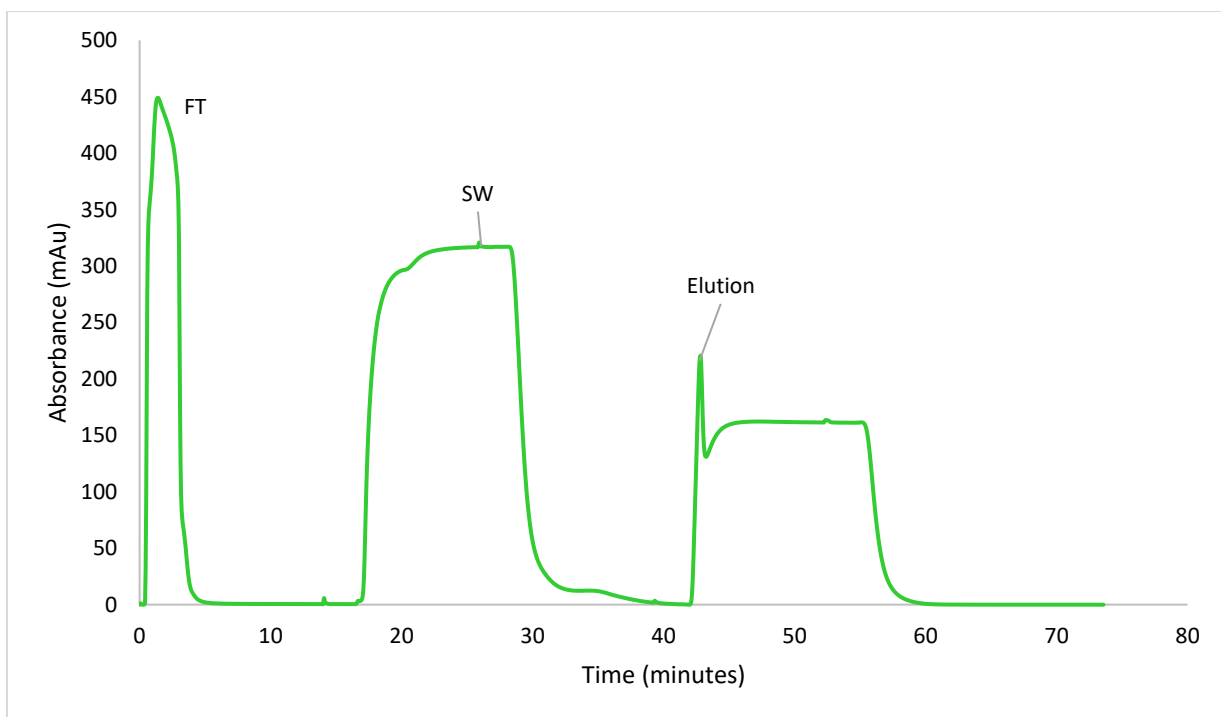


Figure 7.8: Improved IMAC purification of LRP

IMAC purification results of the subsequent synthesis showed, as before, the flow through (FT) was followed by the salt wash (SW) and LRP was eluted off the column in the elution step. The yield was shown to be significantly higher compared to the previous purification (Figure 7.4), as seen by the high elution peak. This shows that there was a marked improvement in the yield of the purified LRP.

For further confirmation of the improved LRP protein yield, the purified LRP was resolved on a coomassie blue stained SDS-PAGE gel.

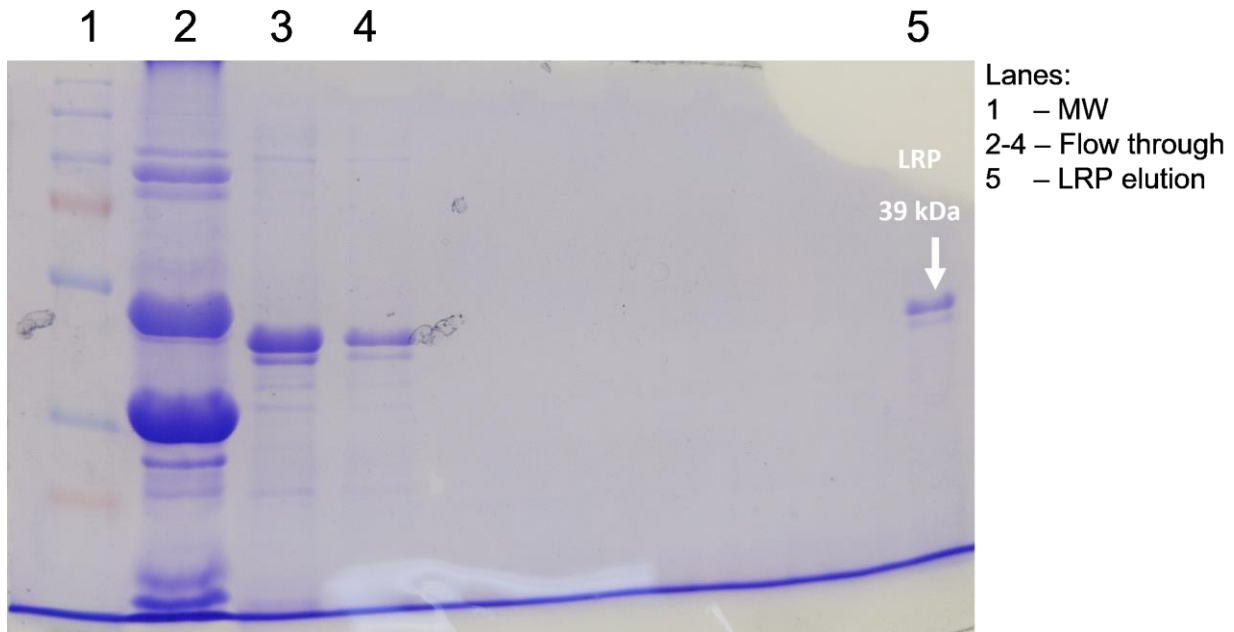


Figure 7.9: Coomassie blue stained SDS-PAGE gel of the purified LRP

An SDS-PAGE gel was stained with coomassie blue to visualise the purified LRP after the second IMAC purification. Lanes 2-4 show the flow through, where the darker band (lane 5) show a relatively high yield of LRP. This confirms the IMAC results (Figure 7.8).

An analysis of the coomassie blue stained SDS-PAGE gel was performed using the molecular weight standards. A standard curve was created and the size of the LRP band was extrapolated against the log molecular weight.

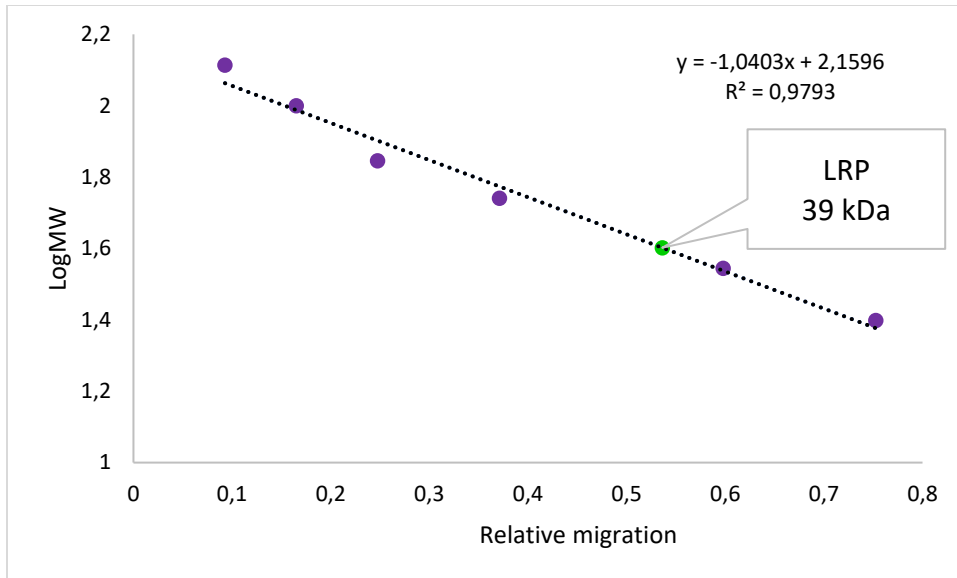


Figure 7.10: Confirmation of purified LRP via standard curve extrapolation

To confirm that the band shown in the coomassie gel does indeed represent LRP, a size analysis of the molecular weight ladder and the suspected LRP band was performed. The molecular weight of the suspected LRP band was calculated using the formula: $y = -1,0403x + 2,1596$ ($R^2 = 0,9793$). The results show that the band is at 39 kDa which confirms the band as being LRP.

8. Supplementary information

8.1. List of reagents and materials:

- Associate chemical enterprise, Southdale, South Africa: DCM; DMSO; EA; Glycerol; HCL; HNO₃; Methanol; PVA; Tween-20
- ATCC, USA: HEK-293 cells
- Biorad Hercules, CA, USA: Clarity™ Western ECL Blotting Substrate; Triton X-100
- Biowest, Nuaille, France: FBS; trypsin-EDTA
- Hyclone, GE Life Sciences, Massachusetts, USA: DMEM
- Inqaba Biotechnical Industries, South Africa: GR-Green
- Merck, Darmstadt, Germany: BSA; CHAPS lysis buffer; EGTA; GFP; Glycine; Gold chloride; Metformin; MgCl₂; PLGA; PIPA buffer; Sodium azide; Sodium citrate; TRAPEze® RT Telomerase Detection Kit; Tris
- NeST Technology, Virginia, USA: 96-well plates; T25 and T75 cell culture flasks
- New England Biolabs, Ipswich, MA, USA: 1 kbp DNA ladder; dNTPs; Luna® Universal qPCR Mastermix
- Thermo Fisher Scientific, Massachusetts, USA: Micro-BCA assay; MST-312; MTT; Penicillin-Streptomycin; TBE

8.2. List of equipment:

- TC 20™ automated cell counter - Bio-Rad
- VICTOR® Nivo™ Multimode Microplate Reader - PerkinElmer
- Roche LightCycler LC480 - Roche, Basel, Switzerland
- Trans-Blot® Turbo™ Transfer System – Biorad
- ChemiDoc – Biorad
- Inverted light microscope - Zeiss Primovert
- FEI Quanta FEG-SEM
- TESCAN MIRA3 FEG-SEM
- FEI Spirit 120 kV TEM

8.3. List of software:

- Agilent Aria Software (v1.5)
- GraphPad Prism (v6.05)
- Image Lab (v5.1)
- Microsoft Excel 365 Pro